Investigating the effects of chronic doxorubicin and ghrelin treatment on hepatic tissue

By

Carmelita B. Abrahams

Thesis presented in fulfilment of the requirements for the degree Master of Science (Physiological Sciences) at Stellenbosch University.

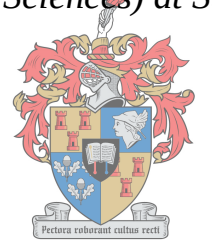

UNIVERSITEIT
iYUNIVESITHI
STELLENBOSCH
UNIVERSITY

Supervisor: Dr. Balindiwe JN Sishi

March 2018

DECLARATION OF ORIGINALITY

Declaration:

1. I understand what plagiarism is and am aware of the University's policy in this regard/

2. I declare that this dissertation is my own original work. Where other people's has been used (either from a printed source, internet or any other source), this has been properly acknowledged and referenced in accordance with departmental requirements.

3. I have not used work previously produced by another student or any other person to hand in as my own.

4. I have not allowed, and will not allow, anyone to copy my work with the intention of passing it off as his or her own work.

5. Where required, I have put my written work through authentication software, with the exclusion of the references, figures and tables and submitted this report to my supervisor or module coordinator.

SIGNATURE STUDENT:

SIGNATURE SUPERVISOR:

Abstract

Introduction: Doxorubicin (DOX) is an effective and widely used chemotherapeutic agent. However, its toxicity on healthy tissue limits its usage. DOX is known to induce damage mainly *via* oxidative stress which stimulates oxidative damage and apoptosis either intrinsically or extrinsically. While literature has primarily focused on the side effects of DOX on the myocardium, very little attention has been paid to the potential toxic effects of DOX on peripheral organs such as the liver which metabolises drugs and various toxins. Ghrelin is a hormone naturally found in the body which has been found to possess some beneficial properties that could protect the liver against DOX toxicity. Up until now, the therapeutic role of ghrelin in a chronic model of DOX toxicity has not been evaluated. Therefore, this study aimed to evaluate the effects of DOX on the liver and whether the use of ghrelin in this context will confer protection.

Methods: Four week old male Sprague-Dawley rats were randomly divided into four experimental groups: vehicle (saline), DOX (2.5 mg/kg/week), ghrelin (300 µg/kg/wk) and DOX+Ghrelin (both treatment regimens). Treatment was administered through intraperitoneal (i.p) injections for eight weeks where body weight and food consumption was monitored. One week after the last injection, the rats were sacrificed and the liver was harvested for histological and molecular analysis. Blood, which was separated into serum and plasma was also collected to evaluate liver function. Histological staining included Haematoxylin and Eosin (H&E), Masson's Trichome, Reticulin and Oil red O, while molecular experiments included oxidative stress analysis, apoptotic and autophagic activity as well as endoplasmic reticulum (ER stress).

Results: Terminal body weights were recorded per week and it was evident by the fourth week that the DOX treated animals (228.30 ± 7.09 g, $p < 0.001$) were not gaining as much weight as the vehicle treated animals (285.50 ± 19.24 g). This lack of weight gain was maintained until the end of the treatment protocol and coincided with reduced food consumption. Ghrelin significantly increased food consumption in the DOX+ghrelin group (159.20 g ± 9.43 g, $p < 0.05$) versus the DOX group (128.50 g ± 7.27), however this effect was not reflected in the body weight measurements of this group. Interestingly, DOX induced the fusion of liver lobes and this was prevented in the presence of ghrelin. While a normal rat liver and those that were treated with ghrelin alone displayed seven lobes, DOX treated

animals presented with an average of four lobes and the combination group, an average of six lobes. This fusion did not affect survival, liver function or oxidative stress parameters. Although autophagic activity was maintained in all treatment groups, DOX+ghrelin prevented caspase-3 cleavage and permitted binding immunoglobin protein (BiP) and activating transcription factor 4 (ATF4) protein expression.

Discussion & Conclusion: This study demonstrated that the liver is a robust organ that can withstand a great deal of stress and toxicity as weekly administration of DOX did not induce severe liver damage. Due to this organs regenerative capabilities, it is highly likely that DOX induced early damage of which the liver was able to recover from. While liver morphology was altered by DOX, structural parameters measured and function tests remained unchanged. No adverse oxidative damage was observed, nor was there any variation in the anti-oxidant status of this tissue. Molecularly, ghrelin reduced apoptosis and elevated autophagy. Therefore, while ghrelin's protective effects were mainly observed as a result of its orexigenic properties, its effect against DOX on the liver requires further investigation.

Acknowledgements

To my **parents and siblings,** thank you for your endless love and support through my tertiary studies, not only financially but emotionally as well. I have always been able to pursue my dreams and various opportunities because your support system has never failed me. I appreciate all the effort that you have gone through to help me succeed. I am fortunate to have you in my life. Lastly, thank you for the laughs, patience, wise advice and encouragment. I will always love you.

To my **friends**, (especially Amanda, Bianca, Curen and Venita), thank you for the unconditional support throughout my studies. This experience has been challenging for all of us but it was also filled with joy, laughter and successes. Thank you for walking this path with me.

To my **Supervisor, Dr. Balindiwe Sishi**, thank you for allowing me to join your research group. I appreciate the effort and time you have invested in me. I have grown not only academically but personally as well. I admire your work ethic, intelligence and determination to succeed. You are truly inspiring and without you, this thesis would not have been possible.

To **Prof.Engelbrecht,** thank you for always being willing to assist me when necessary.

To my research group **CORG**, thank you for your support and advice regarding research. Toni, Topè and staff at the animal facility, thank you for executing the animal study from which I have utilised the liver. Without your input, this research would not have been possible.

Thank you to **Mr. Reggie Williams** from tygerberg campus for your guidance with the histology and hospitality you offered. I thoroughly enjoyed working with you. **Mr. Fani Rautenbach** from the oxidative stress centre at CPUT, thank for providing your facilities and input with the oxidative stress analysis. Thank you to **Jonnifer**, for transporting me to the different campuses and your assistance around the department.

Dr. Lydia Lacerda, thank you for always being of assistance to my experimental plans and I will treasure pleasant conversations we had.

Mr. Ashwin Isaacs, thank you for always being available for advice and assistance with histology and microscopy.

The **staff and students** of the physiology department, thank you for being willing to offer advice and assistance when needed.

List of figures

List of tables

List of abbreviations

ACTH	Adrenocorticotropic hormone
AgRP	Agouti-related protein
ALT	Alanine transaminase
AMPK	Adenosine Monophosphate-Activated Protein Kinase
ANOVA	One-way analysis of variance
AP-1	Activator protein-1
APAF-1	Apoptotic protease activating factor-1
ASK1	Apoptosis signalling-regulating kinase 1
ATF6	Activating transcription factor 6
ATP	Adenosine triphosphate
Bcl-2	B-cell lymphoma 2
BH3	Bcl-2 homology domein 3
BiP	Binding immunoglobin protein
C/EBPβ	CCAAT-Enhancer-Binding Protein β
CAMKK	Calmodulin-dependent kinase kinase
cAMP	Cyclic adenosine monophosphate
CAT	Catalase
CDs	Conjugated dienes
CHF	Congestive heart failure
CHOP	C/EBP homologous protein
CTGF	Connective tissue growth factor
CYP	Cytochrome P450
DAG	Diacylglycerol
DNA	Deoxyribonucleic acid
DOX	Doxorubicin
DOX-Fe	DOX-iron
DTNB	5'-dithiobis-(2-nitrobenzoic acid)
ECM	Extracellular matrix

EGF	Epidermal growth factor
eIF2α	Eukaryotic initiating factor 2 subunit α
eNOS	Endothelial nitric oxide synthase
ER	Endoplasmic reticulum
ERAD	ER associated protein degradation
ERK1/2	Extracellular signal-regulated protein kinases 1 and 2
Fig	Figure
ERO1α	ER Oxidoreductin-1α
GADD34	Growth arrest and DNA damage-inducible protein
GH	Growth hormone
GHRH	Growth-hormone-releasing-hormone
GHS	Growth-hormone secretagogue
GHS-R	Growth hormone secretagogue receptor
GLUT2	Glucose transporter 2
GOAT	Ghrelin O-acyltransferase
GPx	Glutathione peroxidase
GR	Glutathione reductase
Grp78	Glucose regulated protein 78
GSH	Reduced glutathione
GSSG	Oxidized glutathione
H&E	Haematoxylin and Eosin
HDL	High density lipoproteins
HGF	Hepatocyte growth factor
HRP	Horseradish peroxidase
Hsc70	Heat shock protein 70
i.p	Intraperitoneal
IGF-1	Insulin-like growth factor 1
IHC	Immunohistochemistry
IL-1	Interleukin-1
IL-1β	Interleukin-1 beta

IL-6	Interleukin-6
iNOS	Inducible nitric oxide synthase
IP_3	Inositol trisphosphate
IRE1α	Inositol-requiring 1α
IRP	Iron regulatory protein
JNK	Jun N-terminal Kinase
K	Lysine
LDL	Low density lipoproteins
M_2VP	Methyl-2-vinylpyridinium triflate
MAPKs	Mitogen-activated protein kinases
MDA	Malondialdehyde
mPTP	Membrane permeability pore
mRNA	Messenger ribonucleic acid
NADPH	Nicotinamide adenine dinucleotide phosphate
NAFLD	Non-alcoholic fatty liver disease
NBR	Neighbour of BRCA1
NFkB	Nuclear factor kappa-light-chain-enhancer of activated B cells
NH_2	Amino group
NH_3	Ammonia
NPY	Neuropeptide Y
PAS	Periodic acid Schiff.
PDGF	Platelet-derived growth factor
PERK	Double-stranded RNA-dependent protein kinase-like ER kinase
PKA	Protein kinase A
PKB	Serine/threonine kinase Akt
PLC	Phospholipase c
PPARγ	Peroxisome proliferator-activated receptor γ
RIPA	Radio-immunoprecipitation
ROS	Reactive oxygen species
SDS-PAGE	Sodium dodecyl sulphate polyacrylamide gel electrophoresis

SOD	Superoxide dismutase
SREBP	Sterol regulatory binding protein
STAT3	Signal transducer and activator of transcription 3
TBS-T	Tris buffered saline-Tween®20
TGFα	Transforming growth factor alpha
TGFβ	Transforming growth factor beta
VLDL	Very low density lipoproteins
TNFα	Tumour necrosis factor alpha
Ub	Ubiquitin
UPP	Ubiquitin proteasome pathway
UPP	Ubiquitin proteasome pathway
UPR	Unfolded protein response
XBP1	X-box-binding protein 1

List of units

%	Percentage
° C	Degree celsius
µg	Microgram
µg/kg	Microgram per kilogram
µg/ml	Microgram per milliliter
µM	Micromolar
µm	Micromolar
µmol CD/g	Micromolar conjugated diene per gram
µmol MDA/g	Micromolar malondialdehyde per gram
AU	Arbitrary units
G	Gram
g	Gravity
Hrs	Hours
L	Liter
mg/kg	Milligram per kilogram
Mins	Minutes
ml	Millilitre
mM	Millimolar
mU/ml	Milliunits per milliliter
nm	Nanomolar
rpm	Revolutions per minute
Secs	Seconds

Symbols

O_2	Oxygen
$O_2^{\cdot -}$	Superoxide
OH^-	Hydroxyl radicals
H_2O_2	Hydrogen peroxide
Fe	Iron
Fe^{2+}	Ferrous iron
Fe^{3+}	Ferric iron
CO_2	Carbon dioxide
Ca^{2+}	Calcium
α	Alpha
β	Beta
γ	Gamma

Table of contents

Chapter 1

Literature review

1. The liver

1.1 Anatomy and blood supply

The liver accounts for ±1.5 - 2.5% of lean body mass and compared to the skin, it is regarded as the second largest organ present in the human body (Mitra & Metcalf, 2009). The human liver is situated in the abdominal cavity in the right upper quadrant, below the right hemi-diaphragm. While the human liver consists of a right and a left lobe, the livers of rodents have four lobes (Abdel-Misih & Bloomston, 2010). Their livers are divided into the median, right, left and caudate lobes, with all lobes except the left lobe being further divided into two parts. This gives the appearance that mice and rats have seven to eight liver lobes (Malarkey *et al.*, 2005). The liver is protected by the rib cage and maintains its position through avascular ligaments, which stretch from the Glisson capsule, a layer of connective tissue covering the liver, to other organs that surround the liver including the stomach, duodenum and diaphragm (Abdel-Misih & Bloomston, 2010).

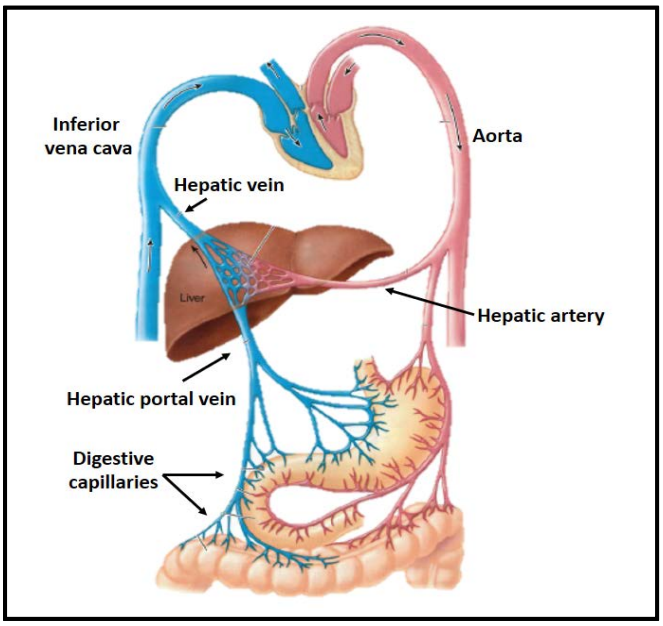

Figure 1.1: Liver blood supply within the human body. The hepatic artery brings blood borne metabolites and the bulk of oxygenated blood to the liver. While the stomach and intestinal veins converge to form the hepatic portal vein which brings venous blood to the liver. (Adapted from Sherwood, 2013).

The liver is a vascular organ and receives a significant amount of blood supply. At rest, it receives up to 25% of cardiac output, more than any other organ (Abdel-Misih & Bloomston, 2010; Campbell, 2006a). In addition, the liver also receives blood from two chief vascular systems, the hepatic artery and the hepatic portal vein (Fig.1.1) (Malarkey *et al.*, 2005). Arterial

blood rich in oxygen (O_2) and blood borne metabolites are transported to the liver by the hepatic artery, while venous blood containing the bulk of nutrients is brought from the digestive tract *via* the hepatic portal system (Sherwood, 2013; Abdel-Misih & Bloomston, 2010). The latter is a complex vascular connection between the digestive tract and the liver, where the stomach and intestinal veins meet to form the hepatic portal vein. The hepatic portal vein and the hepatic artery extend into the liver and branches into a capillary network that runs through the sinusoids between hepatocytes, which are the main cell type found in the liver. This allows for the exchange of metabolites between the blood and hepatocytes, and the blood then drains into the central hepatic venule. Branches of this hepatic venule merge to form the hepatic vein, where blood leaves the liver to enter the inferior vena cava (Sherwood, 2013). From here, the liver parenchyma are responsible for the digestion and metabolism of nutrients and toxins, as well as the production of different proteins.

1.2 Hepatic tissue cell types

Considering that the liver is the second largest organ in the body, it is surprising that there are very few specializations amid the cells present in this organ. Cells found within the liver include the hepatocytes, sinusoidal epithelial cells, biliary epithelium, Kupffer cells and hepatic stellate cells (also known as pericytes), which can transform into myofibroblast-like cells (Young *et al.*, 2013; Pellicoro *et al*., 2014). Hepatocytes are the most abundant comprising approximately 60% of total cells, and constituting ±80% of the liver volume. They are responsible for the execution of metabolic and secretory functions (Sherwood, 2013; Gebhardt, 1992). Hepatocytes are characterized by their polyhedral shape containing circular nuclei, and are considered as the workhorses of the liver (Young *et al.,* 2013). It is for this reason that they contain an abundance of smooth and rough endoplasmic reticulum (ER) which contributes to ±15% of the total cell volume. Furthermore, each hepatocyte contains ±30 lysosomes, ±500 peroxisomes, ±1000 mitochondria and numerous Golgi complexes, ribosomes and cytoskeletal elements. With age however, the amount of hepatocytes decrease, hypertrophy and polyploidy takes place, smooth ER and lysosomes enlarge, while mitochondria remain the same. The capability and ability of the liver to metabolize drugs also declines with age. The sinusoidal endothelial cells form a barrier between hepatocytes and blood where they filter fluids, solutes and particles between the blood and the space of Disse. The space of Disse is found between hepatocytes and the endothelial cells lining the sinusoids, whereas the biliary epithelium serves as a lining for the canaliculi that

transports bile. Kupffer cells are resident macrophages that are derived from circulating monocytes where they produce cytokines which mediate inflammation (Malarkey *et al.*, 2005). The hepatic stellate cells store vitamin A in lipid droplets and under certain stimuli, they lose their perinuclear vitamin A droplets and transform into myofibroblast-like cells that produce extracellular matrix to promote fibrosis (Albanis *et al.*, 1975; Pellicoro *et al.*, 2014). These cells are thus the major determinants of liver regeneration, fibrogenesis and cirrhosis (Malarkey *et al.*, 2005).

1.3 Hepatic lobule and the hepatic acinus

The functional unit of the liver is known as the hepatic lobule which is arranged in a hexagonal structure (Fig.1.2). These hexagonal structures are further assembled into a honeycomb-like configuration where the corners of the hexagon contain three major vessels: the hepatic artery, the portal vein and the bile duct. Together, these vessels are known as the portal triad where branches of the hepatic artery and portal vein transport blood in an opposite direction to the branches of the bile duct (Campbell, 2006a; Gebhardt, 1992). On the one hand, the hepatic artery and portal vein branches from the portal triad into the lobules and form capillary spaces called sinusoids. The sinusoids are outlined by sinusoidal endothelial cells and hepatocytes are arranged in a single layer between two sinusoids. This increases the exchange of metabolites and secretory products between the blood and the hepatocytes (Sherwood, 2013). Between the hepatocytes and the endothelial cells outlining the sinusoids, the space of Disse exists. This space contains extracellular fluid, hepatic stellate cells and Kupffer cells attached to endothelial cells that outline the sinusoids (Pellicoro *et al.*, 2014). The branching of the hepatic artery and portal vein into capillaries that extend through the sinusoids, run to the centre of the lobule where they converge to form the central hepatic venule. With this, metabolites are then exchanged between the hepatocytes and these capillaries (Young *et al.*, 2013). On the other hand, the bile duct follows a different route of entry into the lobule. It diverges into branches known as bile canaliculi that run between the hepatocytes. Hepatocytes themselves secrete bile into these branches which is then transported into the bile duct located at the portal triad. Both the bile and blood are transported in different directions; whereas blood flows from the portal triad towards the central hepatic venule, bile travels from the bile canaliculi towards the bile duct and into the portal triad (Campbell, 2006a). Although the hepatic lobule constitutes the structural unit of the liver, hepatic physiology is best presented by a structure termed the hepatic acinus.

The hepatic acinus (Fig.1.2) is formed from the parenchyma between the portal triad and the central hepatic venule. This area can be divided into three zones: the area closest to the portal triad is referred to as the periportal zone and designated as zone one (1), followed by the intermediate zone designated as zone two (2) in the middle, and the area around the central hepatic venule is the pericentral zone designated as zone three (3) (Hijmans *et al.*, 2013). Zone 1 receives oxygen rich blood and metabolites as it is the closest to the portal triad, while zone 2 and 3 receive a poor supply of oxygen and metabolites. This arrangement also means that the cells present in zone 1 are the ones that are first exposed to blood borne toxins (Young *et al*., 2013).

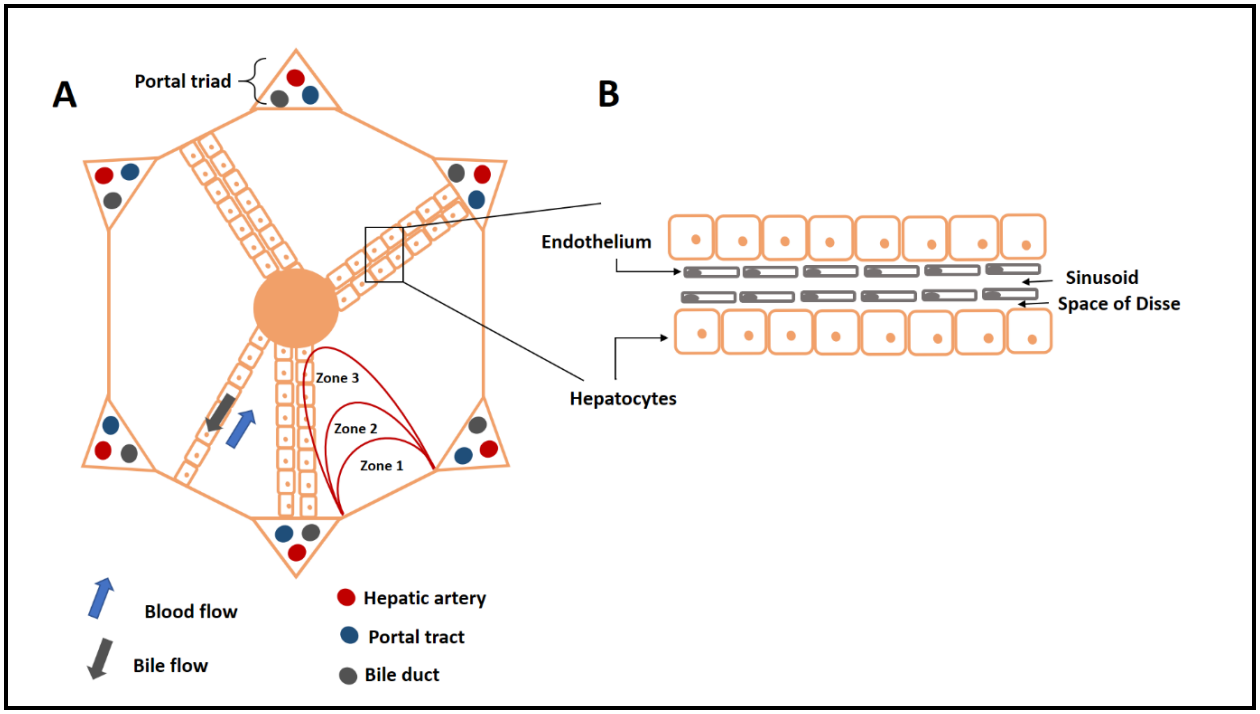

Figure 1.2: Representation of the hepatic lobule and hepatic acinus and the arrangement of the hepatocytes and sinusoids. (A) Illustration of the hepatic lobule with the portal triad at the corners of the hexagonal structure and the central vein in the center. The blue arrows indicate blood flow from the portal triad to the central vein and the grey arrow, bile flow from the hepatocytes to the bile duct in the portal triad. The hepatic acinus is illustrated by the 3 zones. The zones are indicated as zone 1 closest to the portal triad followed by zone 2 and then zone 3 closest to the central vein. **(B)** Magnification of the hepatic lobule, the endothelial cells outline the hepatocytes forming the sinusoids, with the space of Disse between the hepatocytes and the endothelial cells. (Adapted from Campbell, 2006a).

1.4. Functional gradients

The hepatocytes in the above mentioned zones differ in composition and enzyme activity. Hepatocytes closest to the portal triad traditionally have higher levels of oxygen, glucose-6-phosphatase activity, peroxisomes, bile acid uptake, urea cycle activity, glycogen synthesis and glutathione content. This precedes the amounts found in hepatocytes closest to the central hepatic venule (Gebhardt, 1992). During starvation, the hepatocytes closest to the portal triad are first depleted of glycogen and restored following feeding. Interestingly, the hepatocytes closest to the central hepatic venule specialize in a high content of other enzymes including glutamine synthetase, glucokinase, carboxylesterase, and ethanol-inducable cyp 2E. (Hijmans *et al.*, 2013; Malarkey *et al.*, 2013). The latter forms part of the Cytochrome P450 (CYP) family of enzymes responsible for the metabolism of endogenous and exogenous compounds such as steroids, fatty acids, alcohol and a variety of drugs (Cho *et al.*, 2017). Hepatocytes are however not the only cell type in the liver that differs based on localization.

The Kupffer cells found in the periportal zone are larger and have elevated phagocytic activity compared to those present in the pericentral zone (Bykov *et al.*, 2002). When blood enters from the portal triad, the cells closest to this area are first exposed to metabolites and toxins, and the Kupffer cells in this region thus offer the first line of defence (Malarkey *et al.*, 2005: Bykov *et al*., 2002). Overall, the liver is organized into a structure suitable for the digestion and metabolism of macronutrients, the production and secretion of proteins and the elimination of toxins, in addition to the insults it endures that can affect its growth and mass.

1.5 Liver regeneration

Even though hepatocytes are terminally differentiated, they can proliferate in response to metabolic demands, surgical resection and chemical or viral insults (Fausto *et al.*, 2000). Therefore, hepatocyte regeneration following injury is not dependent on progenitor cells (Zaret & Grombe, 2008). Quiescent hepatocytes proliferate and replicate to restore the liver's functional capacity and mass upon stimulation (Fausto *et al.*, 2000). These stimuli include growth factors such as hepatocyte growth factor (HGF), epidermal growth factor (EGF) and transforming growth factor alpha (TGFα). Hepatocytes also need to be primed by cytokines that include interleukin-6 (IL-6) and tumour necrosis factor-alpha (TNF-α) before they can respond to growth factors. At least four transcription factors are required for the initiation of liver regeneration namely, nuclear factor kappa-light-chain-enhancer of activated B cells (NFkB), activator protein-

1 (AP-1), signal transducer and activator of transcription 3 (STAT3) and CCAAT-Enhancer-Binding Protein β (C/EBPβ) (Fausto, 2000; Fausto *et al*., 2006). The ratio between liver and body mass are the main determinants of growth and not the liver mass in isolation. Optimal liver to body mass ratio is reached when the liver performs the amount of metabolic work needed for the body to function optimally (Fausto, 2000; Michalopoulos & DeFrances, 1997).

In conditions where the liver undergoes hyperplasia and/or hypertrophy in response to drug treatment, removal of this stimuli results in a loss of liver mass to restore the normal liver to body mass ratio (Fausto, 2000). Toxic injury, massive necrosis or carcinogenesis may impair or delay hepatic proliferation (Friedman, 2000). Under these conditions, a non-parenchymal cell compartment proliferates and develops into mature hepatocytes to restore the lost liver mass. The adult liver therefore contains facultative progenitor cells identified as the oval cell population (Zaret & Grombe, 2008; Zhang *et al.*, 2009). As the name implies, these cells are oval in shape with a dark stained nucleus and scant basophilic cytoplasm found in the lining of biliary ductules (Zhang *et al.*, 2009; Friedman, 2000). They can differentiate into either hepatocytes or biliary epithelium. However, the oval cell population is not homogenous but rather heterogenous comprising of cells with differing precursor capabilities at different stages of maturation (Zaret & Grombe, 2008). Interestingly, during the postnatal period of the rat, the amount of liver lobules and their size may increase for compensatory growth. When adulthood is reached the liver contains a standard number of lobules and is unable to grow more lobules in the event of a proliferative trigger. However, they are able to grow hepatocytes and increase the size of the hepatic lobules (Papp *et al*., 2009). While the liver has regenerative capacity, chronic insults may impair this trait and instead result in fibrosis.

1.6 Liver fibrosis

Fibrosis is the excessive build-up of extracellular matrix (ECM) proteins (eg. Type I collagen) and if it persists, cirrhosis ensues (Bataller and Brenner, 2005). While fibrosis is reversible, cirrhosis, with rare exceptions is not (Bissel, 1998; Friedman, 2000). Fibrosis becomes clinically relevant when dysregulated and excessive scarring occurs in response to chronic and persistent injury. Normally, the space of Disse contains a basement membrane-like matrix. This normal subendothelial ECM is important for maintaining the differentiated function of all resident liver cells. Once the liver becomes fibrotic, there are qualitative and quantitative changes in the composition of hepatic ECM. There is 3-5 fold increase in the total content of collagen and non-

collagenous components accompanied by a change in the type of ECM in the subendothelial space from the standard low density basement membrane-like matrix, to the interstitial type matrix containing fibril-forming collagens (Friedman, 2000).

As mentioned previously, the cell type mainly associated with fibrosis is the hepatic stellate cells. These cells are activated in response to liver injury which causes them to transform from a quiescent state into a proliferative, fibrogenic and contractile myofibroblast state (Albanis *et al.*, 1975; Pellicoro *et al.*, 2014). The stimuli for activation includes free radicals and leukocytes that are recruited to phagocytose dead or apoptotic hepatocytes. The immune cells intensify the inflammatory response by secreting pro-inflammatory cytokines (TNF, IL-6, IL-1β) and this recruits more T cells to the site of injury. The pro-inflammatory mediators produced by damaged cells and immune cells, includes cytokines and growth factors such as platelet-derived growth factor (PDGF), connective tissue growth factor (CTGF), transforming growth factor beta (TGFβ), all mediate the activation of hepatic stellate cells (Pellicoro *et al.*, 2004). Moreover, myofibroblasts are also implicated in the closure of cutaneous wounds. Taken together, the contractile function of activated stellate cells during chronic liver injury may disrupt normal hepatic morphology by contributing to the distortion of lobular architecture and portal hypertension (Bissel, 1998).

1.7 Metabolism

1.7.1 Fat digestion

The stomach and its gastrointestinal juices are unable to metabolize lipids, therefore the liver produces bile to aid in the digestion of fats. Bile is an alkaline electrolyte solution containing bile salts and pigments which are stored in the gall bladder (Campbell, 2006b). Once dietary lipids and amino acids are present within the small intestine, enteroendocrine I cells present in the duodenal and jejunal mucosa secrete the hormone cholecystokinin which stimulates contraction of the gall bladder and relaxation of the sphincter of Oddi. As a result of this contraction-relaxation cycle, bile is released into the duodenum and assists the enzyme, pancreatic lipase, in fat digestion (Sherwood, 2013; Griifin, 2013). The final products of fat digestion within the small intestine are monoglycerides and free fatty acids which are packaged into vesicles called chylomicrons. These chylomicrons are transported in to the circulation *via* lymphatic vessels and do not enter the liver.

Lipoprotein lipase, situated on a variety of tissues including the liver, is responsible for the release of free fatty acids from plasma chylomicrons (Ory, 2007; Camps *et al.*, 1991). Fatty acids are the liver's predominant source of energy and when in circulation, are recruited into the liver to undergo beta-oxidation within the mitochondria of hepatocytes (Campbell, 2006b). The liver also stores lipids in the form of triglycerides, which are fatty acids attached to a glycerol group *via* esterification. If these triglycerides are not stored in the liver, they are packaged into lipoproteins [very low density lipoproteins (VLDL), low density lipoproteins (LDL) and high density lipoproteins (HDL)] which are released back into the circulation (Mitra & Metcalf, 2009; Brown & Goldstein, 1986). The balance between fatty acid esterification and beta-oxidation is regulated by the hormones insulin and glucagon secreted from the pancreas. Whereas insulin stimulates the formation of triglycerides, glucagon stimulates the process of beta-oxidation (Campbell, 2006b).

The liver not only plays a role in fat digestion by producing bile, it is also involved in the regulation of plasma cholesterol. Hepatocytes have a highly developed and sensitive mechanism for regulating intravascular and intracellular levels of cholesterol. In a stressed state, cells import cholesterol to save energy. Cholesterol is acquired from the circulation by the uptake of lipoproteins, particularly LDL *via* LDL receptors. As the cellular requirement for cholesterol increases, the expression of the receptor increase and the serum LDL levels falls. On the contrary, if there is excess intracellular cholesterol, downregulation of the LDL receptor occurs while serum LDL levels rise. The amount of intracellular free cholesterol thus controls the expression of LDL receptors by stimulating or inhibiting the release of sterol regulatory binding protein (SREBP), which binds to DNA to promote transcription of the LDL receptor gene (Dietschy *et al.*, 1993; Griffin, 2013). Another mechanism by which serum cholesterol can be decreased is through HDL. HDLs are produced in the gut and liver and once in circulation, increase in particle size by acquiring cholesterol from triglyceride rich lipoproteins and peripheral tissues. The cholesterol acquired undergoes a series of enzymatic reactions to form cholesterol esters which are transported back to the liver by HDL. The role of hepatic lipase in this context is to penetrate the surface of HDL to access the cholesterol core and retrieve the contents for the hepatocyte (Griffin, 2013).

1.7.2 Carbohydrate metabolism

The portal vein and hepatic artery bring glucose to the liver following absorption from the small intestine. Glucose enters the hepatocytes *via* the glucose transporter 2 (GLUT2) situated on the hepatocyte cell membrane. The rate of glucose entry into the hepatocytes is directly proportional to the extracellular glucose concentration available within the hepatic portal vein and independent of insulin action. Inside the hepatocytes the enzyme glucokinase phosphorylates glucose molecules to produce glucose-6-phosphate which can follow one of two pathways: glycolysis or glycogenesis (Campbell, 2006b). During glycolysis, glucose-6-phosphate is metabolized to pyruvate in the cytosol and enters the mitochondria to partake in the citric acid cycle for energy production (Maughan, 2013). However, since the liver receives most of its energy from fatty acid and amino acid oxidation, the majority of the glucose absorbed will be converted to glycogen *via* glycogenesis and stored within the liver. The liver is the second largest glycogen store in the body after skeletal muscle. The enzyme glucose-6-phosphatase plays a role in the conversion of glycogen to glucose and this enzyme is not present in the muscle, only in the liver. Therefore, only the liver is able to contribute to blood glucose in the event of low blood glucose levels (Fig. 1.3) (Campbell, 2006b).

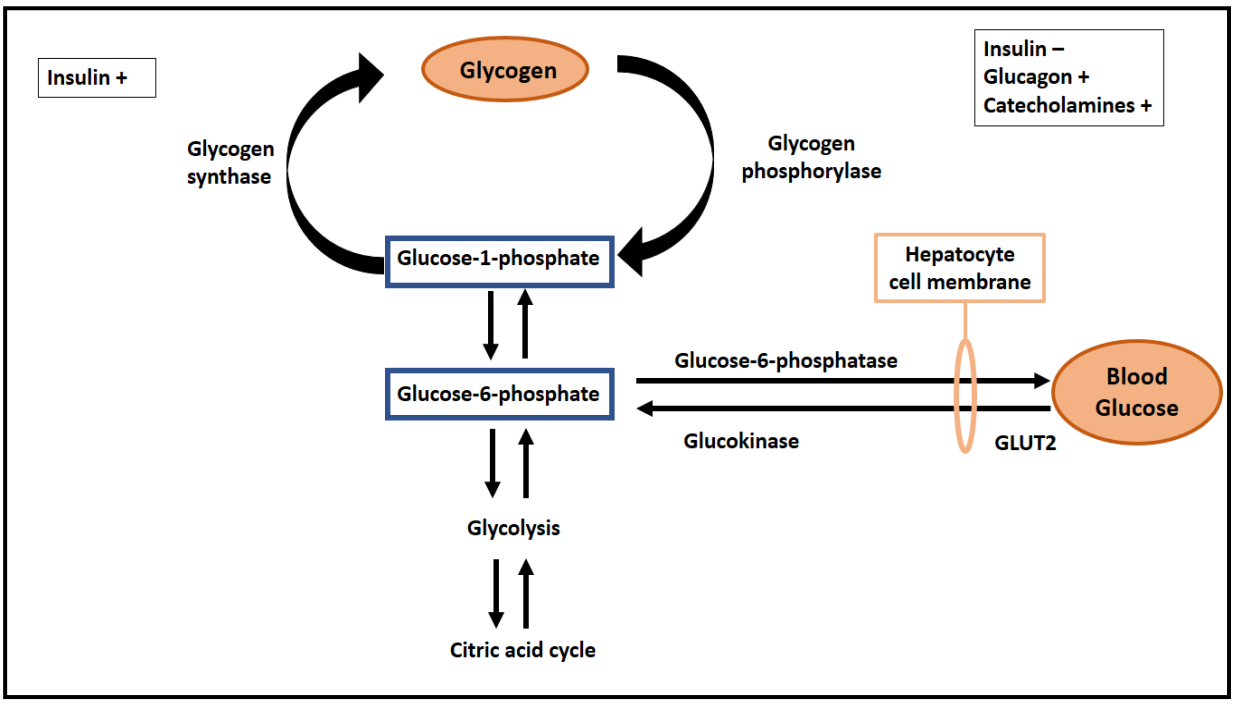

Figure 1.3: Hepatic glycogen synthesis and breakdown. Glucose enters the hepatocyte through the GLUT2 transporter. Glucokinase converts glucose to glucose-6-phosphate where this molecule can either enter glycolysis for energy production or glycogenolysis to form glycogen. Glycogen can also be

metabolized to glucose *via* the enzyme glycogen phosphorylase and glucose-6-phosphatase. These pathways are under the regulation of insulin which promotes glycogen formation and glucagon and catecholamines which promotes glycogen breakdown. Abbreviations: **GLUT2** – glucose transporter 2 (Adapted from Campbell, 2006b).

For glycogenesis to occur, glucose-6-phosphate is first catalysed to glucose-1-phosphate and then synthesized into glycogen *via* the enzyme glycogen synthase. While insulin may not be required for glucose uptake it is essential for the activity of glycogen synthase to produce and store glycogen (Maughan, 2013). During fasting, glucagon stimulates the breakdown of glycogen to form glucose in a process termed glycogenolysis. Glycogen phosphorylase catalyses glycogen to glucose-1-phosphate and subsequently glucose-6-phosphate. Glucose-6-phosphatase reforms the latter into glucose which is released into circulation (Dashty, 2013). Glucagon is however not the only protein that is able to stimulate glycogenolysis. Under conditions of stress, catecholamines stimulate glycogenolysis, while insulin during the fed state facilitates glycogenesis. In addition, the liver can produce glucose from other nutrients such as alanine, lactate and glycerol, *via* a process known as gluconeogenesis (Maughan, 2013). The other hormones that are known to regulate gluconeogenesis in addition to glucagon are cortisol, as well as catecholamines. A healthy relationship between glucagon and insulin is important to stimulate gluconeogenesis during starvation, where high levels of glucagon and a lack of insulin is required. During stress however, elevated levels of catecholamines and cortisol are additional stimuli that induce gluconeogenesis (Campbell, 2006b).

1.7.3 Protein metabolism

The processes of protein synthesis and degradation are tightly controlled throughout the body so that total body protein levels are kept constant. The liver metabolizes proteins by catalysing transamination and deamination reactions. The liver also synthesizes urea as well as some plasma proteins. Transamination is the transfer of an amino group ($-NH_2$) from one amino acid to an α-keto acid (usually α-ketoglutaric acid) to form a new amino acid, glutamate, and α-keto acid from the original amino acid. The enzyme alanine transaminase (ALT) catalyses the transamination between the amino acid alanine and the keto acid, α-ketoglutarate, to produce pyruvate and glutamate. This enzyme can also be used as an indication of hepatic function, with its release into the circulation as indicative of liver damage (Thapa & Walia, 2007). In contrast, deamination is catalysed by the enzyme glutamate dehydrogenase, where $-NH_2$ is removed from glutamate to

form ammonia (NH_3) and α-ketoglutarate (Fig. 1.4) (Mitra & Metcalf, 2009). The α-keto acids generated from transamination and deamination become shunted into the citric acid cycle for energy production with the release of carbon dioxide (CO_2) and water. The keto acids can also serve as precursors for glucose synthesis during gluconeogenesis (Campbell, 2006b). Considering that the NH_3 generated from deamination is toxic to human tissues, the liver converts NH_3 to urea through the ornithine cycle which is eventually excreted by the kidneys (Mitra & Metcalf, 2009). Apart from the metabolism of branch chained amino acids in skeletal muscle, the liver is the only place in the human body where urea is produced (Campbell, 2006b).

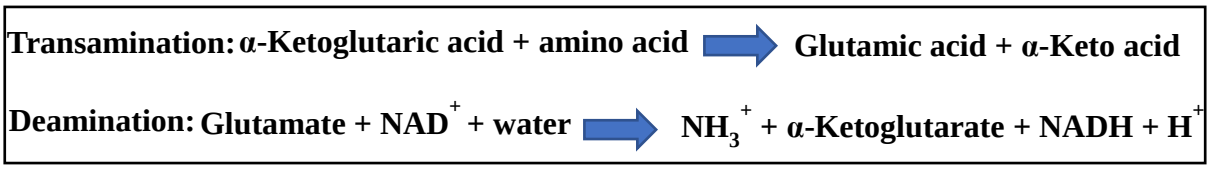

Figure 1.4: Transamination and deamination reactions to metabolize amino acids. Transamination is the transfer of the amino group (-NH_2) from one amino acid to an α-keto acid to form a new amino acid, usually glutamic acid. Deamination is the removal of the -NH_2 from glutamate to form ammonia (NH_3) and α-ketoglutarate.

Plasma proteins produced in the liver include albumin, fibrinogen and globulins. Albumin, while essential in the maintenance of fluid balance within peripheral tissues, it also binds various substances contained within plasma including fatty acids, bile salts and the hormone thyroxine (Campbell, 2006b). Albumin is the most vital protein produced by the liver and is therefore used as an indicator of hepatic function. When the liver is damaged, serum albumin levels are significantly reduced and may also be influenced by nutritional status, osmotic pressure and hormonal balance. In this case, hypoalbuminemia is not specific for liver disease and occurs during malnutrition, nephrotoxicity and chronic protein-losing enteropathies as well (Thapa & Walia, 2007). Globulins are components of lipoproteins that transport lipids and cholesterol between the liver and other tissues. These proteins bind a variety of substances including cortisol and thyroxine, minerals such as iron and copper and vitamin B_{12}. Blood components such as the clotting factor prothrombin and the substance involved in fluid balance, angiotensinogen, are all typical examples of globulins. The liver also produces insulin-like growth factor 1 (IGF-1) for growth, hepcidin for the inhibition of iron absorption and thrombopoietin for the production of platelets (Campbell, 2006b).

1.7.4 Metabolism of drugs and toxins

The metabolism of toxic substances by the liver occurs in two phases. In the first phase, toxic metabolites are inactivated by a group of enzymes called the P450 system. While these enzymes are not restricted to the liver, they are expressed in other tissue types as well. During the second phase, the water solubility of the substance is then increased so that it can be excreted in the urine or in bile**.** Blood draining from the gastrointestinal tract can in some cases be contaminated with bacteria and endotoxins. Resident Kupffer cells attached to the endothelium in the sinusoids, come into direct contact with the blood draining from the gastrointestinal tract. These cells then aid in the clearing of the microbes and release pro-inflammatory cytokines, IL-1 and IL-6 in the process (Campbell, 2006b). Additionally, Kupffer cells remove worn-out erythrocytes from the circulation and excrete the degradation product bilirubin within the bile (Sherwood, 2013). Based on the above roles, the liver is a vital organ involved in the execution of a variety of processes fundamental for the functioning of the human body. However, like any other organ, it is vulnerable to intracellular and extracellular damage that can affect its overall function.

2. Doxorubicin

Doxorubicin (DOX), also known as Adriamycin is an anthracycline antibiotic first isolated in the late 1960s from the fungus *Streptomyces peucetius (*Thorn *et al.,* 2011; Minotti *et al.,* 2004). This anthracycline has shown great potential in the eradication of cancerous cells and is classified by the Food and Drug Administration as one of the most effective antitumor drugs ever developed and as such, it is the most widely used chemotherapeutic agent for the treatment of cancers of the breast, aggressive lymphomas, solid tumours and soft tissue sarcomas (Carvalho *et al.,* 2009; Tacar *et al.*, 2013).

2.1 Pharmacokinetics

Following intravenous administration, the distribution half-life of DOX is between three to five minutes (mins) indicating the rate at which DOX is cleared from the plasma and taken up by the cells (Tacar *et al.* 2013). DOX enters cells *via* passive diffusion and once in the cytoplasm, it attaches to the 20s subunit of proteasomes, where it is translocated to the nucleus (Minotti *et al.,* 2004). It has been reported that the amount of DOX in the nuclear compartment is 50-fold higher compared to the amount found in the cytosplasmic compartment, reaching a saturation level of

340 µM. This can be represented as one DOX molecule intercalated at every fifth DNA base pair on a deoxyribonucleic acid (DNA) strand (Lal *et al.*, 2010). Approximately 2% of DOX is left unbound in the cytoplasm and is distributed among other organelles that include the Golgi apparatus, mitochondria and lysosomes (Tacar *et al.*, 2013). DOX penetrates cells effectively and can remain inside due to its lipophilic and DNA intercalating properties. However, despite these characteristics, DOX is unable to cross the blood brain barrier (Lal *et al.*, 2010). Due to the livers role in metabolism, DOX appears to accumulate in this organ where it becomes biochemically transformed into doxorubicinol by the enzymes aldo-ketoreductase and ubiquitous cytoplasmic carbonyl reductase (Tacar *et al.*, 2013; Kassner *et al.*, 2008). Approximately 50% of DOX leaves the body unchanged whilst the other 50% undergoes metabolism (Kassner *et al.*, 2008). As with all pharmacological agents, DOX needs to be eliminated from the body. The elimination of DOX from tissues takes much longer than its uptake, with a terminal half-life of 24-36 hours (hrs). The hepato-biliary pathway mediates plasma clearance with half of the excreted drug present in the bile. This is usually excreted from the body within five to seven days following chemotherapy. During the same period, 5-12% is excreted in the urine with 3% of the drug being the metabolite, doxorubicinol. Defecation contributes 10-20% towards the elimination of the drug after 24 hrs and after 150 hrs 50% of the drug is excreted via this route (Tacar *et al.*, 2013). In experimental animal models, DOX is often administered *via* intraperitoneal injection. DOX administered *via* this route results in a bioavailability of 40% without altering the elimination capacity. In addition, there is twice the prolongation in the mean residence time (average amount of time a single drug molecule stays in the body) *via* the intraperitoneal route over the intravenous route (Nagai *et al.*, 2013).

2.2 Doxorubicin's mechanism of action against cancer cells

DOX mainly kill cancer cells through DNA damage, while causing damage to other tissue types *via* oxidative stress, apoptosis and organelle dysfunction (Minotti *et al.*, 2004). DOX directly causes damage to DNA by two mechanisms: DNA intercalation and the inhibition of topoisomerase (Mizutani *et al.*, 2005). DOX prevents DNA replication and RNA transcription by spontaneously inserting itself between DNA base pairs in a mechanism referred to as intercalation. Single and double stranded DNA breaks induced by topoisomerase I and II activity, respectively, have also been observed following DOX treatment. (Cummings *et al.*, 1991). During the cell cycle phase, the topoisomerase enzymes cause DNA strand breaks to modify the

supercoiled structure of DNA. These breaks can be resealed again after replication or transcription has been completed. However, DOX exploits topoisomerase II activity by stabilizing the reaction intermediate in which DNA strands are cut and bound to topoisomerase II. This subsequently hampers DNA resealing resulting in cell cycle arrest and death (Minotti *et al.*, 2004). Although DOX is an effective chemotherapeutic agent, its use is limited due to toxic effects observed in non-cancerous cells. Up until now, research has focused on the detrimental effects of DOX on cardiac tissue, while paying little attention to other organs. Therefore, the following mechanisms to be discussed are based mainly on observations from cardiac tissue with supporting literature relevant in the context of the liver.

2.3 Doxorubicin-induced toxicity

2.3.1 Oxidative stress

DOX is a potent inducer of oxidative stress. Following metabolic activation once taken up by the cells, it generates free radicals by one electron being removed from ring C and donated to NADPH to form a semiquinone radical. In the presence of oxygen (O_2), the newly formed semiquinone donates its unpaired electron to O_2 to generate superoxide ($O_2^{\cdot -}$). The semiquinone is then regenerated to its native form, where the cycle continues. This is known as "redox cycling" and the other enzymes involved in this process are the oxidoreductases (NADPH cytochrome P450 reductase, mitochondrial NADH dehydrogenase, endothelial nitric oxide synthase and xanthine oxidase) (Fig. 1.5) (Minotti *et al.*, 2004; Keizer *et al.*, 1990). DOX "redox cycling" occurs in the nucleus, mitochondria, ER as well as the cytoplasm, and the free radicals generated

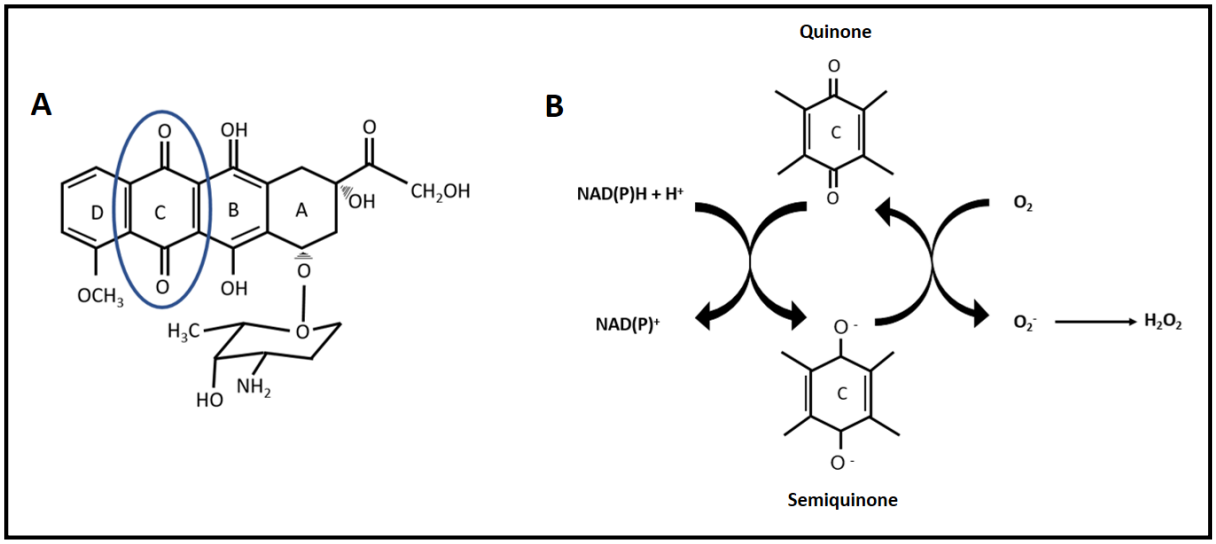

are responsible for the cytotoxic damage of these organelles (Keizer *et al.*, 1990). Considering that the liver is responsible for the metabolism of DOX, and hepatocytes are rich in mitochondria and ER, it is thus likely that DOX induces similar oxidative damage to these organelles in this organ.

Figure 1.5: The chemical structure of DOX and redox cycling of the quinone moiety. (A) Structure of DOX with the quinone moiety circled in blue. **(B)** The Redox cycling of DOX, one electron is removed from the quinone moiety to NADPH, forming a semiquinone. The latter donates the electron to O_2 generating $O_2^{\cdot -}$ and subsequently H_2O_2. Abbreviations: **DOX** – doxorubicin, **O_2** – oxygen, **$O_2^{\cdot -}$** - superoxide, **H_2O_2** – hydrogen peroxide (Adapted from Minotti *et al.*, 2004).

Furthermore, DOX and the $O_2^{\cdot -}$ anions generated also disrupts intracellular iron (Fe) homeostasis which accelerates the generation of reactive oxygen species (ROS). In this case, the iron binding

protein, ferritin, and the iron regulatory protein (IRP) are targeted. Ferritin is responsible for the intracellular storage of iron, and when $O_2^{\cdot-}$ anions are produced from the metabolic activation of DOX, they enter the transprotein channels of ferritin to reduce the iron core resulting in the release of ferrous iron (Fe^{2+}). As the semiquinone has a lower reduction potential than $O_2^{\cdot-}$ anions, it is unable to enter the iron core of ferritin (Minotti *et al.,* 2004). The IRP aconitase, located in the mitochondria and cytoplasm, contains an iron-sulphur [4Fe-S] cluster within its catalytic site. In the mitochondria this enzyme converts citrate to isocitrate as part of its role in the citric acid cycle. When the enzyme is present in the cytoplasm, it participates in iron regulation and is referred to as IRP-1 (Ghigo *et al.,* 2016). $O_2^{\cdot-}$ and hydrogen peroxide (H_2O_2) free radicals sequester the fourth iron from the [4Fe-S] aconitase catalytic site to form [3Fe-S]. This event results in a protein that contains [3Fe-S] and is devoid of aconitase activity. The release of the iron cluster transforms cytoplasmic aconitase into the IRP-1 where it binds with high affinity to the conserved iron-responsive elements in the untranslated regions of the transferrin receptor and ferritin messenger ribonucleic acids (mRNAs). This reduces the expression of ferritin, while increasing that of the transferrin receptor (Ghigo *et al.,* 2016; Minotti *et al.,* 2004). The transferrin receptor recruits transferrin from the circulation into the cell and thereby increasing the intracellular free iron concentration. Together, the sequestration of Fe^{2+} from ferritin and [Fe-S] from aconitase, leads to a reduction in the production of ferritin while increasing expression of the transferritin receptor. This results in elevated free cytoplasmic iron and the formation of DOX-iron (DOX-Fe) complexes (Ghigo *et al.,* 2016).

Free intracellular iron promotes ROS generation not only *via* the Fenton and Harber-Weiss reactions but also through the above mentioned DOX-Fe complexes. Normally, the $O_2^{\cdot-}$ generated from DOX is dismutated to H_2O_2 by the anti-oxidant superoxide dismutase (SOD), where after H_2O_2 is eliminated by glutathione or catalase (CAT). H_2O_2 and $O_2^{\cdot-}$ could also follow a different route under normal physiological conditions, where in the presence of iron, H_2O_2 and $O_2^{\cdot-}$ are readily converted to hydroxyl radicals ($OH^{\cdot}$). As indicated in Fig.1.6 below, the Harber-Weiss reaction may occur on its own at a slow rate (equation 1), while in the presence of iron (Fe^{2+}) this reaction occurs much faster (equation 2). The Fe catalysed Harber-Weiss reaction involves the reduction of ferric iron (Fe^{3+}) to ferrous iron (Fe^{2+}) by $O_2^{\cdot-}$, followed by the Fenton reaction in which Fe^{2+} catalyses the conversion of H_2O_2 into toxic $OH^{\cdot}$ radicals (equation 3). DOX-Fe^{3+} complexes are reduced to DOX-Fe^{2+} in the presence of a reducing system, namely NADPH

cytochrome P450 reductase, cysteine or glutathione thiol residues. DOX-Fe^{2+} in turn reacts with O_2 to form $O_2^{\cdot-}$ and subsequently OH^- radicals. In the absence of the reducing enzymes, DOX-Fe^{3+} undergoes oxidation, generating a DOX-Fe^{2+} complex. This complex catalyses O_2 to form $O_2^{\cdot-}$ anions which react with H_2O_2 to generate OH^- radicals (Šimůnek *et al.*, 2009). The free radicals generated cause lipid peroxidation of unsaturated fatty acids present on cellular and organelle membranes. This process produces toxic aldehydes such as malondialdehyde (MDA) which diffuses within cells and attacks macromolecular targets far from where they were generated. They thus act as secondary cytotoxic messengers (Keizer *et al.*, 1990; Luo *et al.*, 1997). Free radicals further oxidize DNA and proteins leading to the inhibition of enzymes necessary for cellular function. Furthermore, the cytotoxic aldehydes result in impaired energy production, macromolecular damage, and the elicitation of an inflammatory response that culminates in cell death following organelle dysfunction (*Keizer et al.*, 1990; Luo *et al.*, 1997).

Harber-Weiss reaction: $O_2^{\cdot-} + H_2O_2 \rightarrow O_2^{\cdot-} + OH^- + OH^{\cdot}$ **equation 1**

$O_2^{\cdot-} + Fe^{3+} \rightarrow O_2 + Fe^{2+}$ **equation 2**

Fenton reaction: $H_2O_2 + Fe^{2+} \rightarrow OH^{\cdot} + OH^- + Fe^{3+}$ **equation 3**

Figure 1.6: The Harber-Weiss and Fenton reaction. $O_2^{\cdot-}$ and H_2O_2 are converted to hydroxyl radicals by the Harber-Weiss reaction at a slow rate (equation 1). In the presence of Fe, the Harber-Weiss reaction occurs at faster rate and involves the Fenton reaction where $O_2^{\cdot-}$ is catalysed to O_2 by Fe^{3+}(equation 2) followed by Fe^{2+} catalysing the conversion of H_2O_2 to hydroxyl radicals (equation 3). Abbreviations: **$O_2^{\cdot-}$** - superoxide, **H_2O_2** – hydrogen peroxide, **Fe** – iron, **Fe^{3+}** - ferric ion, **Fe^{2+}** - ferrous ion.

2.3.2 Mitochondrial and ER dysfunction

DOX has previously been shown to associate with the mitochondria and ER. While it is not clear which protein it binds to on the ER, it binds with high affinity to cardiolipin, an integral protein enriched in the inner mitochondrial membrane (Sishi *et al.*, 2013a, Sishi *et al.*, 2013b; C Pereirra *et al.*, 2011). The binding of DOX to cardiolipin prevents creatine kinase binding to the inner mitochondrial membrane and decreases the activity of mitochondrial enzymes dependent on cardiolipin (Carvalho *et al.*, 2009). In this case, cardiolipin is not able to interact with key

mitochondrial complexes and this consequence has severe implications for oxidative phosphorylation and adenosine triphosphate (ATP) production (C Pereirra *et al.*, 2011). The binding of DOX to complex I of the respiratory chain also generates single electrons that are transferred to DOX. Similar to the metabolic activation of DOX described previously, a semiquinone intermediate is formed which donates electrons to O_2 producing the $O_2^{\cdot -}$ free radicals. This ROS further damages mitochondrial nucleic acids, proteins and lipids. DOX-induced ROS oxidizes thiol residues of the mitochondrial membrane permeability pore (mPTP) resulting in their opening and the leakage of cytochrome c which initiates the intrinsic (mitochondrial) pathway of apoptosis (Carvalho *et al.*, 2009; Mizutani *et al.*, 2004; Ow *et al.*, 2008). Once in the cytosol, cytochrome c and the initiator caspase, procaspase 9, bind to apoptotic protease activating factor-1 (APAF-1) to form the apoptosome complex. This results in the activation of caspase 9, who activates the effector caspase, caspase 3 and finally the execution of apoptosis (Ow *et al.*, 2008; Elmore *et al.*, 2007; Raychaudhuri *et al.*, 2010).

DOX also interferes with the ability of the ER to regulate calcium (Ca^{2+}) homeostasis. When DOX binds to the ER, it triggers Ca^{2+} release causing an increase in cytosolic Ca^{2+} concentration (Hanna *et al.*, 2014). As the ER is in close proximity to the mitochondria, and the mitochondria are also involved in Ca^{2+} regulation, Ca^{2+} is taken up *via* the Ca^{2+} uniporter in an attempt to restore Ca^{2+} homeostasis. When the Ca^{2+} concentration within the mitochondrial matrix reaches and exceeds its threshold, the mPTP opens where cytochrome c leaks and apoptosis is induced (Deniaud *et al.*, 2007). The ER not only functions as the Ca^{2+} storage center, the majority of membrane and secreted proteins are folded within this organelle where they are released extracellularly or incorporated into cellular compartments (Zhang & Kaufman, 2008; Meusser *et al.*, 2005; Shu *et al.*, 2012; Høyer-Hansen & Jäättelä, 2007). Therefore, the ER has a quality control mechanism where only properly folded proteins are released and the misfolded proteins are translocated to the cytosol for proteasomal degradation in a process termed ER associated protein degradation (ERAD) (Walter & Ron, 2011). As the ER is sensitive to changes in redox status, as observed during DOX treatment, the ER folding capacity and assembly is disrupted resulting in the build-up of misfolded proteins within the ER lumen. This series of events induces ER stress and the cell responds by stimulating the unfolded protein response (UPR) in an attempt to clear these proteins from the lumen. In addition, the UPR inhibits protein translation and upregulates signalling pathways that increase the production of molecular chaperones that assist

in the removal of these damaged proteins (Suh *et al.*, 2010). The UPR is initiated by protein sensors localized on the ER membrane. These include inositol-requiring 1α (IRE1α), double-stranded RNA-dependent protein kinase-like ER kinase (PERK) and activating transcription factor 6 (ATF6). Under normal conditions, these proteins are maintained in position by glucose regulated protein 78 (Grp78), also known as binding immunoglobin protein (BiP). During ER stress, BiP is recruited to bind with unfolded or misfolded proteins and thereby releases the ER stress sensors, resulting in their activation. IRE1, PERK and ATF6 act to upregulate ER chaperones to increase the protein folding capacity of the ER and to initiate the ERAD pathway to clear misfolded proteins (Zhang & Kaufman, 2008; Tsai & Weissman, 2010; Rutkowski & Kaufman, 2007). ERAD involves the translocation of misfolded ER proteins to the cytoplasm where they are degraded by the ubiquitin proteasome pathway (UPP) in a Lysine48 (K48)-dependent manner. (Lecker *et al.*, 2006; Benbrook & Long, 2012).

IRE1, PERK and ATF6 act by signalling downstream proteins to achieve the desired effects (Fig 1.7). Once activated, IRE1 splices an intron from the X-box-binding protein 1 (XBP1) mRNA leading to the translation of the XBP1. XBP1 upregulates the expression of ER chaperones to assist in protein folding, and activates the apoptosis signalling-regulating kinase 1 (ASK1). ASK1 proceeds to activate Jun N-terminal Kinase (JNK) and p38 Mitogen-activated protein kinases (MAPKs) where JNK leads to ER stress-induced apoptosis and increased autophagy, while p38 promotes cellular senescence (Tsai & Weissman, 2010). Activation of PERK results in the phosphorylation of eukaryotic initiating factor 2 subunit α (eIF2α) which inhibits overall protein translation and consequently reduces protein flux into the ER lumen for protein folding. However, eIF2α only prevents the translation of specific mRNAs into proteins, while others such as ATF4 continue to be translated. On the one hand, ATF4 stimulates the expression of ER chaperones and genes involved in the synthesis of glutathione, thereby resisting oxidative stress, and thus promoting cell survival. On the other hand, ATF4 stimulates the expression of C/EBP homologous protein (CHOP) which aggravates ER stress by increasing ER load and expression of the ER oxidase ER Oxidoreductin-1α (ERO1α), which makes the ER lumen more acidic. CHOP therefore acts to induce cell death. ATF6 is first translocated to the Golgi apparatus where it is cleaved by Golgi proteases resulting in its activation. It upregulates the expression of CHOP, ER chaperones and different components of the ERAD system. However, if these mechanisms fail and ER stress persists, the UPR stimulates autophagy to assist in the degradation of proteins,

and if autophagy cannot alleviate ER stress, apoptosis will then be activated (Tsai & Weissman, 2010; Walter & Ron, 2011).

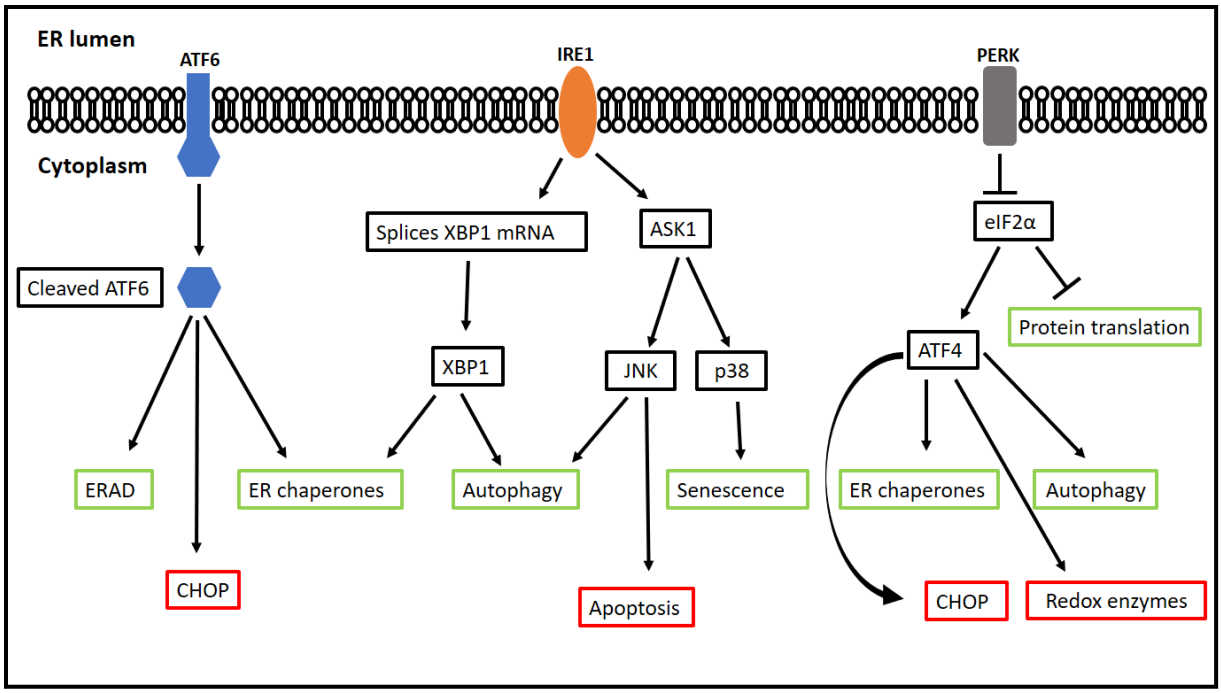

Figure 1.7: Downstream signalling effects of ATF6, IRE1 and PERK during the UPR. ER stress initiates the UPR leading to the activation of ATF6, IRE1 and PERK. These proteins initially function to resolve ER stress. ATF6 becomes cleaved and upregulates ER chaperones and the ERAD. IRE1 activates two proteins. First, it splices XBP1 mRNA leading to its activation. XBP1 then upregulates ER chaperones and autophagy. Second, it activates ASK1 who upregulates autophagy and senescence via JNK and p38, respectively. PERK inhibits eIF2α leading to the inhibition of protein translation and the activation of ATF4 who also upregulates ER chaperones and autophagy. Sustained ER stress may cause the UPR to aggravate ER stress and cause cell death. The proteins then upregulate CHOP, redox enzymes and induce apoptosis. Abbreviations: **ER** – endoplasmic reticulum, **UPR** – unfolded protein response, **ATF6** - activating transcription factor 6 **IRE1**- inositol-requiring 1, **PERK** - protein kinase-like ER kinase, **XBP1** - X-box-binding protein 1, **ASK1** – apoptosis signalling-regulating kinase 1, **JNK** – Jun N-terminal Kinase, **eIF2α** - eukaryotic initiating factor 2 subunit α, ATF4 activating transcription factor 4, **ERAD** – ER associated degradation, **CHOP** - C/EBP homologous protein (Adapted from Tsai & Weissman, 2010).

2.4 Autophagy

Autophagy occurs in three forms in a cell: macroautophagy, chaperone-mediated autophagy and microautophagy. Macroautophagy (referred to as autophagy from this point on) is the degradation of long-lived proteins and organelles sequestered in autophagosomes. The autophagosomes fuse with lysosomes where the contents are digested and released within the cell for recycling. Chaperone-mediated autophagy entails the binding of specific proteins by heat shock protein 70 (Hsc70) and these proteins are transported directly to the lysosome for degradation. Microautophagy necessitates that lysosomes directly engulf defective proteins and organelles where they are immediately digested (Orrenius *et al.*, 2013; Benbrook & Long, 2012). While all forms of autophagy occur at basal levels, they are upregulated to suprabasal levels in response to various stimuli that include oxidative and ER stress, as well as nutrient deprivation (Benbrook & Long, 2012). While Tsai and Weissman (2010) report that the UPR activates autophagy through the IRE1-ASK-JNK axis, others indicate that UPR appears to mediate autophagy through the PERK-eIF2α axis (Suh *et al.*, 2012; Høyer-Hansen & Jäättelä, 2007).

While in the event of ER stress the UPR may induce autophagy, the autophagy pathway may also step in on its own, mediated by adapter proteins such as p62. Usually, the ubiquitin proteasome pathway (UPP), a major degradative pathway, determines whether a protein will be degraded *via* the UPP or autophagy (Benbrook & Long, 2012). The UPP involves the covalent attachment of ubiquitin (Ub) molecules to the protein substrate followed by degradation by the proteasome. The topology of the Ub chain mediates this process. The proteins may be tagged with multiple Ub molecules that form a chain. This chain of Ub molecules can be branched on any of the internal lysine (K) residues (Shang & Taylor, 2011). The proteins tagged with polyubiquitin chains branching at K48 have a more closed conformation and will be degraded *via* the UPP. While proteins with a single Ub molecule or branched on other Lysine residues are degraded *via* autophagy. Some proteins may be degraded by either pathway (Benbrook & Long, 2012). The degradation path to be followed is determined by adapter proteins, p62 and neighbour of BRCA1 (NBR), which shuttle proteins to autophagic vesicles or the adapter proteins, p97, which shuttle proteins to the proteasome. On the one hand p62, has a high affinity for monoubiquitinated and K63 tagged proteins, and these proteins are targeted for autophagic degradation. On the other hand, p62 can also recognize K48 polyubiquitin chains that are targeted for proteasomal degradation. This means that in the event of proteasome overload or dysfunction, p62 can target

proteins meant for proteasomal degradation to autophagic vesicles for degradation (Benbrook & Long, 2012; Popovic & Dikic, 2012).

Sustained ER stress can signal apoptotic cell death *via* the UPR. CHOP and JNK are reported to play essential roles in the induction of cell death in this context. CHOP downregulates the anti-apoptotic protein B-cell lymphoma 2 (Bcl-2), upregulates Bcl-2 homology domain 3 (BH3)-only proteins and the growth arrest and DNA damage-inducible protein 34 (GADD34). The latter functions to inhibit eIF2α and thus releases the suppression on protein translation. This will subsequently increase ER load and aggravate ER stress. JNK phosphorylates Bcl-2 and BH3-only proteins that promote apoptosis (Suh *et al.,* 2012). Furthermore, it has previously been reported that unrestrained autophagy may induce cell death independently of apoptosis resulting in a loss of viable cell mass, or disrupting the balance between pro-survival and pro-apoptotic proteins (Benbrook & Long, 2012).

Taken together, all of the above indicate that DOX toxicity on healthy tissue is a multifactorial process. Not only does DOX cause damage through organelle dysfunction and apoptosis potentially as a result of oxidative stress, much of the literature has focused on reducing oxidative stress to prevent oxidative damage with the use of various antioxidants. While the anti-oxidative agents employed successfully reduced oxidative damage in cellular and pre-clinical models, unfortunately these agents failed to provide the same effects clinically (Minotti *et al.*, 2004)**.** What this means is that we don't have a full understanding of the mechanisms involved that govern toxicity and its downstream effects. Thus, we should aim to investigate other treatment options that not only target oxidative stress, but other mechanisms that are induced as a result of oxidative stress.

3. Ghrelin

The hormone ghrelin has been characterized as a 28 amino acid peptide with an octanoic acid attached to the third serine residue. It was first discovered as a growth-hormone secretagogue (GHS), stimulating the pituitary to release growth hormone (GH) (Kojima *et al*. 1999). It was later found to also stimulate the release of adrenocorticotropic hormone (ACTH) and prolactin from the pituitary as well (Delhanty *et al.,* 2006). Since its discovery, research has shown that this hormone not only acts on the brain, but also the gut and other organs to regulate metabolism.

Today, ghrelin is well-known for its role in energy homeostasis and within the last decade, several *in vivo* studies have demonstrated that ghrelin has anti-oxidative, anti-inflammatory and anti-apoptotic properties (Çetin *et al.*, 2011; Koyuturk *et al.*, 2012; Dobutuvic *et al.*, 2013; Li *et al.*, 2012).

3.1 Synthesis and half-life

The synthesis of ghrelin entails the cleavage of a 117-amino acid pre-prohormone into either a 28 amino acid protein with a C-terminal arginine, or a 27 amino acid protein with a C-terminal proline. The cleaved pre-prohormone undergoes posttranslational modification where the enzyme ghrelin O-acyltransferase (GOAT), found in the ER, acetylates the third serine residue with n-octanoic acid or n-decanoic acid (Hosoda *et al*., 2003; Castañeda *et al.*, 2010). This acetylation is crucial for ghrelin to interact with its receptor and affects its passage across the blood brain barrier (Leite-Moreira & Soares, 2007). While ghrelin is also produced in rodents, it differs by a mere 2 amino acids from the ghrelin expressed in humans (Lysine 11 and Alanine 12 in humans, Arginine11 and Valine12 in rodents) (Hosoda *et al.*, 2003). The pharmacokinetics of total ghrelin elimination from plasma is suggested to be 27-31 mins and that of active ghrelin, a half-life of 9-13 mins (Akamizu *et al.*, 2004). Ghrelin can be removed from the circulation by enzymatic degradation or by binding to lipoproteins that will prevent interaction with its receptor (Castañeda *et al.*, 2010).

3.2 Distribution

Ghrelin is mostly produced by the X/A-like cells present in the digestive tract (Date *et al.*, 2000; Sehirli *et al.*, 2008). The X/A-like cells of the oxyntic mucosa in the gastric fundus produce two-thirds of plasma ghrelin and the rest by those found in the small intestine. Other organs that produce relatively less ghrelin include the kidneys, pancreas, lymphatic tissue, placenta, thyroid and adrenal gland, gonads, heart, eyes, lungs, pituitary and the hypothalamus. It is highly improbable however that the ghrelin produced by these other organs is released into circulation, but rather is used for autocrine or paracrine function (Leite-Moreira & Soares, 2007). Interestingly, while ghrelin may have physiological importance, the biological function of ghrelin in many different tissues is still unclear (Castañeda *et al.*, 2010).

3.3 Stimulators and inhibitors of ghrelin secretion

Hormones that supress ghrelin secretion include insulin, GH, somatostatin and cortistatin. GH's repressing action on ghrelin secretion indicates a negative feedback loop between the hypothalamus and the stomach, as ghrelin stimulates the release of GH. Secretion of ghrelin is stimulated by acetylcholine, oestrogen, testosterone, IGF-1 and combined administration of growth-hormone-releasing-hormone (GHRH) and arginine (Leite-Moreira & Soares, 2007). Since ghrelin is known for its orexigenic properties, it is thus influenced by nutritional status; where during fasting glucose and lipid levels are low, or during conditions such as anorexia nervosa and cachexia, ghrelin levels are upregulated. In contrast, during feeding or obese states, circulating plasma levels of ghrelin are downregulated or dysregulated (Barazzoni *et al.*, 2005; Smith *et al.*, 2005).

3.4 Receptor distribution, interaction and transduction pathways

Ghrelin acts through its G-protein coupled receptor, growth hormone secretagogue receptor (GHS-R), which has two isoforms; GHS-R1α and GHS-R1β (Kojima *et al.*, 1999; Smith *et al.*, 2005). Ghrelin acts through the GHS-R1α largely found in the arcuate nucleus, an area in the hypothalamus essential for the neuroendocrine and orexigenic properties of ghrelin, as well as in the somatotroph pituitary cells (Muccioli *et al.*, 2002). Although, the GHS-R1α has not been found on hepatocytes, ghrelin has been found to stimulate glucose output in hepatocytes, thus suggesting an uncharacterized receptor for ghrelin on liver tissue exist (Gauna *et al.*, 2005). The binding of ghrelin to its receptor induces the activation of different signalling transduction pathways on different tissues through the increase in intracellular Ca^{2+}. For example, in pituitary cells, ghrelin activates the phospholipase C (PLC)/diacylglycerol (DAG)/Inositol trisphosphate (IP_3) signalling pathway, while in neuropeptide Y (NPY) expressing cells of the arcuate nucleus, ghrelin stimulates adenylate-cyclase/cyclic adenosine monophosphate (cAMP)/protein kinase A (PKA) pathway (Muccioli *et al.*, 2002: Castañeda *et al.*, 2010). In vascular epithelium ghrelin acts to inhibit inflammation by activating the calmodulin-dependent kinase kinase (CAMKK), AMP-activated protein kinase (AMPK) and endothelial nitric oxidase synthase (eNOS). AMPK activation in the hypothalamus regulates food intake in response to fasting (Castañeda *et al.*, 2010). Due to the variation in signalling pathways activated in different tissue types, it is clear that the activation of the GHS-R1α signal transduction pathway is tissue and function specific (Leite-Moreira & Soares, 2007).

3.5 Ghrelin's role in metabolism

Ghrelin has always been thought to play a fundamental role in metabolism by stimulating food intake with a subsequent increase in the adiposity index (Wortley *et al.,* 2004). Literature also indicates that ghrelin does not regulate energy homeostasis directly but rather other mechanisms compensate for ghrelin's appetite stimulating properties. Ghrelin's orexigenic properties are compensated for by the NPY and agouti-related protein (AgRP) neurons which co-localize with GHS-R1α in the arcuate nucleus found in the nutrient centre of the brain. By ghrelin binding to this receptor in this region, it triggers spontaneous activity of NPY and AgRP neurons (Albarrab-Zeckler *et al.,* 2011; Müller *et al.,* 2015). Therefore, the activity of ghrelin in the brain could modulate both appetite and body weight. Although ghrelin appears to indirectly stimulate appetite, other studies have demonstrated that ghrelin acts directly on peripheral tissues and to regulate metabolism and/or digestion (Gauna *et al.,* 2005). In this scenario, ghrelin promotes gastric motility, as well as gastric acid secretion and is also involved in carbohydrate and lipid metabolism (Van der Lely *et al.,* 2004). Ghrelin's role in carbohydrate metabolism is to increase plasma glucose levels by stimulating glycogenolysis and gluconeogenesis in hepatocytes (Leite-Moreira & Soares, 2007). Barazonni and colleagues (2005) reported that prolonged ghrelin treatment induces hyperglycemia by upregulating the activity of the glycolytic enzyme glucose-6-phosphatase in hepatocytes. In return, glucose decreases ghrelin secretion. Vestergaard and colleagues (2008) demonstrated that ghrelin promoted peripheral insulin resistance through the inhibition of pancreatic β-cell function, while promoting hepatic glucose secretion in healthy young men. This study further reported that glucagon had no impact on ghrelin stimulating hepatic glucose production.

In the context of lipid metabolism, exogenously administered ghrelin in rodents has been demonstrated to reduce 5' AMP-activated protein kinase (AMPK) levels, a potent inducer of fatty acid oxidation, and promote the expression of genes that favour lipogenesis and triglyceride storage in the liver. However in skeletal muscle, ghrelin reduces triglyceride content and upregulates the activity of mitochondrial oxidative enzymes independent of changes in AMPK levels (Barazonni *et al.,* 2004). Furthermore, ghrelin activates peroxisome proliferator-activated receptor γ (PPARγ) which reduces fat content in skeletal muscle. Based on these findings, ghrelin favours the deposition of triglycerides in the liver rather than in skeletal muscle and acts on adipocytes to favour lipogenesis over lipolysis

3.6 Anti-oxidative, anti-inflammatory and anti-apoptotic properties

Cellular systems are protected from harmful agents by having an endogenous anti-oxidant defence system consisting of anti-oxidants and enzymes. The anti-oxidants include reduced glutathione (GSH), vitamins A, C and E and the enzymes include reduced peroxidase (GPx) and glutathione reductase (GR), SOD and CAT (Jafari *et al.*, 2007) The liver is responsible for the detoxification of drugs and toxins, therefore the liver should have a good anti-oxidant defence system. *De novo* synthesis of the anti-oxidant reduced GSH occurs in the liver, and is distributed to the rest of the body which contributes almost 90% of reduced GSH under normal physiological conditions. Although reduced GSH is distributed to other tissues, the liver still contains the highest reduced GSH concentration in the body (Limón-Pacheco & Gonsebatt, 2008). However, in disease states the anti-oxidant defence system may not be sufficient to prevent damage and additional help is required. Therefore, studies has investigated the effects of ghrelin in hepatic pathophysiology.

The administration of ghrelin into the cerebro-ventricules of male Wistar rats was shown to upregulate protein expression of different intracellular antioxidant enzymes in the liver (Dobutovic *et al.*, 2014). This indicates that ghrelin can promote protection against oxidative stress in hepatocytes**.** These findings have led ghrelin to be utilized as an adjuvant therapeutic agent in various pathological conditions. Li and colleagues (2013) reported that ghrelin administration during the induction of non-alcoholic fatty liver disease (NAFLD) reduced oxidative stress, restored the expression of GPx and reduced the pro-inflammatory cytokines, TNF-α and IL-6, at both the transcriptional and translation level. The decline in oxidative stress and pro-inflammatory cytokines was associated with a reduction in cleaved caspase 3 expression. Interestingly, a recent study conducted by Koyuturk and colleagues (2015) found that ghrelin does not reduce the rate of apoptosis in hepatocytes of diabetic neonatal rats. The controversial reports on the anti-apoptotic property of ghrelin could be due to variation in pathophysiological conditions and experimental models used.

Moreover, ghrelin administration prior to inducing carbon tetrachloride toxicity in the rat liver, has shown increased activity of the anti-oxidant enzyme, SOD, CAT and GPx with a subsequent reduction in lipid peroxidation and inducible nitric oxide synthase (iNOS) (Cetin *et al.*, 2011). Other studies have also utilized ghrelin as a therapeutic agent in hepatic pathology. Chronic cholestatic disease is characterised by damage to biliary epithelium that results in the defective

transport of bile from the liver to the intestine. This results in damage to hepatocytes that induces an inflammatory response and activation of Kupffer cells leading to hepatic fibrosis. Iseri and colleagues (2008) found that long term ghrelin treatment in chronic cholestatic hepatic injury decreased serum pro-inflammatory cytokines and serum lactate dehydrogenase (LDH) activity, while improving liver function. Furthermore, hepatic lipid peroxidation and collagen deposition were decreased. The above *in vivo* studies on various hepatic pathologies exhibit ghrelin's anti-oxidative, anti-inflammatory, anti-apoptotic and in addition, anti-fibrotic properties.

4. Summary

DOX is the most effective antitumor drug used against a wide range of cancers. However, its clinical use is limited due to the development of chronic cardiomyopathy and congestive heart failure (CHF) years after treatment, as a result of the toxicity on healthy tissues (Minotti *et al.*, 2004). Research has invested its resources into DOX-induced cardiotoxicity and has neglected to investigate potential damaging effects on other peripheral organs. The liver is responsible for metabolizing DOX, which has been found to accumulate in this organ. Tacar and colleagues (2013) reported that 40% of patients receiving DOX suffer from liver injury caused by oxidative stress. However, based on the above mentioned literature, DOX toxicity is multifactorial and therefore therapeutic interventions should also be multifactorial. Ghrelin is a hormone naturally found in the body which has been found to possess beneficial properties that could protect the liver against DOX toxicity. Up until now, the therapeutic role of ghrelin in a chronic model of DOX toxicity has not been evaluated. Therefore, this study hypothesises that long term DOX treatment induces toxicity in hepatic tissue that will negatively affect liver function while the use of ghrelin, will prevent the damaging effects induced by DOX.

The aim of this study was to investigate:

(i) The effect of DOX on liver function and if damaging effects are found, whether the use of ghrelin will improve liver function in the presence of DOX.

(ii) DOX induced oxidative stress on liver tissue and the use of ghrelin as an intervention.

(iii) Upregulation of autophagy, apoptosis and ER stress following DOX treatment alone and whether co-treatment with ghrelin will decrease these markers.

Chapter 2

Materials and Methods

2.1 Experimental procedure

In an effort to investigate the effects of DOX on the liver, a model simulating chronic DOX-induced cardiotoxicity was utilised. This disease is mainly observed in survivors of childhood cancer years to decades following DOX therapy. A repeated measures experimental design were utilised for this study. Four week old male Sprague-Dawley rats (90 – 130 g) were acclimatised for one week, where after they were randomly allocated into four experimental groups, namely: vehicle (n=7), DOX (n=9), ghrelin (n=7) and DOX+Ghrelin (n=9). While the vehicle group received physiological saline, the DOX group (LKT Laboratories, D5794, USA) received 2.5 mg/kg once weekly, the ghrelin group (LKT Laboratories, G2869, USA) received 100 µg/kg three times a week and the DOX+Ghrelin group received both treatment regimens. All injections were conducted intraperitoneally (i.p) for a duration of eight weeks. Animals were housed in sterile rat cages at an ambient temperature of 25 °C with a 12hr light-dark cycle, while receiving standard rat chow and tap water *ad libitum*. All experiments were ethically approved and executed according to the guidelines for the care and use of laboratory animals implemented at Stellenbosch University (reference number: SU-ACUD15-00038) and conformed to the accepted standards for the use of animals in research and teaching as reflected in the South African National Standards 10386: 2008. Body weight measurements, food consumption and general well-being of the animals was monitored regularly.

2.2 Sample collection

One week after the last injection, the animals were euthanized with a lethal dose of sodium pentobarbitone (60 mg/kg) (Euthapent Kyron Laboratories, 130540, SA). Animals were checked for a pedal reflex before the abdominal cavity was cut open to harvest the liver. During this time, blood was collected from the thoracic cavity using a 10 mL syringe and immediately placed into plasma (Lasec, VGRV450474R, SA) and serum (Lasec, VGRV450470R, SA) separation tubes. Followed by centrifugation at 4000 rpm (1.4 x *g*) for ten minutes (4 °C), where after the plasma and serum was aliquoted at 200 µL volumes into centrifuge tubes and frozen at – 80 °C until required. The liver was weighed and examined grossly with the lobular segmentation counted

before it was divided into two parts. One half was snap frozen in liquid nitrogen for biochemical analysis, while the other was preserved in 4% formaldehyde (Merck Millipore, 1.00496.5000, SA) solution for histological staining.

2.3 Liver function tests

To determine the effects of this study's treatment regimen on liver function, ALT (Abcam, ab105134, SA) and albumin (Abcam, ab108790, SA) concentration in the serum and plasma respectively, was evaluated using commercially available kits. Briefly, a standard curve was setup and a dilution series of the samples was performed to determine the appropriate concentrations of these proteins that fall within the range. After the reagents were prepared according to the manufacturer's instructions, the samples were transferred into 96-well plates with their reaction reagents and the activity of ALT and albumin content was measured. ALT absorbance (BMG Labtech, SPECTROstar nano, Germany) was measured at a wavelength of 570 nm at 37 ˚C every 2 minutes (mins) for a total of 60 mins, whereas albumin content was determined at room temperature at a wavelength of 450 nm (Bio-tek instruments Inc., EL800, USA). The absorbance measurements were then converted into mU/ml for ALT and µg/ml for albumin (see Appendix D, pg. 84 for full protocol).

2.4 Histological Analysis

2.4.1 Tissue processing and sectioning

Liver tissue fixed in 4% formaldehyde underwent a series of dehydration steps followed by infiltration of Paraplast® wax (Sigma-Aldrich, A6330-4LB, SA) using a tissue processor (Sakura Finetechnical Co. Ltd, Tissue Tek II 4634, Japan). Once embedded onto a cassette (Lasec, PLPS191023, SA), tissue was sectioned into 5 µm thick sections with a microtome (Leica Biosystems, Leica RM 2125 RT, Germany) and placed onto glass microscope slides (Lasec, GLAS4S22M3000F, SA) (see Appendix E, pg. 90 for full protocol). The slides were then allowed to air-dry and adhere on a 20 °C heating block.

2.4.2 Haematoxylin and Eosin stain

The Haematoxylin and Eosin (H&E) stain was used to observe general histological structure of liver tissue. While acidic components such as the nucleus are stained blue by the haematoxylin dye, basic components such as the cytoplasm are stained pink by the eosin dye. This stain was

performed using an automated staining machine (Leica Biosystems, Leica ST5010 Autostainer XL, Germany), where micro- or macro-vesicular ballooning (hydropic changes) would be observed. The staining protocol followed is available in the Appendix section (see Appendix E, pg. 92 for full protocol). After staining, the slides were mounted using DPX mountant (Associated Chemical Enterprises, D0738NN00500, SA) and covered with a cover slip (Lasec, GLAS2C29M2250REC, SA). The slides were left to dry overnight. The stained slides were viewed using a bright-field Nikon ECLIPSE E400 microscope, mounted with a Nikon DS-Fi2 camera, and processed through a Nikon Digital Sight DS-U3 processor (Nikon, Japan). Image processing was performed using NIS elements software v4.10.

2.4.3 Masson's Trichrome stain

The Masson's trichrome technique stains connective tissue to indicate fibrosis. The tissue sections were prepared as previously described and were deparaffinized and rinsed in distilled water. The slides containing tissue sections were placed in a haematoxylin solution for 5 mins followed by tap water until a dark blue colour formed. The sections were then placed in a working solution of fuchsin ponceau-orange G for 15 mins and rinsed in 0.2% acetic acid water (Radchem, 600113). The slides were flushed in 5% phosphotungstic acid (Merck Millipore, 100582) for 5 mins and again rinsed in 0.2% acetic acid water to differentiate the colour tones. The sections were then stained in light green solution (Sigma-Aldrich, L1886, SA) for 20 min and treated with acetic acid for 5 min. This step was followed by dehydration through a series of alcohol solutions and xylene (Merck Millipore, 1086619190, SA) (see Appendix E, pg. 99 for full protocol). Finally, the slides were mounted using DPX mounting medium and covered with a cover slip. The stained slides were viewed using the same microscope as previously described.

2.4.4 Reticulin stain

The reticulin stain detects the reticulin fibres that form the supportive reticulin network in hepatic tissues. The tissue sections were prepared as previously described and slides were initially oxidized in 0.5% acidified potassium permanganate (Merck Millipore, 109930, SA), decolourised with 2% oxalic acid (Radchem, 6153-56-6, SA), fixed in 4% iron alum (Merck Millipore, 103776, SA) and impregnated in ammoniacal silver solution. This was followed by reducing sections with 10% formalin, where after the slides were rinsed using tap water and distilled water

and fixed with 2% aqueous sodium triphosphate (Sigma-Aldrich, T5041, SA). Tissue slides were counterstained with light green solution (Sigma-Aldrich, L1886, SA) and after dehydration, slides were mounted using DPX mounting medium and covered with a cover slip. The stained slides were viewed using the same microscope as previously described (see Appendix E, pg. 95 for full protocol).

2.4.5 Periodic acid Schiff (PAS) stain

The PAS stain was used to detect glycogen content in liver tissue. The tissue sections were prepared as previously described and slides were oxidized in 1% periodic acid solution (Sigma-Aldrich, 210064, SA) rinsed in distilled water and placed in Schiff reagent (Merck Millipore, 109034, SA) where the sections turned a light pink colour. After washing in lukewarm water, the sections developed into a dark pink colour. This was followed by counterstaining with Mayer's haematoxylin (Merck Millipore, SAAR2822001LC, SA) and washing in tap water. The sections are then dehydrated and mounted accordingly. The stained slides were viewed using the same microscope as previously described (see Appendix E, pg. 97 for full protocol).

2.4.6 Oil Red O stain

The oil red O stain was used to observe lipid accumulation in hepatic tissue. For this stain, frozen liver tissue was placed in liquid nitrogen and sectioned into 7 µm thick sections with a cryostat (Leica CM 3050 S Research Cryostat, Leica Biosystems, Germany) and placed onto positively charged Histobond microscope slides (Lasec, GLAS2S13M0810401). The sections were left to defrost followed by placing in the oil red O staining solution (Sigma-Aldrich, O1391, SA) The excess solution was briefly washed in cold tap water and counterstained with 50% crystal violet (Sigma-Aldrich, V5265) followed by another wash step using tap water. The sections were left to air dry, where after aqueous mounting media (Sigma-Aldrich, G 0918) was placed onto the sections with a coverslip. The stained slides were viewed using the same microscope as previously described (see Appendix F, pg. 104 for full protocol).

2.4.7 Immunohistochemistry (IHC)

The immunohistochemistry staining was used to stain for ALT in formaldehyde fixed liver tissue. The slides were sectioned as mentioned above and placed on positively charged glass microscope

slides. The IHC staining protocol was performed with an automated machine (Leica Biosystems, Bond-Max™ Autostainer, Germany) and the Bond™ Polymer Refine detection kit (Leica Biosystems, DS9800, Germany). An ALT primary antibody (Santa Cruz Biotechnology, sc-271861, SA) was used to detect ALT present in the tissue using a horseradish peroxidase (HRP)-linked antibody conjugate system (see Appendix E, pg. 100 for full protocol). ALT stained as a brown precipitate and was quantified with the IHC Profiler plugin in Image J version 1.50i. The software pixel intensity ranges from 0 to 255, with 0 representing the darkest shade and 255 the lightest shade of brown. With the assistance of a pathologist, the different shades were assigned a score where the darkest shade received a high score and the lighter shade a lower score. The scores were divided as high positive (3+), positive (2+), low positive (1+) or negative (0). The software determines the percentage (%) of pixels that falls within a category and if 60% or more falls within one category, that score is assigned to the image. If not, then the software uses an equation to assign a score to an image. The stained slides were viewed using the same microscope as previously described.

2.5 Oxidative stress analysis

As DOX is a known inducer of oxidative stress, oxidative damage was evaluated by measuring conjugated dienes (CDs), malondialdehyde (MDA) and glutathione. For these assays, 100 mg liver tissue was used and added to phosphate buffer (7.5 mM, pH: 7.4) in a 1:10 ratio. For the glutathione assay specifically, two separate assays were performed measuring reduced (GSH) and oxidized (GSSG) glutathione. For the GSSG assay, a similar process was followed but a solution of Methyl-2-vinylpyridinium triflate (M_2VP) was added to the phosphate buffer and this solution was then added to the tissue. The tissue was subsequently homogenised (Kinematica AG, Polytron PT 2100, Switzerland) and then sonicated at an amplitude of 10 Hz for 10 seconds (secs) (Qsonica, Misonix Sonicator S-400, USA). The foam layer was allowed to settle after which the lysate was centrifuged (Labnet, Spectrafuge 16M, USA) at 4 ˚C at 12 000 rpm (9660 *g*) for 10 mins. The supernatant was removed and used for further analysis (see Appendix G, pg. 105 for full protocol).

2.5.1 Conjugated Dienes

The prepared tissue lysates were added to a solution of methanol and chloroform and centrifuged

(Labnet, Spectrafuge 24D, USA) at room temperature at 14 000 rpm (13148 *g*). After the formation of a top protein layer and a bottom liquid layer, the liquid layer was removed and placed into centrifuge tubes and left overnight at 4 ˚C over a flow of nitrogen, where the chloroform and methanol solution evaporated and the fatty components left behind. Cyclohexane was added to each centrifuge tube, vortexed and the mixture was transferred into clear 96-well UV plates (Thermoscientific Inc, Microplate Uv Flat Bttm CS40, Netherlands). The conjugated diene (CD) content was measured with a spectrophotometer (Thermo Electron Corporation, Multiskan spectrum, Finland) at a wavelength of 230 nm. The absorbance measurements were converted into µmol CD/g of tissue (see Appendix G, pg. 106 for full protocol).

2.5.2 TBARS assay

The prepared tissue lysates were added to various reagents namely: 4 mM 3,5-Di-tert-4-butylhydroxytoluene (BHT) (Sigma-Aldrich, 442377, SA), 0.2 M ortho-phosphoric acid (OPA) (Merck Millipore, 1.00573.2500, SA) and 0.11 M Thiobarturic acid (TBA) (T5500, Sigma-Aldrich, SA). To catalyse the reaction, the mixture was vortexed and heated at 90 ˚C and the samples in centrifuge tubes were then placed into an ice bath to stop the reaction. Butanol (Sigma-Aldrich, B7906, SA) was added followed by centrifugation (Labnet, Spectrafuge 24D, USA) at room temperature at 14 000 rpm (13148 *g*). MDA content of each sample was measured with a spectrophotometer (Thermo Electron Corporation, Multiskan spectrum, Finland) at a wavelength of 532 nm in clear 96-well plates. The absorbance measurements were converted into µmol MDA/g of tissue (see Appendix G, pg. 107 for full protocol).

2.5.3 Glutathione assay

As explained above, the liver tissue for GSH and GSSG measurement were prepared into lysates with two different buffers. The protocol used to measure GSH and GSSG remained the same. For each analysis, a standard curve was prepared and the lysates were transferred into clear 96-well plates. The following reagents were added to the lysates: 5,5'-dithiobis-(2-nitrobenzoic acid) (DTNB) (Sigma-Aldrich, D21820, SA), glutathione reductase (Sigma Aldrich, G3664, SA) and reduced nicotinamide adenine dinucleotide phosphate (NADPH) (Sigma-Aldrich, N6785, SA). The plate was read with a spectrophotometer (Thermo Electron Corporation, Multiskan spectrum,

Finalnd) at 412 nm every 30 secs for 5 mins. Total GSH and GSSG were then calculated from the linear slope of the standard curve (see Appendix G, pg. 108 for full protocol).

2.6 Western Blotting

2.6.1 Preparation of tissue lysates

Snap frozen liver tissue was thawed and protein was extracted by adding modified radio-immunoprecipitation (RIPA) buffer (pH 7.4) followed by homogenization into a lysate (Kinematica, POLYTRON® PT 2100 Homogenizer Switzerland). The lysates were centrifuged (Labnet, Spectrafuge 16M, USA) at 14 000 rpm (13148 *g*) for 60 mins at 4° C to isolate the fat layer formed at the top, the protein layer in the middle and the pellet at the bottom of the centrifuge tubes. The fat layer was separated from the protein layer and the pellet discarded. To ensure that the protein layer was not contaminated, the lysate retrieved was centrifuged again for 40 mins where after protein concentration was determined (see Appendix H, pg. 110 for full protocol).

2.6.2 Protein determination

The Direct Detect ™ Spectrometer (Merck Millipore, DDHW00010-WW, Germany) was used to determine the protein concentration within each lysate. This system measures the absorbance of amide bonds in protein chains using infrared quantitation thereby determines intrinsic components of every protein without relying on amino acid composition, dye binding properties and redox potential. 2 µl blank (RIPA buffer) and 2 µl of samples were pipetted onto the windows of the Direct Detect™ card. The card was then placed vertically inside the sampling accessory, which dries and then measures each sample as mg/mL of protein. 30 µg protein samples were prepared in Laemmli's loading buffer, boiled at 95 ˚C for 5 mins and stored at -80 °C until needed. In addition, the fat layer that was reserved was used to determine lipid content in each sample (see Appendix H, pg. 110 for full protocol).

2.6.3 Sodium dodecyl sulphate polyacrylamide gel electrophoresis (SDS-PAGE)

Samples previously prepared in Laemmli's buffer were thawed on ice and boiled again at 95 ˚C for five min. 30 µg protein of each sample was separated by 12% TGX stain-free™ FastCast™ acrylamide gels (Bio-Rad, 1610183, SA) for 10 mins at 100 V and 400 mA (constant), followed by 120 V for 60 mins. The stain-free gel was activated by placing the gel directly onto the Bio-

Rad UV transilluminator plate (Bio-Rad, ChemiDoc™ XRS+ system, USA) and by selecting the 'gel activation' step in the Image Lab™ software (Version 5.2.1). After activation, the proteins were transferred onto polyvinylidene fluoride (PVDF) membranes (Bio-Rad, Trans-Blot® Turbo™ ready-to-assemble mini low fluorescent PVDF transfer kit, 1707274, USA) using the TransBlot® Turbo™ Transfer System (Bio-Rad, USA) for 30 min at 25 V. After transfer, the stain-free blot was imaged for use in total protein normalization. Membranes were then blocked for 60 min at room temperature 5% fat free milk dissolved in 1x tris buffered saline-Tween®20 Solution (1x TBS-T). After blocking, the membranes were washed 3 times for 5 min in 1x TBS-T and incubated overnight at 4 ˚C with gentle agitation in primary antibody (1:1000) dissolved in 1X TBS-T (Table 2). Following primary antibody incubation, the wash step was repeated and the membranes were incubated in HRP-linked anti-rabbit or anti-mouse secondary antibody dissolved in 1x TBS-T for 60 mins at room temperature. Membranes were washed with 1x TBS-T (3 x 5 min) and incubated with Clarity™ ECL western blotting substrate (Bio-Rad, 1705061, USA). The bands were detected using the ChemiDoc™ XRS+ System with the Image Lab™ software and discrepancies in loading were corrected for by using total protein normalization.

Table 2.1. List of primary and secondary antibodies used for Western blotting

Primary Antibodies			
Name	**Size (kDa)**	**Company (catalogue number)**	**Dilution**
Cleaved Caspase-3	17, 19	Cell Signalling Technology (9662)	1:1 000
Cleaved PARP	89	Cell Signalling Technology (5625)	1:1 000
BiP	68	Cell Signalling Technology (3177)	1:1 000
ATF4	48	Cell Signalling Technology (11815)	1:1 000
LC3	16, 18	Cell Signalling Technology (3868)	1:1 000
p62	62	Cell Signalling Technology (5114)	1:1 000
ALT	48	Santa Cruz Biotechnology (Sc-271861)	1:1 000
	Secondary Antibodies		
Anti-Rabbit IgG HRP-linked	-	Cell Signalling Technology (7074)	1:10 000
Anti-mouse IgG HRP-linked	-	Cell Signalling Technology (58802)	1:10 000

Abbreviations: **PARP**: Poly (ADP-ribose) polymerase, **BiP**: immunoglobulin heavy chain-binding protein, **ATF4**: Activating Transcription Factor 4, **LC3**: microtubule associated protein 1 light chain 3, **ALT**: alanine transaminase.

2.7 Statistical analysis

GraphPad Prism 5.0 (GraphPad Inc.) software was used for statistical analysis and visual representation of data. Statistical analysis was determined with one-way analysis of variance (ANOVA) followed by the Bonferonni posthoc test. All data are presented as mean ± standard error (SEM) and a *p* value less than (<) 0.05 was considered statistical significant.

Chapter 3

Results

3.1 Body weight

Chemotherapeutic agents are known to result in weight loss in cancer patients, and considering that ghrelin promotes appetite, this study monitored body weight throughout the treatment duration. It was already evident by the fourth week that the DOX treated animals (228.30 g ± 7.09 g, $p < 0.01$) were not gaining as much weight as the vehicle (control) treated animals (285.50 g ± 19.24 g). While comparing the DOX treated animals (247.30 g ± 6.51 g, $p < 0.01$) to the ghrelin treated animals, there was a significant difference (297.20 g ± 11.80 g) from the fifth week (Fig. 3.1). This lack of weight gain within the DOX group was maintained until the end of the treatment protocol. While the experimental animals that received both treatment regimens (DOX+Ghrelin) were affected by DOX, they fared better when compared to the DOX group, albeit insignificantly so.

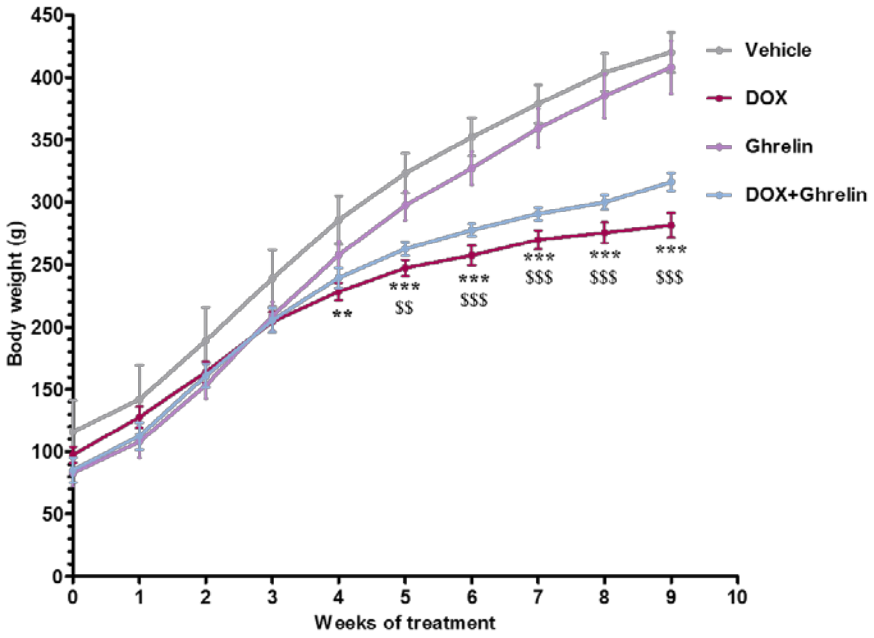

Fig. 3.1: Average body weight recorded per week. Body weight measurements recorded weekly per group following an eight week treatment regimen. Animals were treated (i.p) with saline (vehicle), DOX, ghrelin and a combination of the two drugs. Results are presented as mean ± SEM (n = 7-9). ****** $p < 0.01$ vs. vehicle, ******* $p < 0.001$ vs. vehicle, $^{\$\$}$ $p < 0.01$ vs. ghrelin and $^{\$\$\$}$ $p < 0.001$ vs. ghrelin. Abbreviations: **DOX** – doxorubicin **g** – grams **vs** – versus.

3.2 Liver weight

In contrast to how body weight was monitored, liver weight could only be measured at the end of the study. At face value, the weight of the livers in the DOX treated group appeared to be smaller (10.60 g ± 0.47 g, $p < 0.001$) versus the vehicle group (14.69 g ± 0.77 g) (Table 3.1), and no significant changes were observed in any of the other treatment groups. However, in order to get a better understanding of these results, the liver to body weight ratio was also calculated. When this was done, no considerable changes were observed and thus indicating that the weights of the livers were in proportion to the body weight of the animals in the different experimental groups.

Table 3.1. Average body and liver weight and the ratio of liver to body weight at the end of the experimental procedure.

Treatment group	Body weight (g)	Liver weight (g)	Liver weight: Body weight ratio
Vehicle	420.10 ± 16.19	14.69 ± 0.77	0.035 ± 0.001
DOX	281.40 ± 9.78	10.60 ± 0.47***	0.037 ± 0.001
Ghrelin	408.20 ± 21.30	14.53 ± 0.94	0.036 ± 0.001
DOX+Ghrelin	316.30 ± 7.09	12.16 ± 0.36	0.039 ± 0.001

Results are presented as mean ± SEM (n = 7-9). *** $p < 0.001$ vs. vehicle. Abbreviations: **DOX** – doxorubicin **g** – grams **vs.** – versus.

3.3 Food consumption

In addition to monitoring body weight, the average food consumed per group was recorded weekly for the duration of the study. As indicated in Fig. 3.2, DOX treated animals consumed less food as early as the third week of treatment (144.80 g ± 3.97 g, $p < 0.001$) when compared to the vehicle group (176.00 g ± 1.37 g). This loss in appetite was maintained throughout the treatment protocol suggesting that DOX has appetite repressive effects. Even though the food consumed in the combination group (DOX+Ghrelin) did not significantly differ from the earlier time points, significance was obtained on the sixth (159.20 g ± 9.43 g, $p < 0.05$) and seventh (158.30 g ± 5.31 g, $p < 0.05$) week of treatment when compared to the DOX group (128.50 g ± 7.27 g and 136.60 g ± 5.83 g) respectively.

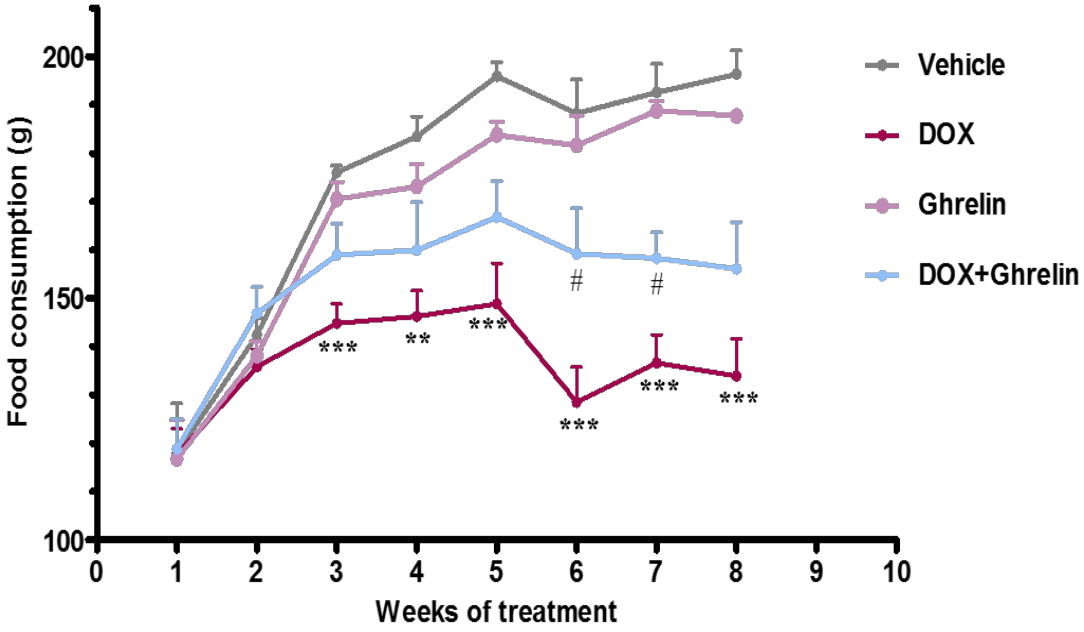

Fig. 3.2: Average food consumption (g) recorded per week. Food consumption measurements recorded weekly per group following an eight week treatment regimen. Animals were treated (i.p) with saline (vehicle), DOX, ghrelin and a combination of the two drugs. Results are presented as mean ± SEM (n = 7-9). ****** $p < 0.01$, ******* $p < 0.001$ vs. vehicle and $^{\#}$ $p < 0.05$ vs. DOX. Abbreviations: **DOX** – doxorubicin **g** – grams **vs** – versus.

3.4 Gross anatomy of the liver

Once the animals were sacrificed, and the livers harvested from the various treatment groups, an interesting but novel phenomenon was observed. All the animals treated with DOX presented with significantly less lobes than all the other groups (Fig. 3.3). While the vehicle and ghrelin groups presented with seven lobes, the DOX treated group presented with only four lobes. The combination group prevented this fusion and this group presented with six lobes. Although the significance of this observation is currently unknown, all animals survived the treatment duration and thus the fusion of the lobes in the DOX group did not influence the survival.

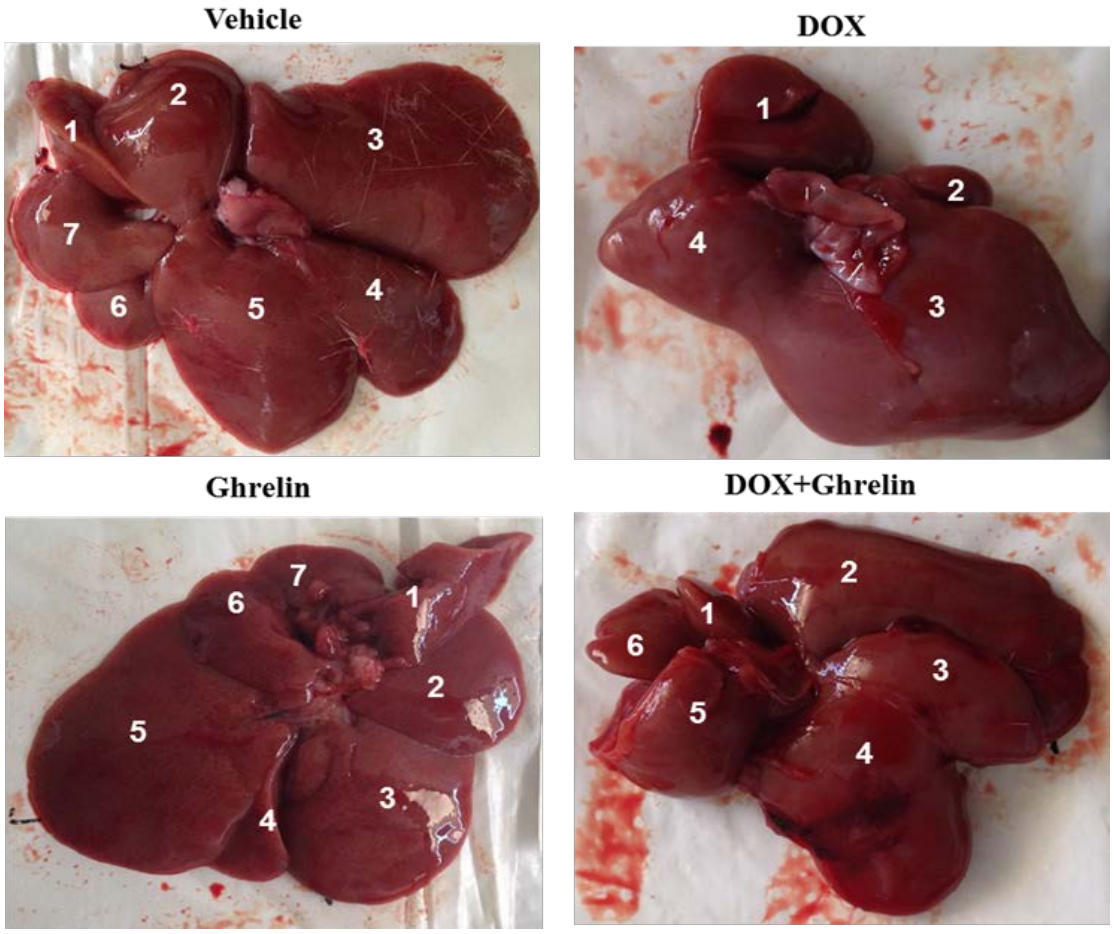

Fig 3.3: Representative image of the gross anatomy of the liver. The amount of liver lobes observed when the animals were sacrificed and the livers harvested. Animals were treated (i.p) with saline (vehicle), DOX, ghrelin and a combination of the two drugs. The liver lobes are numbered 1-7. Image Resolution: 364x2448. (n = 7-9). Abbreviations: **DOX** – doxorubicin.

3.5 Liver function assessment

3.5.1 Alanine transaminase

The alanine transaminase (ALT) assay measures the concentration of ALT in the blood. This enzyme is normally found inside liver cells (hepatocytes), and when the liver is damaged or inflamed, ALT is released into the bloodstream in significant amounts. As the liver is also responsible for DOX metabolism, this study aimed to determine the influence of both DOX and ghrelin on liver function by utilizing different assays. Firstly, an ALT assay was used to test for the presence of ALT in the serum (Fig. 3.4**A**), however no considerable changes were observed between the experimental groups. Secondly, western blotting was employed to determine the protein expression of ALT from tissue samples (Fig. 3.4**B**). Although all treatment groups except

for the vehicle expressed more ALT, these were not statistically different from one another. Finally, to supplement the western blot data, staining for ALT by IHC was used (Fig. 3.4**C**). In this case, a grading system was employed either indicating a low positive or a positive result depending on the intensity of the brown precipitate which is indicative of ALT presence. All groups except for the DOX treated group were marked as low positives while the DOX group was marked as positive. This means that the DOX group had the most ALT present in these tissue samples, but since this did not leak into the blood, these results indicate that DOX did not induce extensive liver damage.

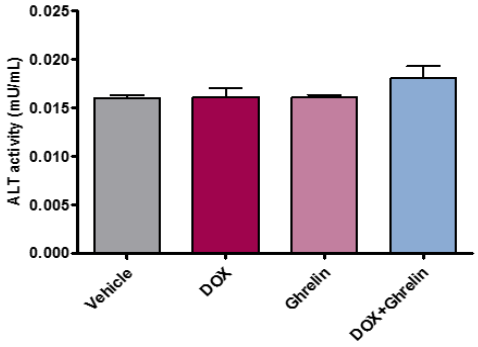

Fig. 3.4A: Serum ALT concentration. ALT concentration (mU/ml) was measured in serum following treatment to determine liver damage. Animals were treated (i.p) with saline (vehicle), DOX, ghrelin and a combination of the two. Results are presented as mean ± SEM (n = 7-9). Abbreviations: **DOX** – doxorubicin.

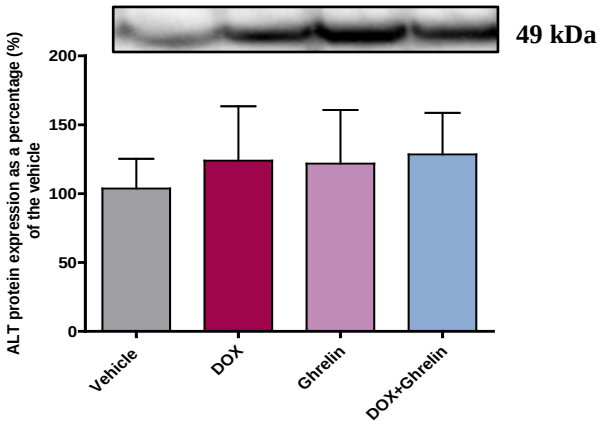

Fig. 3.4B: ALT protein expression detected by western blotting. Quantitative analysis of ALT expressed in liver tissue. The lane analysis and western blot are shown. Protein expression of ALT was normalized to total lane protein and the results were expressed as a percentage (%) of the vehicle. Animals were treated (i.p) with saline (vehicle), DOX, ghrelin and a combination of the two. Results are presented as mean ± SEM (n = 5-6). Abbreviations: **DOX** – doxorubicin **kDa** - kilo Daltons

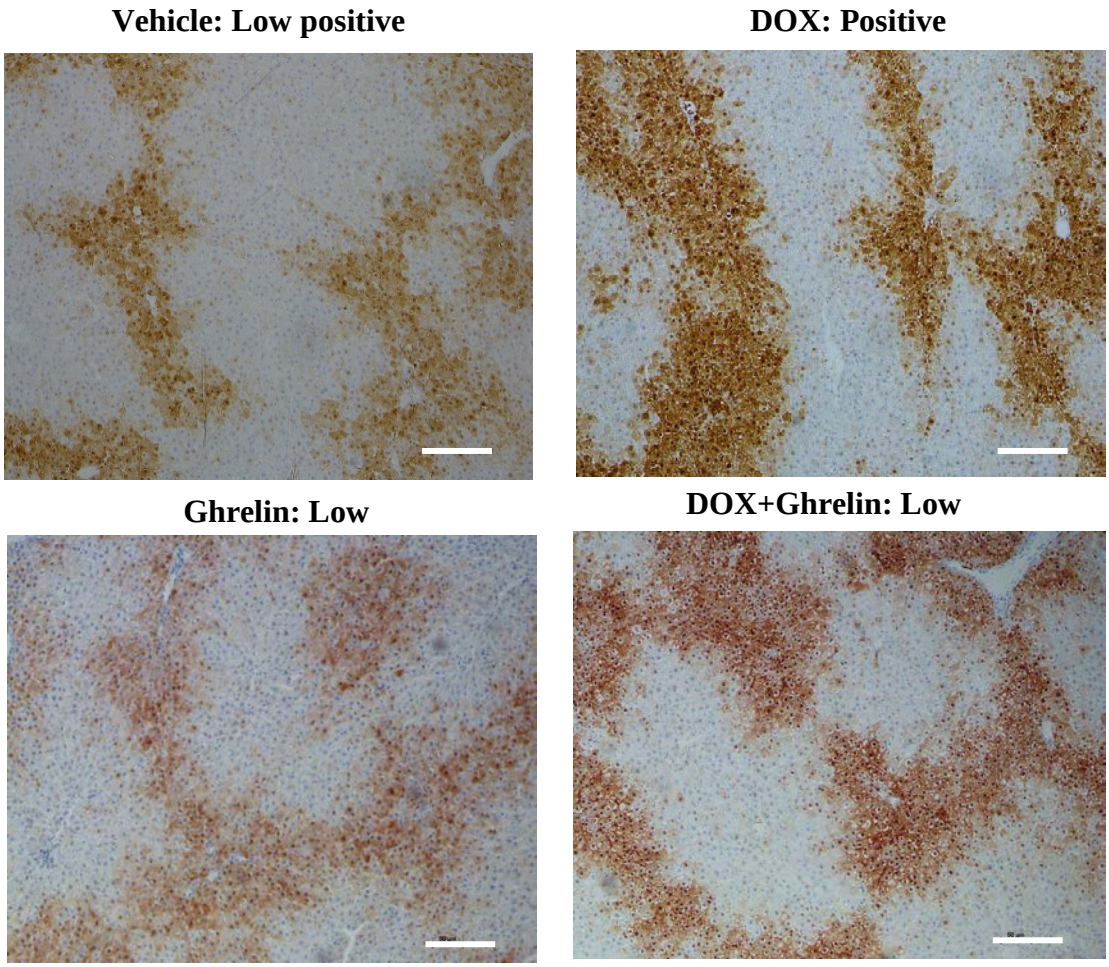

Figure 3.4C: Representative images of IHC detection of ALT. Animals were treated (i.p) with saline (vehicle), DOX, ghrelin and a combination of the two. The overall score was assigned based on the pixel intensity of the brown pigment. Images taken at 10x magnification (scale bar = 200 µm) (n = 3-5). Abbreviations: **DOX** – doxorubicin **IHC** – immunohistochemistry.

3.5.2 Albumin

Albumin, produced by the liver, is the most abundant protein contained in blood. Not only does this protein regulate colloid osmotic pressure to prevent leakage from blood vessels, it also

transports essential proteins required for growth and tissue repair in the blood. Therefore, having a low plasma albumin level is a sign that amongst other causes either the liver or the kidneys are not working as they should. As demonstrated on Fig 3.5, the serum albumin levels remained

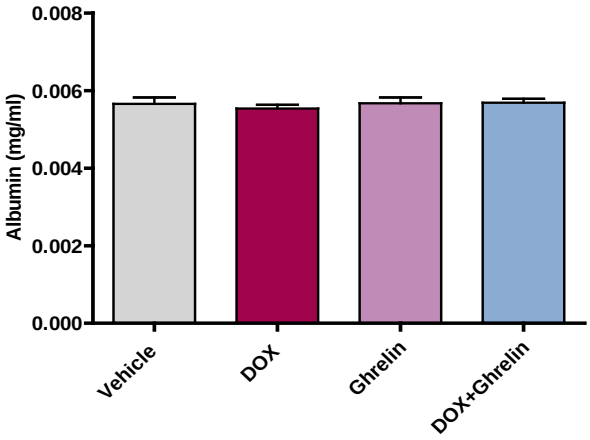

constant throughout all experimental groups without change. Taken together, these results indicate that no adverse effects were induced by DOX or ghrelin on the livers capacity to synthesise albumin in of experimental animals.

Fig. 3.5: Plasma albumin concentration. Albumin concentration (mg/ml) measured in the plasma. Animals were treated (i.p) with saline (vehicle), DOX, ghrelin and a combination of the two drugs. Results are presented as mean ± SEM (n = 7-9). Abbreviations: **DOX** – doxorubicin.

3.6. Histological analysis of hepatic tissue

3.6.1 Haematoxylin and Eosin (H&E) stain

In the event of liver damage, the first structural changes that occur are the formation of non-uniform fluid filled sacs in the cytoplasm of the hepatocytes, known as ballooning or hydropic changes. These are observed as micro-vesicular, if restricted to the cytoplasm with the nucleus intact or, macro-vesicular if they extend and displace the nucleus from its position. In this study, micro-vesicular ballooning (indicated with black arrows) were observed in the liver tissue following H&E staining (Fig 3.6). These were semi-quantified by constructing a grading system (Table 3.2) where the percentage hydropic changes per image of 4 lobes per rat was determined. An average was then calculated and grades assigned per treatment group.

Table 3.2: Grading system for micro-vesicular ballooning (see Appendix E, pg. 94)

Percentage (%) change	0 > 25	25 > 50	50 > 75	75 > 100
Grade	Minimal	Mild	Moderate	Severe

Micro-vesicular ballooning in the vehicle group was minimal as very few hydropic changes were observed (Fig. 3.6). While the hydropic changes seen in the ghrelin and DOX groups were classified as mild and moderate respectively, the ballooning in the combination group was mild suggesting that ghrelin may be protecting the liver against severe damage.

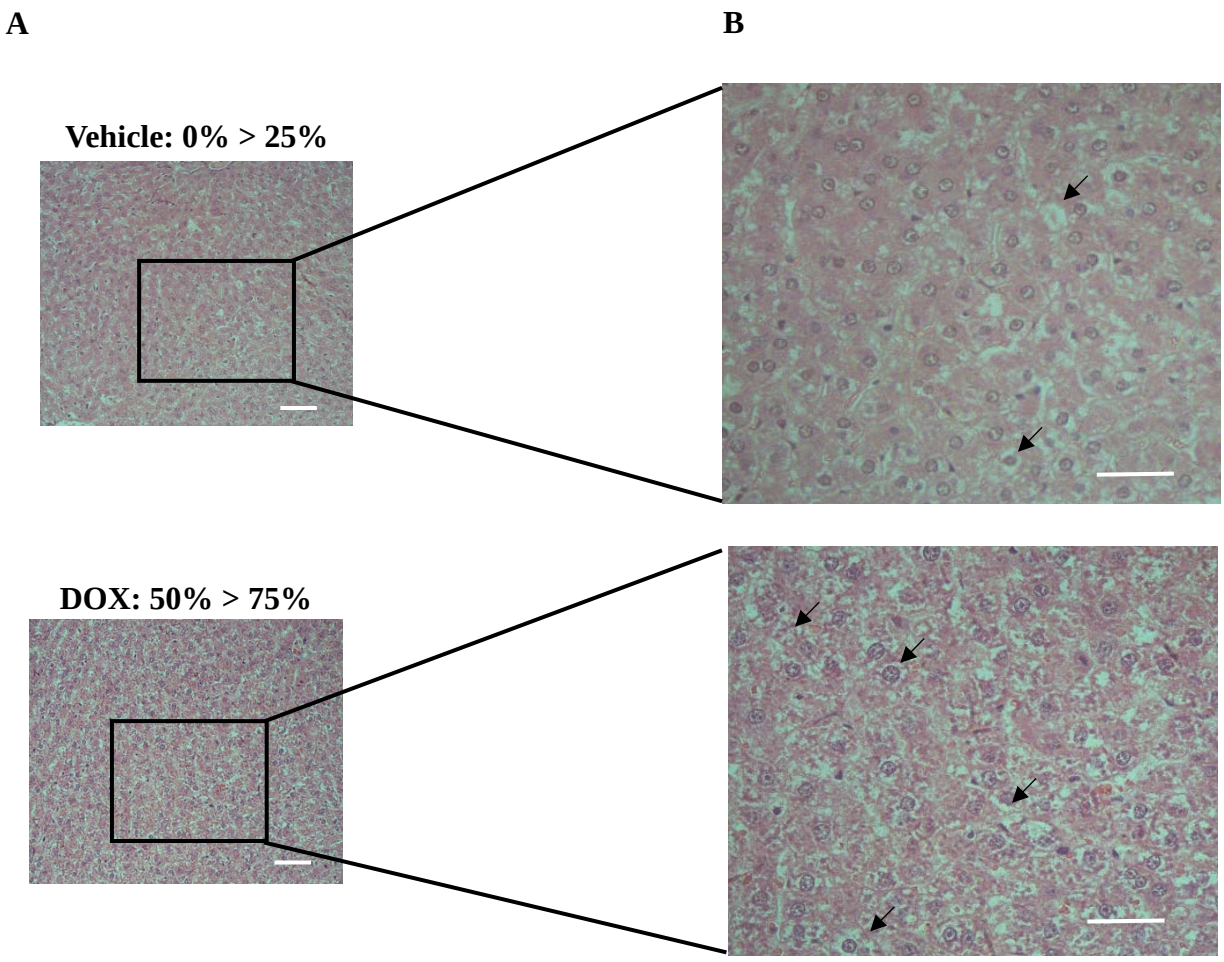

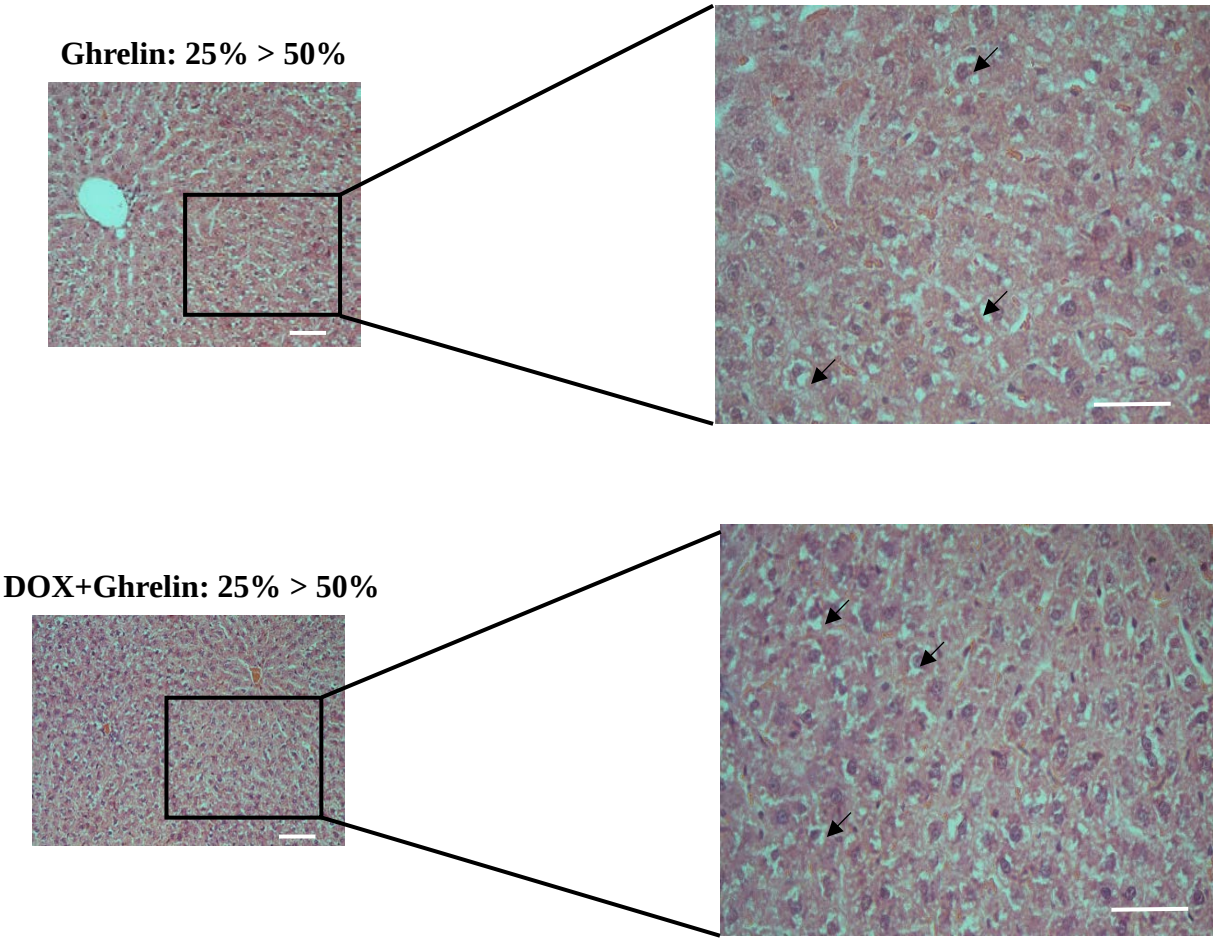

Fig. 3.6: Haematoxylin and Eosin (H&E) stain to observe structural modifications of liver tissue. Micro-vesicular ballooning (indicated by black arrows) in liver tissue in the various treatment groups. Animals were treated (i.p) with saline (vehicle), DOX, ghrelin and a combination of the two. 2-4 lobes per liver was analysed (n = 5-6). Images were taken at (A) 10x and (B) 20x magnification (scale bar of 200 µm and 100 µm). Abbreviations: **DOX** – doxorubicin.

3.6.2 Masson's trichrome stain

When a harmful stimulus intensifies or persists, the functional liver parenchyma become replaced with scar tissue which consists of type I and type III collagen, as well as ground substance. This is known as fibrosis and can progress to cirrhosis, which is indicative of end stage liver damage. To evaluate potential liver damage, type I and type III collagen (indicated by the blue hue) was detected using the Masson's Trichome stain in an effort to determine the presence of fibrosis. According to our results, this study did not observe significant fibrotic tissue in any of the treatments groups other than the expected type I collagen surrounding the portal triad and central veins, and type III collagen within sinusoids (Fig. 3.7).

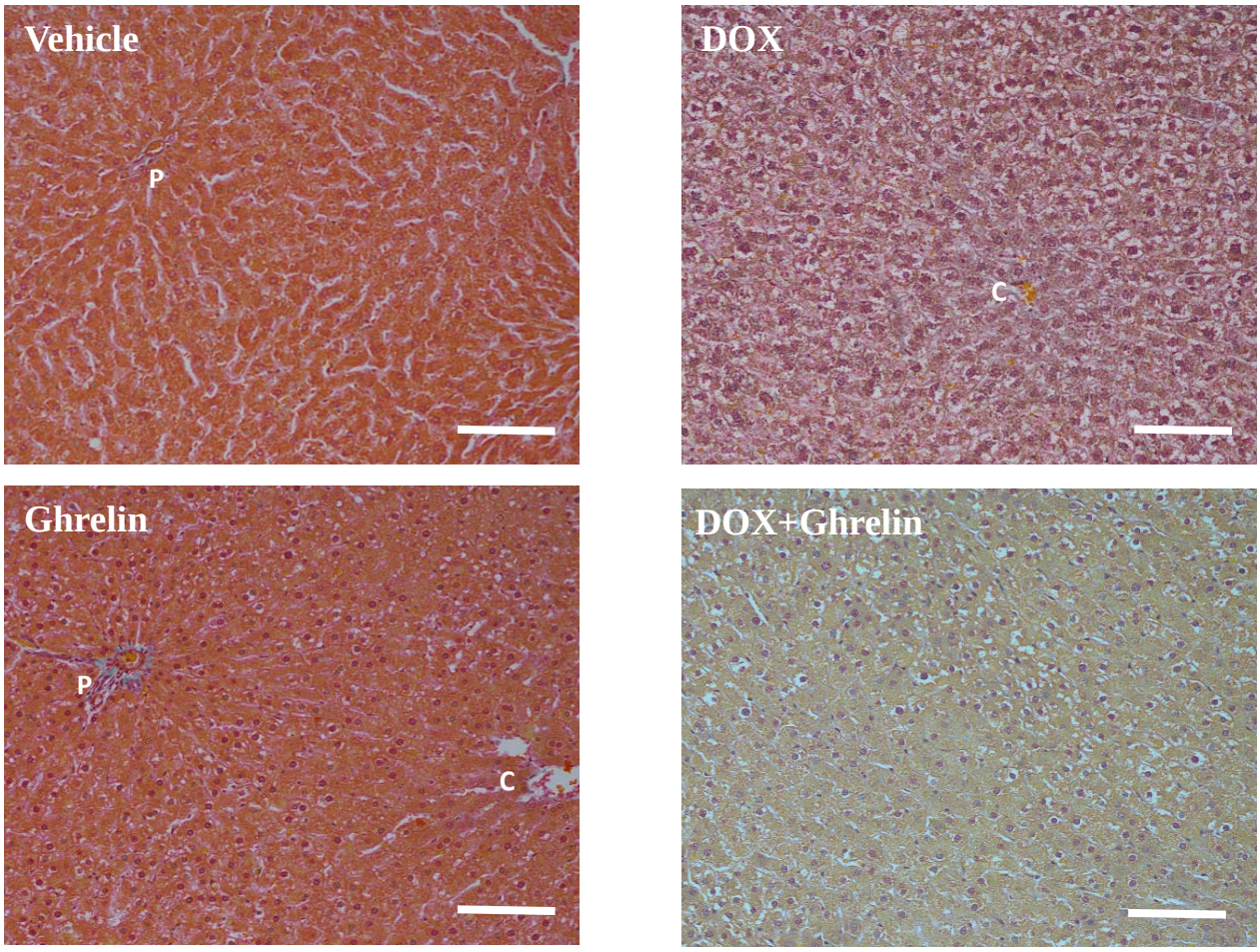

Fig. 3.7: Representative images of fibrosis detected by the Masson's trichrome stain. Animals were treated (i.p) with saline (vehicle), DOX, ghrelin and a combination of the two drugs (n = 5-6). Images were taken at 20x magnification (scale bar = 100 µm). Abbreviations: **DOX** – doxorubicin **P** – portal triad **C** – central vein.

3.6.3 Reticulin stain

Reticular fibers are a type of fiber found in connective tissue which crosslink to form a fine structure termed reticulin. The latter supports hepatocytes and endothelial cells that outline the sinusoids. The collapse or condensation of the reticulin network is indicative of a loss in underlying liver parenchyma. To further evaluate the effect of DOX and ghrelin on the liver, this study evaluated whether there is a loss of reticulin through the use of the reticulin stain (Fig. 3.8). Reticulin is stained as fine black lines that outline the sinusoids and the central vein and portal triad while the hepatocytes were stained light green. A significant reduction in reticulin is observed in the DOX treated group when compared to the vehicle. While ghrelin treated rats presented with less reticulin when compared to the vehicle, the rats treated with both DOX and ghrelin had more reticulin content when compared to the rats treated with DOX alone.**Fig. 3.8:**

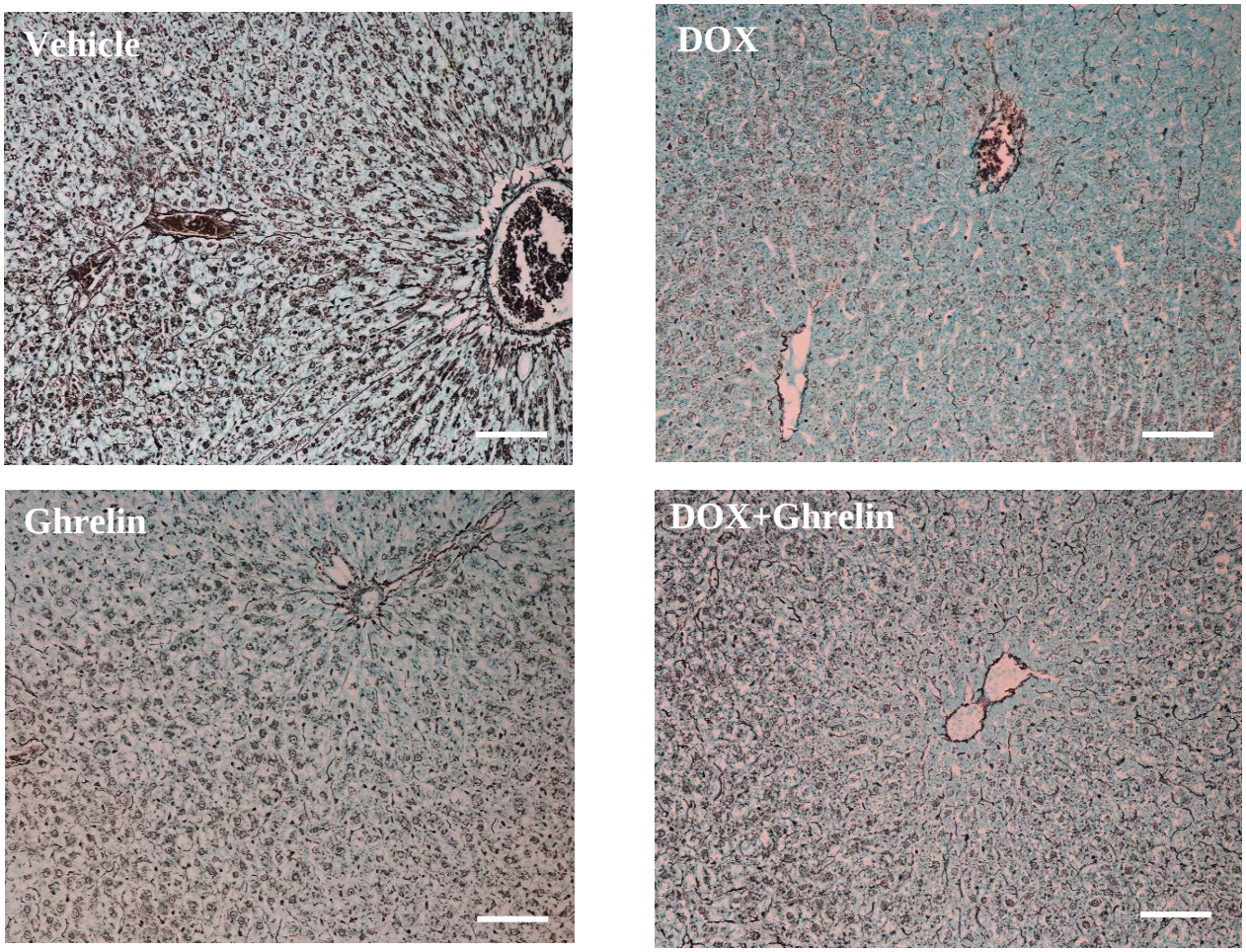

Reticulin presence in liver tissue. Representative images are taken at 20x magnification (scale bar = 100 µm). Animals were treated (i.p) with saline (vehicle), DOX, ghrelin and a combination of the two drugs (n = 5-6). Abbreviations: **DOX** – doxorubicin.

3.6.4. Periodic Acid Schiff (PAS) stain.

The liver plays an integral role in metabolism and stores glucose in the form of glycogen. While ghrelin has previously been found to promote the release of glucose from the liver, literature does not report on the effect of DOX in this context. The Periodic Acid Schiff stain was therefore used to detect glycogen content (indicated by the magenta hue) in all treatment groups (Fig. 3.9**A**), and this was quantified with the grey scale threshold on Image J software (Fig.3.9**B**). Based on our results, the glycogen content remained the same throughout the treatment groups with no major differences observed. This means that both DOX and ghrelin did not affect the amount of glycogen present in the liver.

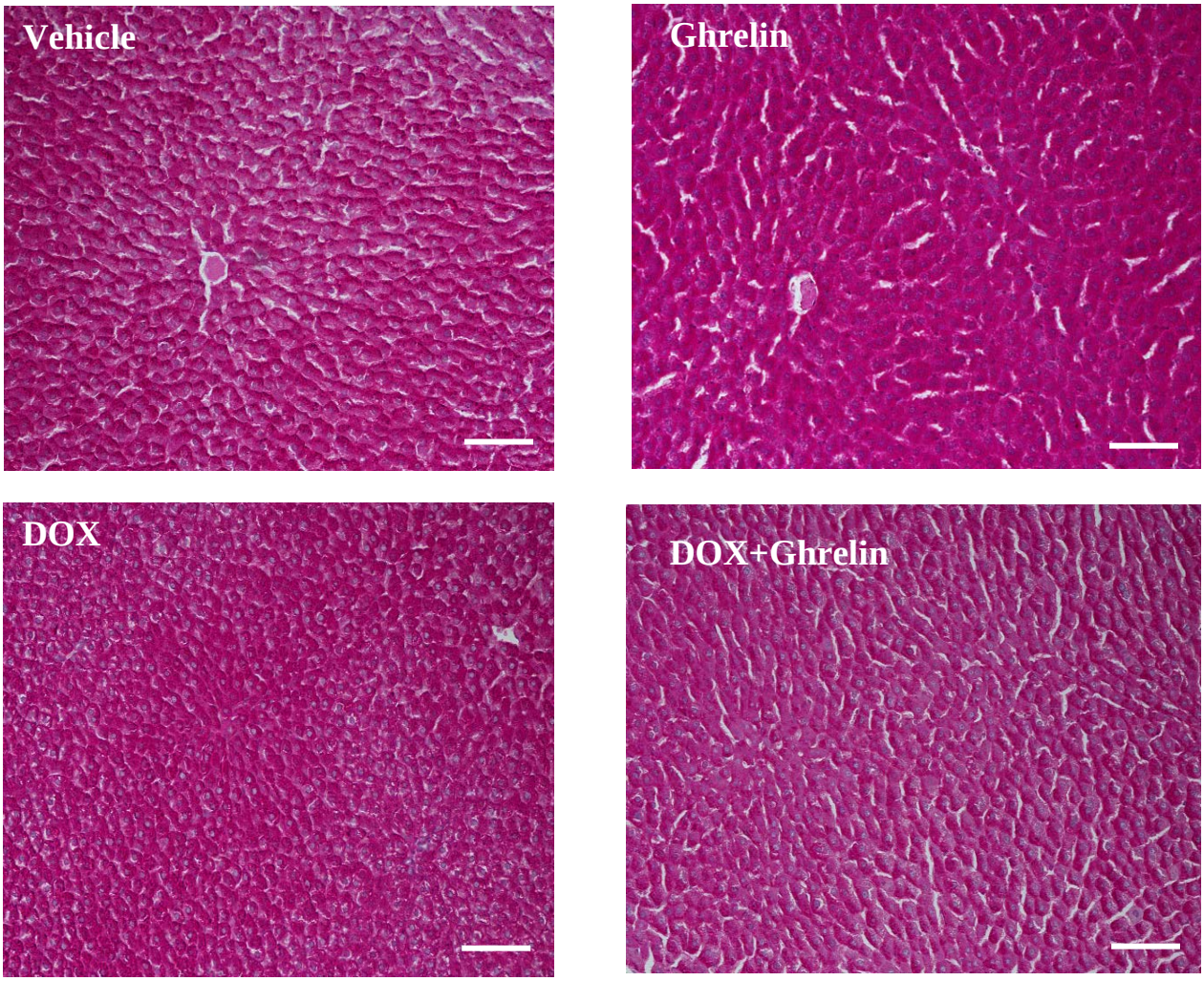

Fig. 3.9A: Periodic Acid Schiff stain detects glycogen in liver tissue. Representative images were taken at 20x magnification (scale bar = 100 µm). Animals were treated (i.p) with saline (vehicle), DOX, ghrelin and a combination of the two drugs (n = 5-6). Abbreviations: **DOX** – doxorubicin

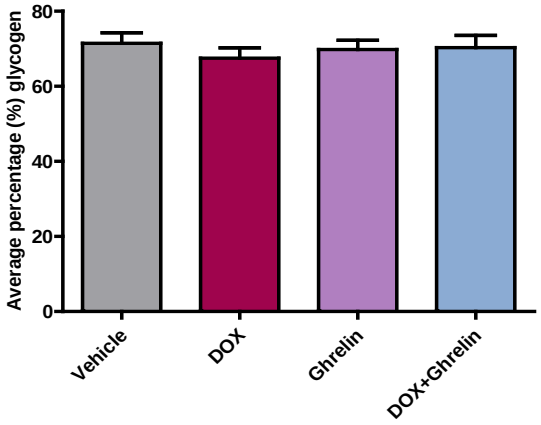

Fig. 3.9B: Quantification of glycogen content detected by the Periodic acid Schiff stain. The average percentage glycogen content was quantified with the grey scale threshold on the Image J software. Animals were treated (i.p) with saline (vehicle), DOX, ghrelin and a combination of the two drugs. Results are presented as mean ± SEM (n = 5-6). Abbreviations: **DOX** – doxorubicin.

3.6.5 Oil Red O stain

A fatty liver is a reversible condition where large vacuoles of triglyceride fat accumulate in liver cells via a process known as steatosis. This occurs as a result of disturbances in fat metabolism which causes excessive accumulation of fat in the liver. While the effects of DOX on fat accumulation in the liver are currently unknown, ghrelin promotes lipid accumulation within liver tissue and can result in lipotoxicity if the accumulation is severe. This study evaluated fat accumulation by performing an Oil Red O stain on frozen liver tissue samples (Fig. 3.10). The hepatocytes stain a purple/blue colour, whereas the lipid droplets within hepatocytes stain red. The lipid content within the tissues was determined by infrared-based quantitation (Table 3.3). Our findings reveal that while DOX reduced lipid accumulation, ghrelin significantly (0.13 ± 0.009 AU, p <0.001) increased lipid accumulation when compared to the vehicle (0.05 ± 0.003 AU). The result found that lipids in the DOX+Ghrelin experimental group were similar compared to the DOX group.

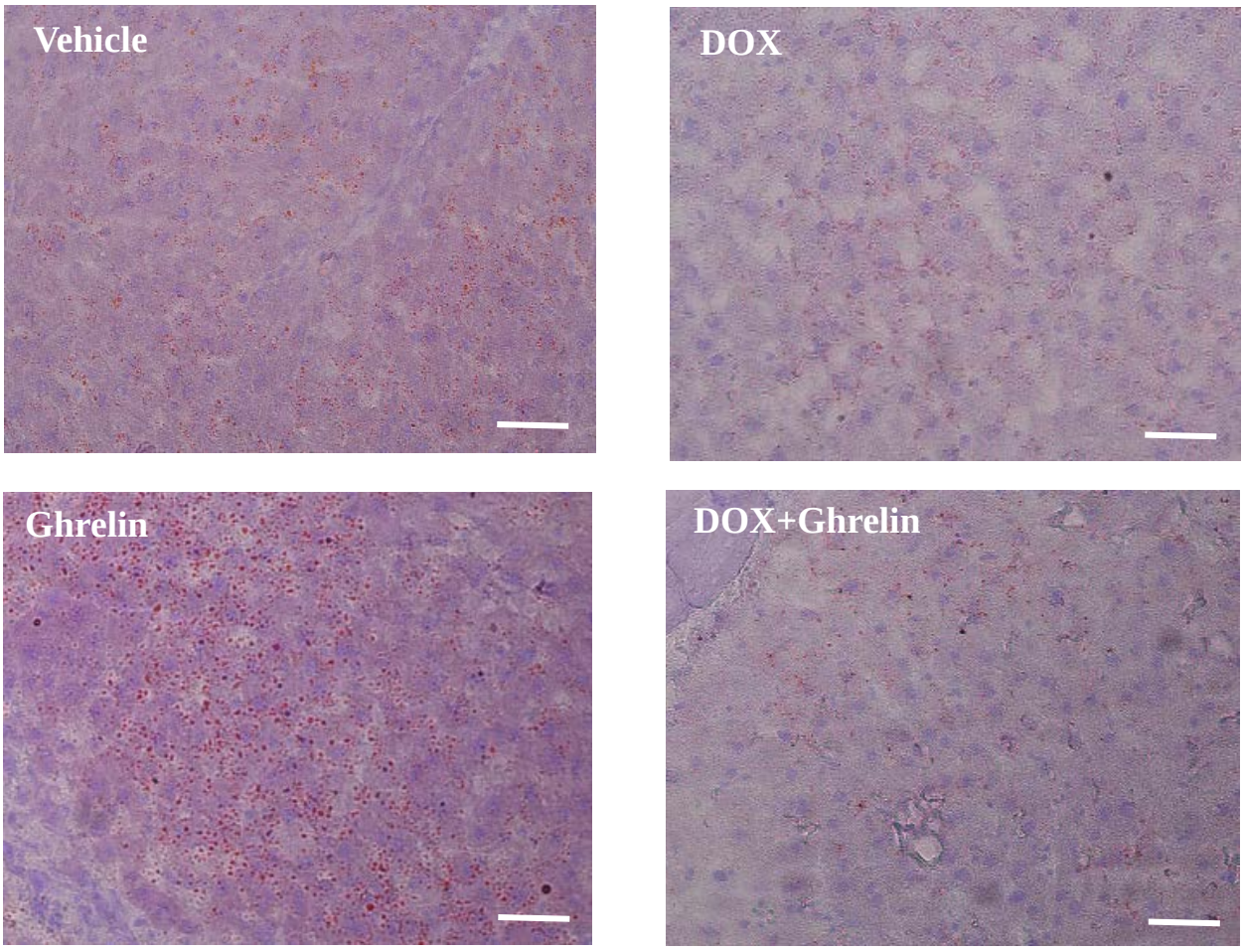

Fig. 3.10: Oil Red O stain for the detection of fat accumulation in liver tissue. Representative images were taken at 20x magnification (scale bar = 100 µm). Animals were treated (i.p) with saline (vehicle), DOX, ghrelin and a combination of the two drugs (n = 5-6). Abbreviations: **DOX** – doxorubicin.

Table 3.3: Relative lipid content present in hepatic tissue

Group	Vehicle	DOX	Ghrelin	DOX+Ghrelin
Lipid absorbance (AU)	0.05 ± 0.003	0.03 ± 0.009	0.13 ± 0.009***	0.04 ± 0.004

Results are presented as mean ± SEM (n = 3-5). *** $p < 0.001$ vs. vehicle. Abbreviations: **DOX** – doxorubicin, **AU** - arbitrary units, **vs.** - versus.

3.7. Oxidative Stress

3.7.1 Lipid Peroxidation

DOX induced toxicity on healthy tissues is mainly as a result of the production of ROS creating a condition of oxidative stress when the anti-oxidant systems become overwhelmed. As ghrelin has been found to possess anti-oxidative properties, this study evaluated oxidative stress indirectly by assessing lipid peroxidation. Although ROS have a short half-life, they oxidize cellular membranes to produce conjugated dienes (CDs) (early marker) that are converted to malondialdehyde (MDA) (late marker). As indicated in Fig. 3.11, no significant differences were observed in either CDs or MDA content in the liver tissue.

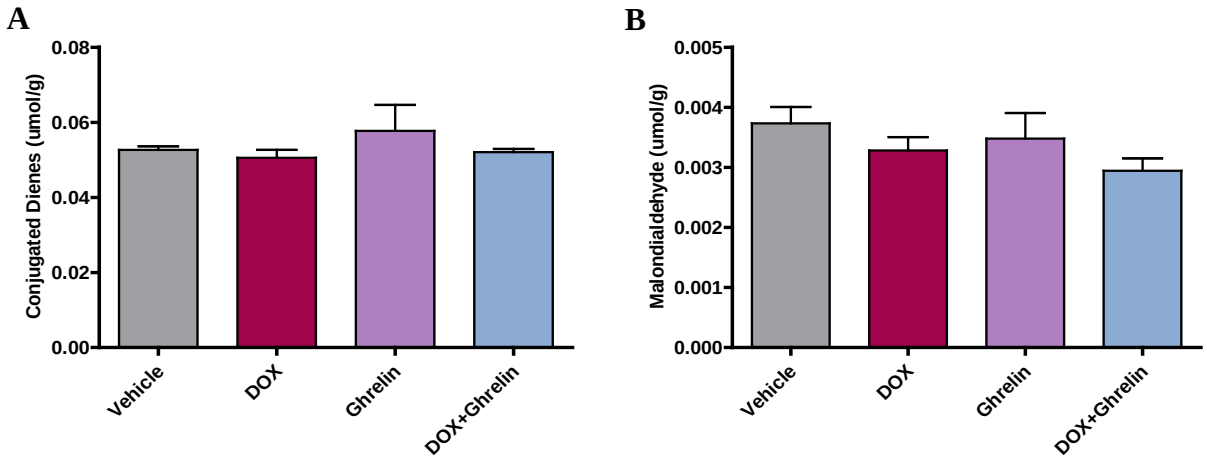

Fig. 3.11: Lipid peroxidation of rat liver tissue. Markers for lipid peroxidation were assessed by measuring conjugated diene (umol/g) (**A**) and malondialdehyde (µmol/g) (**B**) content as early and late markers respectively. Animals were treated (i.p) with saline (vehicle), DOX, Ghrelin or DOX+Ghrelin. Results are presented as mean ± SEM (n = 5-6). Abbreviations: **DOX** – doxorubicin.

3.7.2 Anti-oxidant status

To supplement the lipid peroxidation data, the anti-oxidant status of liver tissue was examined. Glutathione is the most significant non-enzymatic oxidant defence system. It undergoes a redox reaction where reduced glutathione (GSH) neutralizes free radicals through donating an electron, resulting in the rise of oxidized glutathione (GSSG). Due to the rapid nature of the formation of GSSG relative to synthesis or secretion of GSH, the ratio of GSH to GSSG is a good indicator of oxidative stress (Table 3.4). The results obtained in this experiment echoed those observed for

oxidative damage where no considerable changes were detected. This was rather surprising due to the known ROS producing effects of DOX, as well as the high iron content within this tissue.

Table 3.4: Glutathione analysis of rat liver tissue

Treatment group	GSH (umol/g)	GSSG (umol/g)	GSH:GSSG
Vehicle	1.52 ± 0.39	0.45 ± 0.10	1.53 ± 0.08
DOX	1.68 ± 0.34	0.33 ± 0.02	1.48 ± 0.19
Ghrelin	1.95 ± 0.19	0.37 ± 0.04	1.58 ± 0.20
DOX+Ghrelin	1.99 ± 0.20	0.39 ± 0.04	1.60 ± 0.23

Results are presented as mean ± SEM (n = 5-6). Abbreviations: **DOX** – doxorubicin **g** – grams.

3.8. Autophagy, Apoptosis and Endoplasmic Reticulum (ER) Stress

Despite the controversies in the literature regarding the effects of DOX on autophagy, this process contributes to the regulation of hepatic lipid metabolism by facilitating the degradation of lipid droplets to sustain energy homeostasis during energy exhaustion. p62 degradation and LC3 lipidation are two major hallmarks of autophagy execution. Our results show a decrease in the protein expression of p62 and an increase in LC3-II in all treatment groups when compared to the vehicle (Fig. 3.12). This is suggestive of elevated autophagic activity and increased flux through this pathway.

There are numerous reasons why autophagy in this context may be elevated. Firstly, autophagy may be induced as a result of oxidative stress; however since oxidative stress was not detected in this study, autophagy may be induced to prevent apoptosis from taking place. This study shows that both cleaved caspase-3 and cleaved PARP were upregulated by DOX and ghrelin alone versus the vehicle (Fig. 3.13). However, DOX treatment in the presence of ghrelin reduced the protein expression of these apoptotic proteins when compared to the DOX group. This result exemplifies ghrelin's anti-apoptotic effects.

Interestingly, apoptosis and autophagy in this context may be induced as a result of ER stress, a condition that arises when there is an accumulation of misfolded proteins or a depletion of the ER calcium stores. In response to this stress, the UPR is triggered to limit protein synthesis and to initiate protein degradation *via* ERAD (endoplasmic associated degradation). This study demonstrates that under basal conditions, the liver presents with relatively elevated levels of ER stress as indicated by the increased expression of BiP and AFT4 (Fig. 3.14). Similar observations were seen in the ghrelin group. Although DOX reduced BiP and ATF4 when compared to the vehicle, the DOX+Ghrelin group maintained elevated levels of ATF4 when compared to the DOX treated group.

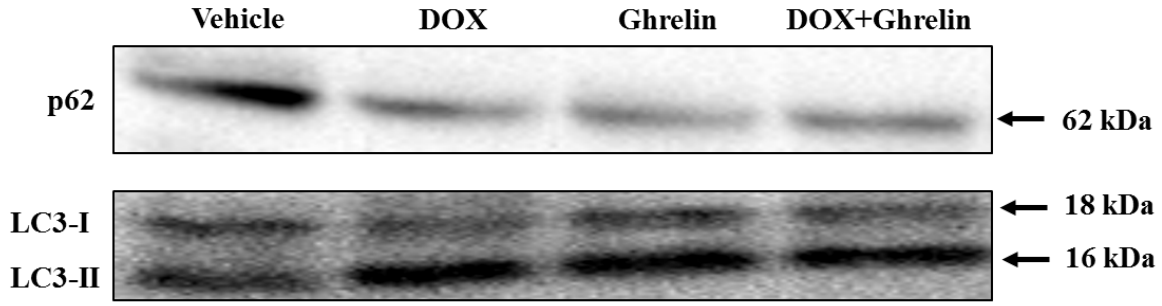

Fig. 3.12: Relative protein expression of p62 and LC3 in hepatic tissue determined by Western blotting. Abbreviations: **DOX** – doxorubicin **LC3** - microtubule associated protein 1 light chain 3 **kDa** - kilo Daltons.

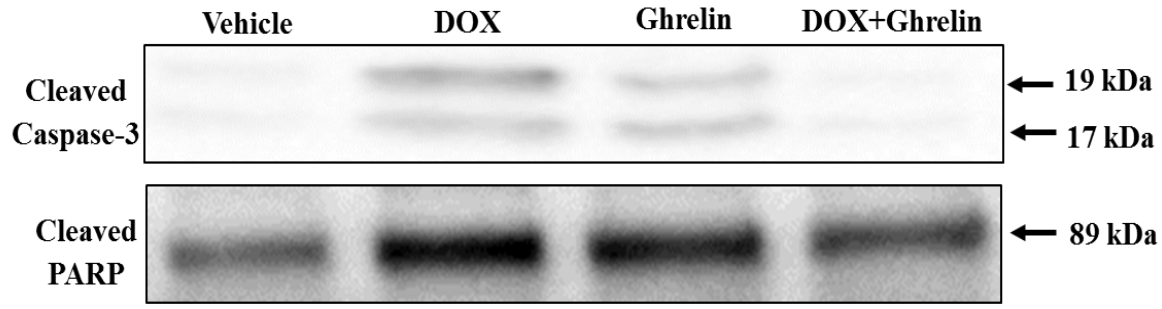

Fig. 3.13: Relative protein expression of cleaved caspase-3 and cleaved PARP in hepatic tissue determined by Western blotting. Abbreviations: **DOX** – doxorubicin **PARP** - Poly (ADP-ribose) polymerase **kDa** - kilo Daltons.

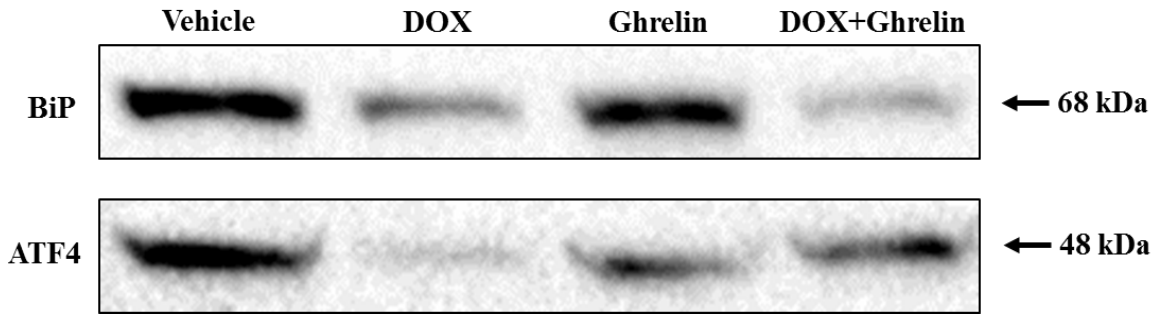

Fig. 3.14: Relative protein expression of BiP and ATF4 in hepatic tissue determined by Western blotting. Abbreviations: **DOX** – doxorubicin **BiP** - binding immunoglobulin heavy chain-binding protein **ATF4** - Activating Transcription Factor 4 **kDa** - kilo Daltons.

Chapter 4

Discussion

This study set out to determine the effects of DOX, a potent chemotherapeutic agent, on the liver using a chronic model of DOX-induced cardiotoxicity. As there is no cure for this disease, current research is aimed at identifying therapeutic interventions that counteract the damaging effects of this anti-cancer regimen. Ghrelin, a brain-gut peptide, known for its appetite inducing effects has previously been shown to possess anti-oxidant, anti-apoptotic, anti-fibrotic and anti-inflammatory effects, all of which contributes to the development of cardiotoxicity. While literature has mainly focused on cardiovascular injury induced by DOX, few studies has paid attention to the liver which is responsible for DOX's metabolism and exit out of the body. The model used in this study simulated long-term dose-dependent toxicity often observed in patients who develop adverse cardiovascular complications following DOX therapy. Therefore, the cumulative DOX concentration (20 mg/kg) provided to the experimental animals fell within the range of 60 - 75 mg/m^2 that is administered to humans (human equivalent dose) (Desai *et al*., 2013; Von Hoff *et al*., 1979). In addition, the age of the animals at the start of the study was taken into consideration. Experimentation began when animals were five weeks old which indicates a young age, and by the time the study was concluded, the animals were 13 weeks old which is comparable to adulthood in humans. Finally, since cardiotoxicity takes some time to manifest, usually when cancer has been treated or in remission, it is for this reason that cancer was not induced in this module before treatment commenced.

4.1 Ghrelin promotes food consumption and prevents severe body weight loss

A well-known side effect of chemotherapeutic agents including DOX, is the loss of appetite resulting in weight loss (Kalender *et al.*, 2005). Severe weight loss reduces a patient's quality of life and limits the dose and the duration of a potential curative treatment. Therefore, appetite stimulants such as ghrelin provide an advantage towards the prevention of weight loss and the improvement of a patient's nutritional status (Neary *et al.*, 2004). This study demonstrated reduced weight gain in the animals that received DOX treatment (Fig. 3.1) and this was caused by a reduction in the food consumed by these animals (Fig. 3.2). Although the animals that received both treatment regimens ate significantly more food when compared to the DOX group,

this effect was not reflected in the body weight data as expected. Rodents are small animals that have a higher surface-to-volume ratio, and thus lose relatively larger heat loss to the environment per unit in time. In an effort to maintain body temperature despite rapid heat loss, these animals oxidize food at an elevated rate (Glider, 2011). This study therefore proposes that due to the appetite repressive effects of DOX, as well as the high metabolic rate of these animals, the food consumed was metabolised and immediately used to maintain normal physiological functions instead of it being stored. In support of our observations, numerous studies have shown decreased weight gain and food consumption due to DOX treatment (Wang *et al.,* 2014; Injac *et al.,* 2009), whereas others have demonstrated increased appetite and subsequent food intake after exogenous ghrelin administration independently of GH secretion (Wren *et al.,* 2000, Neary *et al.,* 2004).

It was expected that treatment with ghrelin alone would induce a potent increase in food intake, however this effect was not observed in this study. In a similar manner, Shintani and colleagues (2001) illustrated a significant increase in food intake four hours following ghrelin administration, but this effect was lost after 24 hours. Increased food intake following ghrelin administration is said to occur within 60 mins in rodents, which means that daily (24 hours) monitoring of food intake can be missed. Even though ghrelin's orexigenic effects are indicated to be more powerful when ghrelin is administered centrally (intra-cerebroventricular), rather than peripherally (i.p), ghrelin does not regulate energy homeostasis directly (Wren *et al.,* 2000). Instead, ghrelin increases the expression of NPY and AgRP neurons which co-localize with GHS-R1α in the arcuate nucleus in the nutrient centre of the brain, and by stimulating glycogenolysis and gluconeogenesis in hepatocytes (Leite-Moreira & Soares, 2007) and the promotion of genes that favour lipogenesis and triglyceride storage in the liver (Barazonni *et al.,* 2005).

4.2 DOX induces fusion of hepatic tissue

The liver regulates its mass in response to body weight. The optimal liver to body weight ratio is reached when the liver performs the amount of metabolic work required for the body to function optimally (Fausto, 2000; Michalopoulos & DeFrances, 1997). This organ will either proliferate to increase its mass in response to body weight gain or undergo apoptosis in response to body weight loss (Fausto, 2000; Wang *et al.,* 2014). In this study there were no changes among the treatment groups when liver weight was expressed relative to body weight (Table 3.1). Although

ghrelin administration with DOX treatment did not significantly alter liver mass, additional loss of liver mass was inhibited.

As mentioned previously, the liver is divided into median, right, left and caudate lobes. The median, right and caudate lobes are further subdivided into two more parts, giving the appearance that rat liver has seven lobes (Malarkey *et al.,* 2005). In this study the morphological appearance of the rat liver in the vehicle and ghrelin treatment groups presented with seven lobes (Fig. 3.3), while those that were treated with DOX only presented with four lobes (except for one out of the nine animals in this group), which is suggestive of fusion. Interestingly, this fusion of liver lobes was not prominent in the animals co-treated with DOX and ghrelin as they presented with six lobes. To the best of our knowledge, this novel observation has not previously been reported and further implies that ghrelin impedes this fusion. While this observation may infer a protective effect by ghrelin, all animals survived the treatment duration and therefore the significance of these results warrant further investigation.

As mentioned previously, DOX administered intraperitoneally *versus* intravenously, has a 40% bioavailability and remains in the abdominal cavity for an extended period (Nagai *et al.,* 2013). In addition, in the clinical setting DOX administered intraperitoneally to treat patients with ovarian cancer has resulted in peritoneal irritation (Ozols *et al.,* 1982). In our study, peritoneal irritation with intestinal adhesions was observed when the rats were sacrificed. Therefore, this study proposes that DOX administration *via* i.p injection possibly initiated peritoneal irritation where the corrosive property of DOX eroded the Glisson capsule surrounding the liver, and induced tissue injury that led to the fusion of adjacent lobes. The standard response to tissue injury in all mammalian organ systems is to prevent blood loss (Gurtner *et al.,* 2008). A platelet plug is initially formed to arrest bleeding from breached blood vessels to signal blood coagulation. Once bleeding has been stopped and tissue healing occurs, the plug is removed through a process termed clot retraction. The platelets within the clot contract and pull the edges of the damaged vessels together (Sherwood, 2013). Therefore, erosion of the Glisson capsule exposes hepatocytes of adjacent lobes to one another and through coagulation and clot retraction, hepatic fusion ensues. An important factor to be considered in this scenario is the fact that treatment began when the animals were at a relatively young age where the liver was still in a process of growth and development, and it is likely that DOX impaired these processes. Finally,

since the liver is a regenerative organ that can undergo partial hepatectomy, where two thirds of the liver can be removed; this organ is able to regenerate with the remaining lobes enlarging to compensate for the loss of liver mass. However, the lost lobes never grow back, and the livers are able to function normally with less lobes (Michalopoulos & Defrances, 1997). It should also be noted that the lobes of a rat liver has different susceptibilities to toxicity depending on the agent being used. For example, rats treated with dimethylnitrosamine had more damage in the left and left median lobes compared to the rest of liver lobes. Similary, carbon tetrachloride induced greater damage in the right lobes compared to the left lobes. These effects were observed independent of the route of administration (Lawson and Pound, 1974).

4.3 DOX treatment does not impair liver function

ALT is highly expressed in the liver where it plays a fundamental role in gluconeogenesis and amino acid metabolism (Reagan *et al.* 2012). Injury to the liver results in the release of ALT into the serum. Thus, elevated serum ALT is an indication of liver damage. Although ALT is largely localized in the liver, it is also expressed in other tissue types including muscle, heart and digestive tract (Giannini *et al.*, 2005)**.** While hepatotoxicity induced by DOX therapy has previously been shown *in vivo* (Swamy *et al*., 2012) and clinically (Damodar *et al*., 2014), this study did not demonstrate differences in ALT between the groups (Fig. 3.4). The major difference between these studies was the frequency and duration at which DOX was administered. Whereas at this current study administered DOX once weekly for eight weeks, Swamy and colleagues (2012) injected DOX six times over a period of two weeks to make a cumulative dose of 15 mg/kg. Although our study administered a higher cumulative dose (20 mg/kg) over time, the frequency at which DOX was administered may have accounted for the differences observed. A similar result was also obtained for plasma albumin where no changes were observed (Fig. 3.5). Albumin is exclusively produced by the hepatocytes and a decrease in circulation is indicative of not only liver damage (Thapa & Walia, 2007) but also nephrotoxicity and protein losing enteropathies. A marked reduction in albumin synthesis has been demonstrated in DOX treated animals following hepatic resection which coincided with necrosis of hepatocytes not observed in this study (Tanaka *et al*., 1982). Like other studies, the frequency and duration of DOX treatment differed. It can thus be concluded that while treatment with DOX is toxic to the

liver, where toxicity is dependent on frequency and duration of treatment, over time this organ can regenerate and heal itself once the harmful stimulus is prevented.

4.4 DOX and ghrelin induce minor structural changes in liver histology

When the liver is damaged, one of the first structural changes that occurs is ballooning, also known as hydropic changes. Hepatocyte ballooning indicates the presence of a non-uniform fluid filled sac found in the cytoplasm of the hepatocytes. Literature reports that ballooning arises due to: (i) damage of hepatocyte membranes that allows entry of sodium into a cell with osmotically obliged water, or (ii) a lack of ATP to furnish the energy required for the sodium pump to function optimally, and thereby allows excess sodium and water to accumulate (Edmondson *et al.,* 1967). It could also occur due to cytoskeletal alterations where keratin 8 and 18 are disrupted and no longer spread throughout the cytoplasm (Takahashi *et al.,* 2014). While DOX and ghrelin demonstrated moderate and mild hydropic changes respectively, the co-administration of DOX and ghrelin together showed mild ballooning (Fig. 3.6). Our results are in stark contrast to the literature where structural changes have not been observed as a result of ghrelin treatment. The reason for this could be the fact that this study utilised a higher ghrelin concentration (300 µg/kg/week) than Li *et al.* (2013) and Cetin *et al.* (2011) who administered lower ghrelin concentrations of 30 ng/kg/week and 50 ng/kg/week respectively.

When a harmful stimulus is chronically persistent and occurs frequently enough, scarring occurs and liver parenchyma are replaced with collagen in a phenomenon termed fibrosis. Fibrosis can progress to cirrhosis which is indicative of end stage liver damage. A cirrhotic liver lacks normal hepatic lobules and the hepatocytes are enclosed in a fibrotic circle, also termed a nodule (Anthony *et al.,* 1978). Hepatic fibrosis is characterized by an increase in extracellular matrix constituents that include type I and type III collagen forming a hepatic scar (Friedman, 1993). Since normal type I and type III collagen are naturally found around the portal triad, central vein and sinusoids, care should be taken not to term blue staining (Masson Trichome) in these areas as fibrotic tissue (Lefkowitch *et al.,* 2006; Murli, 2013). No prominent fibrosis was observed in this study other than where it was expected (Fig. 3.7). This could be attributed to the limitation of our light microscopic observations but also the frequency of DOX treatment as observed by others (El-Sayyad *et al*., 2009).

Reticulin, composed of type II collagen, is found within the extracellular matrix of the space of Disse outlining the sinusoids. It functions to support hepatocytes and endothelial cells outlining the hepatocytes (Krishna, 2013). The loss or condensation of reticulin signals the loss of underlying liver parenchyma and also used in the diagnosis of fatty liver disease (Lefkowitch, 2006; Dixon *et al.,* 2001).This study illustrates a significant loss of reticulin in the liver of the rats treated with DOX and this was not recovered by ghrelin adjuvant therapy (Fig. 3.8). In fact, ghrelin itself reduced reticulin expression and this result may imply a degree of toxicity. A loss of reticulin is an indication of fat accumulation, and in this study ghrelin treatment alone resulted in a significant fat accumulation. DOX treatment did not result in fat accumulation, hence, the loss of reticulin as a result of DOX treatment should further be investigated. Although studies evaluating the effects of DOX on reticulin expression in the liver are rare, the use of reticulin stain has been found to be valuable mainly in the differential identification of well-differentiated hepatocellular carcinoma and benign hepatic nodules (Hong *et al*., 2011).

4.5 Ghrelin promotes fat accumulation and not glycogen storage in the liver

The liver is the second largest organ to store glycogen in the body and consequently supplies glucose in the event of low circulating levels (Campbell, 2006b). Several studies have reported that ghrelin promotes glucose release from hepatocytes by upregulating the activity of the enzyme glucose-6-phosphatase (Gauna *et al.*, 2005; Barazonni *et al.*, 2005). No changes in glycogen content within hepatocytes in this study was observed (Fig. 3.9). Additionally, the liver is involved in lipid metabolism through the incorporation of fatty acids into complex lipids such as triglycerides. These are further assembled into lipoproteins to be transported into circulation. Although lipids are stored subcutaneously or in adipose tissue, they may accumulate in vital peripheral organs such as the liver. This ectopic fat has been associated with the development of non-alcoholic fatty liver disease (NAFLD) and insulin resistance (Griffin, 2013). By reducing the activity of AMPK, a potent inducer of fatty acid oxidation (Barazonni *et al.,* 2005), exogenous ghrelin administration has been found to reduce fat utilization and promote fat storage (Tschöp *et al.*, 2000). Similar observations were made in this study as ghrelin treatment increased fat storage, while DOX amplified its utilization resulting in its reduction (Fig. 3.10). Considering that the liver utilizes free fatty acids as an energy source (Zámbó *et al.*, 2013), this may have accounted for the reduced lipid accumulation when both treatments were combined.

4.6 DOX does not induce oxidative damage or changes in antioxidant status

DOX is well known for its stimulatory oxidative properties which induces oxidative damage to healthy tissues. The ROS generated oxidizes lipid structures of organelles and cellular membranes, resulting in conjugated dienes and malondialdehydes which are markers of lipid peroxidation (Jafari *et al.,* 2007; Gutteridge, 1995; Halliwell & Chirico, 1993). Even though lipid peroxidation has been observed following DOX treatment (Kalender *et al.,* 2005, Pieniążek *et al.,* 2013; Wang *et al.,* 2014), the current study did not observe any considerable changes in the different experimental groups (Fig. 3.11). Unlike the heart, the liver has superior antioxidant levels and operates at a lower oxidative environment (Carvalho *et al.,* 2009), and is thus not prone to oxidative damage unless it is severe. Glutathione is produced in the cytoplasm of hepatocytes and from here, it is distributed to the rest of the bodily tissues. Mainly present in two forms, glutathione is reduced following oxidation to form GSSG from GSH (Arrick & Nathan, 1984). GSH plays a vital role in ROS scavenging and the detoxification of drugs and toxins, and therefore a decrease in the ratio of GSH to GSSG is suggestive of oxidative stress (Jafari *et al.,* 2007). Our findings regarding glutathione status (Table 3.4) echoed those observed for lipid peroxidation. Despite our non-significant findings, ghrelin is a potent inducer of antioxidant enzyme activity such as glutathione reductase, which catalyses the conversion of GSSG back to GSH (Dobutovic *et al.,* 2014; Couto *et al.,* 2016).

4.7 Ghrelin prohibits DOX-induced cell death

Apoptosis is one of the hallmarks of DOX-induced toxicity and has been observed to occur in liver tissue following DOX administration (Wang *et al.,* 2014). It can occur *via* two mechanisms; intrinsically as a result of cytochrome c leakage from mitochondria (Owe *et al.,* 2008), or extrinsically due to the presence of inflammatory cytokines (Gustaffson and Gottlieb, 2003; Hsu *et al.,* 1995). These pathways initiate the caspase cascade converging at caspase-3 which cleaves PARP. PARP functions to repair oxidatively damaged DNA but when cleaved by caspase-3, the cell will resort in apoptotic cell death. As expected, DOX induced significant apoptosis as demonstrated by the increased presence of caspase-3 and PARP cleavage (Fig. 3.13). While ghrelin is known to be anti-apoptotic (Lee *et al*., 2016), this effect was only observed when DOX treatment was provided in combination with ghrelin. The manner in which this happens is the prevention of cleavage of pro-apoptotic proteins, but also through the phosphorylation and

activation of serine/threonine kinase Akt (PKB) and extracellular signal-regulated protein kinases 1 and 2 (ERK1/2) (Baldanzi *et al*., 2002). Together, these findings propose that ghrelin inhibits apoptosis by modulating the stress-induced apoptotic signalling pathways.

Autophagy is known as a double edged sword as its activation may be protective or detrimental depending on the stimulus and the context of which it is studied (Dirks-Naylor, 2013; Kawagachu *et al.,* 2012). This process removes damaged proteins or organelles from cells and the by products are then recycled for energy production. In the context of DOX toxicity, autophagic activity is controversial as some studies demonstrate elevated activity (Smuder *et al.,* 2013; Lu *et al.,* 2009), while others show reduced activity (Sishi *et al.,* 2013b; Kawagachu *et al.,* 2012). Autophagic degradation begins with the formation of an isolation membrane (phagophore) that sequesters cytoplasmic components into double membraned autophagosomes. These autophagosomes fuse with lysosomes containing digestive enzymes where the autophagosomal cargo is degraded (Mizushima, 2007). To date, only LC3 has been acknowledged as an autophagosomal inner membrane protein that serves as a receptor for p62/SQSTM1 (sequestome 1), an adapter protein with ubiquitin-binding domains, which is selectively degraded by autophagy (Bjørkøy *et al*., 2005). This study demonstrates that both DOX and ghrelin induced autophagic activity as p62/SQSTM1 expression was reduced, suggesting degradation, and LC3-I was converted LC3-II (Fig. 3.12). Since autophagy is accompanied with other forms of cell death such as apoptosis, it is often challenging to discern whether it is pro-death or pro-survival (Kobayashi *et al*., 2010). Thus, autophagy and apoptosis can act together to cause cell death or, autophagy can inhibit apoptosis by acting as an antagonist to promote survival or, autophagy may enable apoptosis by permitting apoptosis to take place without resulting in death by autophagy (Eisenberg-Lerner *et al*., 2009). Autophagy in this context may also be upregulated to assist proteasomal degradation, as it has previously been demonstrated to be obstructed by DOX molecules which hijack its activity to gain entry into the nucleus (Fekete *et al*., 2005; Kiyomiya *et al*., 2002).

The proteasome is a constituent of the ubiquitin-proteasome pathway, a major bulk degradation system contained in all mammalian cells. It functions to remove long-lived, damaged or misfolded proteins in an ATP- and ubiquitin-dependent manner. Protein folding mainly takes place within the ER and when disturbances in the REDOX status and ER folding capacity occur,

ER stress is triggered due to the build-up of these misfolded proteins within the ER lumen. In response to this stress, the UPR is initiated to relay formation about the degree of protein folding capacity from the rough ER to other cellular locations. In this regard, activation of the UPR momentarily mitigates the rate of protein synthesis and increases genes responsible for encoding chaperones, ER-associated degradation (ERAD) proteins, ER membrane biogenesis enzymes and autophagy regulators (Hetz *et al*., 2008). Essentially, the UPR signalling pathway reduces the build-up of misfolded proteins by amplifying the functional capacity of the ER to promote folding and to eradicate abnormal proteins. This study demonstrated a stark difference in the effect of both DOX and ghrelin on UPR activation (Fig. 3.14). While an expected basal level of UPR activity was observed in the control group which was maintained by ghrelin, DOX downregulated activation of this signalling pathway, whereas both treatments together sustained relative activity. Literature however does not support our observations as DOX is known to induce ER stress due to disruptions in calcium homeostasis and calcium receptors either located on the ER (Mitry *et al*., 2016) or mitochondria (Zhou *et al*., 2001). It is thus plausible to speculate that the effect of DOX on ER stress may be tissue specific in much the same way as its toxic effects are different from its anti-neoplastic activity.

In conclusion, this study demonstrates that the liver is a robust organ that can withstand a great deal of stress and toxicity as weekly administration of DOX did not induce severe liver damage. While liver morphology was altered by DOX, structural parameters measured and function tests remained unchanged. No adverse oxidative damage was observed, nor was there any variation in the anti-oxidant status of this tissue. Molecularly, ghrelin reduced caspase-3 cleavage and increased p62 degradation and LC3-II protein expression. Therefore, while ghrelin's protective effects were mainly observed as a result of its orexigenic properties, its effect against DOX on the liver requires further investigation.

Chapter 5

5.1 Limitations

The major limitation in this study was the fact that this only had one time point of analyses. Additional time points would add value to the study in order to determine the very early changes that may have been induced by either DOX, ghrelin or both treatment regimens.

5.2 Future directions

- To further investigate the cause of liver lobe fusion due to DOX treatment.
- To evaluate the potential role of reticulin in liver lobe fusion.
- To determine the extent of the inflammatory response in this context.
- Due to the fact that the liver is a highly metabolic organ with numerous mitochondria, mitochondrial dynamics should be assessed to better understand the relative molecular changes that take place within this organ as a result of DOX and ghrelin treatment.

Reference list

Abdel-Misih, S.R. and Bloomston, M., 2010. Liver anatomy. *Surgical Clinics of North America*, *90*(4), pp.643-653.

Akamizu, T., Takaya, K., Irako, T., Hosoda, H., Teramukai, S., Matsuyama, A., Tada, H., Miura, K., Shimizu, A., Fukushima, M. and Yokode, M., 2004. Pharmacokinetics, safety, and endocrine and appetite effects of ghrelin administration in young healthy subjects. *European Journal of Endocrinology*, *150*(4), pp.447-455.

Albanis, E., Safadi, R. and Friedman, S.L., 2003. Treatment of hepatic fibrosis: almost there. *Current gastroenterology reports*, *5*(1), pp.48-56.

Albarran-Zeckler, R.G., Sun, Y. and Smith, R.G., 2011. Physiological roles revealed by ghrelin and ghrelin receptor deficient mice. *Peptides*, *32*(11), pp.2229-2235.

Anthony, P.P., Ishak, K.G., Nayak, N.C., Poulsen, H.E., Scheuer, P.J. and Sobin, L.H., 1978. The morphology of cirrhosis. Recommendations on definition, nomenclature, and classification by a working group sponsored by the World Health Organization. *Journal of clinical pathology*, *31*(5), pp.395-414.

Arrick, B.A. and Nathan, C.F., 1984. Glutathione metabolism as a determinant of therapeutic efficacy: a review. *Cancer Research*, *44*(10), pp.4224-4232.

Baldanzi, G., Filigheddu, N., Cutrupi, S., Catapano, F., Bonissoni, S., Fubini, A., Malan, D., Baj, G., Granata, R., Broglio, F. and Papotti, M., 2002. Ghrelin and des-acyl ghrelin inhibit cell death in cardiomyocytes and endothelial cells through ERK1/2 and PI 3-kinase/AKT. *The Journal of cell biology*, *159*(6), pp.1029-1037.

Barazzoni, R., Bosutti, A., Stebel, M., Cattin, M.R., Roder, E., Visintin, L., Cattin, L., Biolo, G., Zanetti, M. and Guarnieri, G., 2005. Ghrelin regulates mitochondrial-lipid metabolism gene expression and tissue fat distribution in liver and skeletal muscle. *American Journal of Physiology-Endocrinology and Metabolism*, *288*(1), pp.E228-E235.

Bataller, R. and Brenner, D.A., 2005. Liver fibrosis. *Journal of clinical investigation*, *115*(2), p.209.

Benbrook, D.M. and Long, A., 2012. Integration of autophagy, proteasomal degradation, unfolded protein response and apoptosis. *Exp Oncol*, *34*(3), pp.286-97.

Bissell, D.M., 1998. Hepatic fibrosis as wound repair: a progress report. *Journal of gastroenterology*, *33*(2), pp.295-302.

Bjørkøy, G., Lamark, T., Brech, A., Outzen, H., Perander, M., Øvervatn, A., Stenmark, H. and Johansen, T., 2005. p62/SQSTM1 forms protein aggregates degraded by autophagy and has a protective effect on huntingtin-induced cell death. *The Journal of cell biology*, *171*(4), pp.603-614.

Bykov, I., Ylipaasto, P., Eerola, L. and Lindros, K.O., 2004. Functional differences between periportal and perivenous Kupffer cells isolated by digitonin-collagenase perfusion. *Comparative hepatology*, *3*(1), p.34.

C Pereira, G., M Silva, A., V Diogo, C., S Carvalho, F., Monteiro, P. and J Oliveira, P., 2011. Drug-induced cardiac mitochondrial toxicity and protection: from doxorubicin to carvedilol. *Current pharmaceutical design*, *17*(20), pp.2113-2129.

Campbell, I., 2006a. Liver: functional anatomy and blood supply. *Anaesthesia & intensive care medicine*, *7*(2), pp.49-51.

Campbell, I., 2006b. Liver: metabolic functions. *Anaesthesia & Intensive Care Medicine*, *7*(2), pp.51-54.

Camps, L., Reina, M., Llobera, M., Bengtsson-Olivecrona, G., Olivecrona, T. and Vilaro, S., 1991. Lipoprotein lipase in lungs, spleen, and liver: synthesis and distribution. *Journal of lipid research*,*32*(12), pp.1877-1888.

Carvalho, C., Santos, R.X., Cardoso, S., Correia, S., Oliveira, P.J., Santos, M.S. and Moreira, P.I., 2009. Doxorubicin: the good, the bad and the ugly effect. *Current medicinal chemistry*, *16*(25), pp.3267-3285.

Castaneda, T.R., Tong, J., Datta, R., Culler, M. and Tschöp, M.H., 2010. Ghrelin in the regulation of body weight and metabolism. *Frontiers in neuroendocrinology*, *31*(1), pp.44-60.

Çetin, E., Kanbur, M., Çetin, N., Eraslan, G. and Atasever, A., 2011. Hepatoprotective effect of ghrelin on carbon tetrachloride-induced acute liver injury in rats. *Regulatory peptides*, *171*(1), pp.1-5.

Cho, Y.E., Mezey, E., Hardwick, J.P., Salem, N., Clemens, D.L. and Song, B.J., 2017. Increased ethanol-inducible cytochrome P450-2E1 and cyto chrome P450 isoforms in exosomes of alcohol-exposed rodents and patients with alcoholism through oxidative and endoplasmic reticulum stress. *Hepatology Communications*, *1*(7), pp.675-690.

Couto, N., Wood, J. and Barber, J., 2016. The role of glutathione reductase and related enzymes on cellular redox homoeostasis network. *Free Radical Biology and Medicine*, *95*, pp.27-42.

Damodar, G., Smitha, T., Gopinath, S., Vijayakumar, S. and Rao, Y.A., 2014. An evaluation of hepatotoxicity in breast cancer patients receiving injection Doxorubicin. *Annals of medical and health sciences research*, *4*(1), pp.74-79.

Dashty, M., 2013. A quick look at biochemistry: carbohydrate metabolism. *Clinical biochemistry*, *46*(15), pp.1339-1352.

Date, Y., Kojima, M., Hosoda, H., Sawaguchi, A., Mondal, M.S., Suganuma, T., Matsukura, S., Kangawa, K. and Nakazato, M., 2000. Ghrelin, a Novel Growth Hormone-Releasing Acylated Peptide, Is Synthesized in a Distinct Endocrine Cell Type in the Gastrointestinal Tracts of Rats and Humans** This work was supported in part by grants-in-aid from the Ministry of Education, Science, Sports, and Culture, Japan, and the Ministry of Health and Welfare, Japan (to MN). *Endocrinology*, *141*(11), pp.4255-4261.

Deniaud, A., Maillier, E., Poncet, D., Kroemer, G., Lemaire, C. and Brenner, C., 2008. Endoplasmic reticulum stress induces calcium-dependent permeability transition, mitochondrial outer membrane permeabilization and apoptosis. *Oncogene*, *27*(3), pp.285-299.

Desai, V.G., Herman, E.H., Moland, C.L., Branham, W.S., Lewis, S.M., Davis, K.J., George, N.I., Lee, T., Kerr, S. and Fuscoe, J.C., 2013. Development of doxorubicin-induced chronic

cardiotoxicity in the B6C3F 1 mouse model. *Toxicology and applied pharmacology*, *266*(1), pp.109-121.

Dietschy, J.M., Turley, S.D. and Spady, D.K., 1993. Role of liver in the maintenance of cholesterol and low density lipoprotein homeostasis in different animal species, including humans. *Journal of lipid research*, *34*(10), pp.1637-1659.

Dirks-Naylor, A.J., 2013. The role of autophagy in doxorubicin-induced cardiotoxicity. *Life sciences*, *93*(24), pp.913-916.

Dixon, J.B., Bhathal, P.S. and O'brien, P.E., 2001. Nonalcoholic fatty liver disease: predictors of nonalcoholic steatohepatitis and liver fibrosis in the severely obese. *Gastroenterology*, *121*(1), pp.91-100.

Dobutovic, B., Sudar, E., Tepavcevic, S., Djordjevic, J., Djordjevic, A., Radojcic, M. and Isenovic, E.R., 2014. Effects of ghrelin on protein expression of antioxidative enzymes and iNOS in the rat liver. *Archives of medical science: AMS*, *10*(4), p.806.

Edmondson, H.A., Peters, R.L., Frankel, H.H. and Borowsky, S., 1967. The early stage of liver injury in the alcoholic. *Medicine*, *46*(2), pp.119-129.

Eisenberg-Lerner, A. and Kimchi, A., 2009. The paradox of autophagy and its implication in cancer etiology and therapy. *Apoptosis*, *14*(4), pp.376-391.

Elmore, S., 2007. Apoptosis: a review of programmed cell death. *Toxicologic pathology*, *35*(4), pp.495-516.

El-Sayyad, H.I., Ismail, M.F., Shalaby, F.M., Abou-El-Magd, R.F., Gaur, R.L., Fernando, A., Raj, M.H. and Ouhtit, A., 2009. Histopathological effects of cisplatin, doxorubicin and 5-flurouracil (5-FU) on the liver of male albino rats. *International journal of biological sciences*, *5*(5), p.466.

Fausto, N., 2000. Liver regeneration. *Journal of hepatology*, *32*, pp.19-31.

Fausto, N., Campbell, J.S. and Riehle, K.J., 2006. Liver regeneration. *Hepatology*, *43*(S1).

Fekete, M.R., McBride, W.H. and Pajonk, F., 2005. Anthracyclines, proteasome activity and multi-drug-resistance. *BMC cancer*, *5*(1), p.114.

Friedman, S.L., 2000. Molecular regulation of hepatic fibrosis, an integrated cellular response to tissue injury. *Journal of Biological Chemistry*, *275*(4), pp.2247-2250.

Gauna, C., Delhanty, P.J., Hofland, L.J., Janssen, J.A., Broglio, F., Ross, R.J., Ghigo, E. and van der Lely, A.J., 2005. Ghrelin stimulates, whereas des-octanoyl ghrelin inhibits, glucose output by primary hepatocytes. *The Journal of Clinical Endocrinology & Metabolism*, *90*(2), pp.1055-1060.

Gebhardt, R., 1992. Metabolic zonation of the liver: regulation and implications for liver function. *Pharmacology & therapeutics*, *53*(3), pp.275-354.

Ghigo, A., Li, M. and Hirsch, E., 2016. New signal transduction paradigms in anthracycline-induced cardiotoxicity. *Biochimica et Biophysica Acta (BBA)-Molecular Cell Research*, *1863*(7), pp.1916-1925.

Giannini, E.G., Testa, R. and Savarino, V., 2005. Liver enzyme alteration: a guide for clinicians. *Canadian medical association journal*, *172*(3), pp.367-379.

Glider, W.V., 2011. Using Mammal Study Skins to Investigate the Relationship between Surface Area to Volume Ratio and Mass of Two Size Classes of Mammals. *Proceedings of the Association for Biology Laboratory Education (32),* pp. 346 -353, viewed: 5 December 2017 from http://www.ableweb.org/volumes/vol-32/v32reprint.php?ch=34

Griffin, B.A., 2013. Lipid metabolism. *Surgery (Oxford)*, *31*(6), pp.267-272.

Gurtner, G.C., Werner, S., Barrandon, Y. and Longaker, M.T., 2008. Wound repair and regeneration. *Nature*, *453*(7193), pp.314-321.

Gustafsson, Å.B. and Gottlieb, R.A., 2003. Mechanisms of apoptosis in the heart. *Journal of clinical immunology*, *23*(6), pp.447-459.

Gutteridge, J.M., 1995. Lipid peroxidation and antioxidants as biomarkers of tissue damage. *Clinical chemistry*, *41*(12), pp.1819-1828.

Halliwell, B. and Chirico, S., 1993. Lipid peroxidation: its mechanism, measurement, and significance. *The American journal of clinical nutrition*, *57*(5), pp.715S-724S.

Hanna, A.D., Lam, A., Tham, S., Dulhunty, A.F. and Beard, N.A., 2014. Adverse effects of doxorubicin and its metabolic product on cardiac RyR2 and SERCA2A. *Molecular pharmacology*, *86*(4), pp.438-449.

Hetz, C., Lee, A.H., Gonzalez-Romero, D., Thielen, P., Castilla, J., Soto, C. and Glimcher, L.H., 2008. Unfolded protein response transcription factor XBP-1 does not influence prion replication or pathogenesis. *Proceedings of the National Academy of Sciences*, *105*(2), pp.757-762.

Hijmans, B.S., Grefhorst, A., Oosterveer, M.H. and Groen, A.K., 2014. Zonation of glucose and fatty acid metabolism in the liver: mechanism and metabolic consequences. *Biochimie*, *96*, pp.121-129.

Hong, H., Patonay, B. and Finley, J., 2011. Unusual reticulin staining pattern in well-differentiated hepatocellular carcinoma. *Diagnostic pathology*, *6*(1), p.15.

Hosoda, H., Kojima, M., Mizushima, T., Shimizu, S. and Kangawa, K., 2003. Structural divergence of human ghrelin identification of multiple ghrelin-derived molecules produced by post-translational processing. *Journal of Biological Chemistry*, *278*(1), pp.64-70.

Høyer-Hansen, M. and Jäättelä, M., 2007. Connecting endoplasmic reticulum stress to autophagy by unfolded protein response and calcium. *Cell Death & Differentiation*, *14*(9), pp.1576-1582.

Hsu, H., Xiong, J. and Goeddel, D.V., 1995. The TNF receptor 1-associated protein TRADD signals cell death and NF-κB activation. *Cell*, *81*(4), pp.495-504.

Injac, R., Perse, M., Cerne, M., Potocnik, N., Radic, N., Govedarica, B., Djordjevic, A., Cerar, A. and Strukelj, B., 2009. Protective effects of fullerenol C 60 (OH) 24 against doxorubicin-induced cardiotoxicity and hepatotoxicity in rats with colorectal cancer. *Biomaterials*, *30*(6), pp.1184-1196.

İşeri, S.Ö., Şener, G., Saglam, B., Ercan, F., Gedik, N. and Yeğen, B.Ç., 2008. Ghrelin alleviates biliary obstruction-induced chronic hepatic injury in rats. *Regulatory peptides*, *146*(1), pp.73-79.

Jafari, M., 2007. Dose-and time-dependent effects of sulfur mustard on antioxidant system in liver and brain of rat. *Toxicology*, *231*(1), pp.30-39.

Kalender, Y., Yel, M. and Kalender, S., 2005. Doxorubicin hepatotoxicity and hepatic free radical metabolism in rats: the effects of vitamin E and catechin. *Toxicology*, *209*(1), pp.39-45.

Kassner, N., Huse, K., Martin, H.J., Gödtel-Armbrust, U., Metzger, A., Meineke, I., Brockmöller, J., Klein, K., Zanger, U.M., Maser, E. and Wojnowski, L., 2008. Carbonyl reductase 1 is a predominant doxorubicin reductase in the human liver. *Drug Metabolism and Disposition*, *36*(10), pp.2113-2120.

Kawaguchi, T., Takemura, G., Kanamori, H., Takeyama, T., Watanabe, T., Morishita, K., Ogino, A., Tsujimoto, A., Goto, K., Maruyama, R. and Kawasaki, M., 2012. Prior starvation mitigates acute doxorubicin cardiotoxicity through restoration of autophagy in affected cardiomyocytes. *Cardiovascular research*, *96*(3), pp.456-465.

Keizer, H.G., Pinedo, H.M., Schuurhuis, G.J. and Joenje, H., 1990. Doxorubicin (adriamycin): a critical review of free radical-dependent mechanisms of cytotoxicity. *Pharmacology & therapeutics*, *47*(2), pp.219-231.

Kiyomiya, K.I., Kurebe, M., Nakagawa, H. and Matsuo, S., 2002. The role of the proteasome in apoptosis induced by anthracycline anticancer agents. *International journal of oncology*, *20*(6), pp.1205-1209.

Kobayashi, S., Volden, P., Timm, D., Mao, K., Xu, X. and Liang, Q., 2010. Transcription factor GATA4 inhibits doxorubicin-induced autophagy and cardiomyocyte death. *Journal of Biological Chemistry*, *285*(1), pp.793-804.

Kojima, M., Hosoda, H., Date, Y., Nakazato, M., Matsuo, H. and Kangawa, K., 1999. Ghrelin is a growth-hormone-releasing acylated peptide from stomach. *Nature*, *402*(6762), pp.656-660.

Koyuturk, M., Sacan, O., Karabulut, S., Turk, N., Bolkent, S., Yanardag, R. and Bolkent, S., 2015. The role of ghrelin on apoptosis, cell proliferation and oxidant-antioxidant system in the liver of neonatal diabetic rats. *Cell biology international*, *39*(7), pp.834-841.

Krishna, M., 2013. Role of special stains in diagnostic liver pathology. *Clinical Liver Disease*, *2*(S1).

Lal, S., Mahajan, A., Ning Chen, W. and Chowbay, B., 2010. Pharmacogenetics of target genes across doxorubicin disposition pathway: a review. *Current drug metabolism*, *11*(1), pp.115-128.

Lecker, S.H., Goldberg, A.L. and Mitch, W.E., 2006. Protein degradation by the ubiquitin–proteasome pathway in normal and disease states. *Journal of the American Society of Nephrology*, *17*(7), pp.1807-1819.

Lee, J.H., Kim, T.J., Kim, J.W., Yoon, J.S., Kim, H.S. and Lee, K.M., 2016. The Anti-apoptotic Effect of Ghrelin on Restraint Stress-Induced Thymus Atrophy in Mice. *Immune network*, *16*(4), pp.242-248.

Lefkowitch, J.H., 2006, November. Special stains in diagnostic liver pathology. In *Seminars in diagnostic pathology* (Vol. 23, No. 3, pp. 190-198). WB Saunders.

Leite-Moreira, A.F. and Soares, J.B., 2007. Physiological, pathological and potential therapeutic roles of ghrelin. *Drug discovery today*, *12*(7), pp.276-288.

Li, Y., Hai, J., Li, L., Chen, X., Peng, H., Cao, M. and Zhang, Q., 2013. Administration of ghrelin improves inflammation, oxidative stress, and apoptosis during and after non-alcoholic fatty liver disease development. *Endocrine*, *43*(2), pp.376-386.

Limón-Pacheco, J. and Gonsebatt, M.E., 2009. The role of antioxidants and antioxidant-related enzymes in protective responses to environmentally induced oxidative stress. *Mutation Research/Genetic Toxicology and Environmental Mutagenesis*, *674*(1), pp.137-147.

Lu, L., Wu, W., Yan, J., Li, X., Yu, H. and Yu, X., 2009. Adriamycin-induced autophagic cardiomyocyte death plays a pathogenic role in a rat model of heart failure. *International journal of cardiology*, *134*(1), pp.82-90.

Luo, X., Evrovsky, Y., Cole, D., Trines, J., Benson, L.N. and Lehotay, D.C., 1997. Doxorubicin-induced acute changes in cytotoxic aldehydes, antioxidant status and cardiac function in the rat. *Biochimica et Biophysica Acta (BBA)-Molecular Basis of Disease*, *1360*(1), pp.45-52.

Malarkey, D.E., Johnson, K., Ryan, L., Boorman, G. and Maronpot, R.R., 2005. New insights into functional aspects of liver morphology. *Toxicologic pathology*, *33*(1), pp.27-34.

Maughan, R., 2013. Carbohydrate metabolism. *Surgery (Oxford)*, *31*(6), pp.273-277.

Meusser, B., Hirsch, C., Jarosch, E. and Sommer, T., 2005. ERAD: the long road to destruction. *Nature cell biology*, *7*(8), pp.766-772.

Michalopoulos, G.K. and DeFrances, M.C., 1997. Liver regeneration. *Science*, *276*(5309), pp.60-66.

Minotti, G., Menna, P., Salvatorelli, E., Cairo, G. and Gianni, L., 2004. Anthracyclines: molecular advances and pharmacologic developments in antitumor activity and cardiotoxicity. *Pharmacological reviews*, *56*(2), pp.185-229.

Mitra, V. and Metcalf, J., 2009. Metabolic functions of the liver. *Anaesthesia & Intensive Care Medicine*, *10*(7), pp.334-335.

Mitry, M.A. and Edwards, J.G., 2016. Doxorubicin induced heart failure: Phenotype and molecular mechanisms. *IJC Heart & Vasculature*, *10*, pp.17-24.

Mizushima, N., 2007. Autophagy: process and function. *Genes & development*, *21*(22), pp.2861-2873.

Mizutani, H., Tada-Oikawa, S., Hiraku, Y., Kojima, M. and Kawanishi, S., 2005. Mechanism of apoptosis induced by doxorubicin through the generation of hydrogen peroxide. *Life sciences*, *76*(13), pp.1439-1453.

Muccioli, G., Tschöp, M., Papotti, M., Deghenghi, R., Heiman, M. and Ghigo, E., 2002. Neuroendocrine and peripheral activities of ghrelin: implications in metabolism and obesity. *European journal of pharmacology*, *440*(2), pp.235-254.

Müller, T.D., Nogueiras, R., Andermann, M.L., Andrews, Z.B., Anker, S.D., Argente, J., Batterham, R.L., Benoit, S.C., Bowers, C.Y., Broglio, F. and Casanueva, F.F., 2015. Ghrelin. *Molecular metabolism*, *4*(6), pp.437-460.

Nagai, K., Nogami, S., Egusa, H. and Konishi, H., 2014. Pharmacokinetic evaluation of intraperitoneal doxorubicin in rats.*Die Pharmazie-An International Journal of Pharmaceutical Sciences*,*69*(2), pp.125-127.

Neary, N.M., Small, C.J., Wren, A.M., Lee, J.L., Druce, M.R., Palmieri, C., Frost, G.S., Ghatei, M.A., Coombes, R.C. and Bloom, S.R., 2004. Ghrelin increases energy intake in cancer patients with impaired appetite: acute, randomized, placebo-controlled trial. *The Journal of Clinical Endocrinology & Metabolism*, *89*(6), pp.2832-2836.

Ory, D.S., 2007. Chylomicrons and lipoprotein lipase at the endothelial surface: bound and GAG-ged.*Cell metabolism*, *5*(4), pp.229-231.

Ow, Y.L.P., Green, D.R., Hao, Z. and Mak, T.W., 2008. Cytochrome c: functions beyond respiration. *Nature Reviews Molecular Cell Biology*, *9*(7), pp.532-542.

Ozols, R.F., Young, R.C., Speyer, J.L., Sugarbaker, P.H., Greene, R., Jenkins, J. and Myers, C.E., 1982. Phase I and pharmacological studies of adriamycin administered intraperitoneally to patients with ovarian cancer. *Cancer research*, *42*(10), pp.4265-4269.

Pellicoro, A., Ramachandran, P., Iredale, J.P. and Fallowfield, J.A., 2014. Liver fibrosis and repair: immune regulation of wound healing in a solid organ. *Nature Reviews Immunology*, *14*(3), pp.181-194.

Pieniążek, A., Czepas, J., Piasecka-Zelga, J., Gwoździński, K. and Koceva-Chyła, A., 2013. Oxidative stress induced in rat liver by anticancer drugs doxorubicin, paclitaxel and docetaxel. *Advances in medical sciences*, *58*(1), pp.104-111.

Popovic, D. and Dikic, I., 2012. The molecular basis of selective autophagy. *Biochemist*, *34*, pp.24-30.

Raychaudhuri, S., Skommer, J., Henty, K., Birch, N. and Brittain, T., 2010. Neuroglobin protects nerve cells from apoptosis by inhibiting the intrinsic pathway of cell death. *Apoptosis*, *15*(4), pp.401-411.

Reagan, W.J., Yang, R.Z., Park, S., Goldstein, R., Brees, D. and Gong, D.W., 2012. Metabolic adaptive ALT isoenzyme response in livers of C57/BL6 mice treated with dexamethasone. *Toxicologic pathology*, *40*(8), pp.1117-1127.

Rutkowski, D.T. and Kaufman, R.J., 2007. That which does not kill me makes me stronger: adapting to chronic ER stress. *Trends in biochemical sciences*, *32*(10), pp.469-476.

Şehirli, Ö., Şener, E., Şener, G., Çetinel, Ş., Erzik, C. and Yeğen, B.Ç., 2008. Ghrelin improves burn-induced multiple organ injury by depressing neutrophil infiltration and the release of pro-inflammatory cytokines. *Peptides*, *29*(7), pp.1231-1240.

Shang, F. and Taylor, A., 2011. Ubiquitin–proteasome pathway and cellular responses to oxidative stress. *Free Radical Biology and Medicine*, *51*(1), pp.5-16.

Sherwood, L., 2013. *Introduction to human physiology*. Brooks/Cole.

Shintani, M., Ogawa, Y., Ebihara, K., Aizawa-Abe, M., Miyanaga, F., Takaya, K., Hayashi, T., Inoue, G., Hosoda, K., Kojima, M. and Kangawa, K., 2001. Ghrelin, an endogenous growth hormone secretagogue, is a novel orexigenic peptide that antagonizes leptin action through the activation of hypothalamic neuropeptide Y/Y1 receptor pathway. *Diabetes*, *50*(2), pp.227-232.

Šimůnek, T., Štěrba, M., Popelová, O., Adamcová, M., Hrdina, R. and Geršl, V., 2009. Anthracycline-induced cardiotoxicity: overview of studies examining the roles of oxidative stress and free cellular iron. *Pharmacological Reports*, *61*(1), pp.154-171.

Sishi, B.J., Loos, B., van Rooyen, J. and Engelbrecht, A.M., 2013a. Doxorubicin induces protein ubiquitination and inhibits proteasome activity during cardiotoxicity. *Toxicology*, *309*, pp.23-29.

Sishi, B.J., Loos, B., van Rooyen, J. and Engelbrecht, A.M., 2013b. Autophagy upregulation promotes survival and attenuates doxorubicin-induced cardiotoxicity. *Biochemical pharmacology*, *85*(1), pp.124-134.

Smith, R.G., Jiang, H. and Sun, Y., 2005. Developments in ghrelin biology and potential clinical relevance. *Trends in Endocrinology & Metabolism*, *16*(9), pp.436-442.

Smuder, A.J., Kavazis, A.N., Min, K. and Powers, S.K., 2013. Doxorubicin-induced markers of myocardial autophagic signaling in sedentary and exercise trained animals. *Journal of applied physiology*, *115*(2), pp.176-185.

Suh, D.H., Kim, M.K., Kim, H.S., Chung, H.H. and Song, Y.S., 2012. Unfolded protein response to autophagy as a promising druggable target for anticancer therapy. *Annals of the New York Academy of Sciences*, *1271*(1), pp.20-32.

Swamy, A.V., Gulliaya, S., Thippeswamy, A., Koti, B.C. and Manjula, D.V., 2012. Cardioprotective effect of curcumin against doxorubicin-induced myocardial toxicity in albino rats. *Indian journal of pharmacology*, *44*(1), p.73.

Tacar, O., Sriamornsak, P. and Dass, C.R., 2013. Doxorubicin: an update on anticancer molecular action, toxicity and novel drug delivery systems. *Journal of Pharmacy and Pharmacology*, *65*(2), pp.157-170.

Takahashi, Y. and Fukusato, T., 2014. Histopathology of nonalcoholic fatty liver disease/nonalcoholic steatohepatitis. *World journal of gastroenterology: WJG*, *20*(42), p.15539.

Tanaka, Y., Nagasued, N., Kanashima, R., Inokuchi, K. and Shirota, A., 1982. Effect of doxorubicin on liver regeneration and host survival after two–thirds hepatectomy in rats. *Cancer*, *49*(1), pp.19-24.

Thapa, B.R. and Walia, A., 2007. Liver function tests and their interpretation. *Indian Journal of Pediatrics*, *74*(7), pp.663-671.

Tsai, Y.C. and Weissman, A.M., 2010 The Unfolded Protein Response, Degradation from Endoplasmic Reticulum and Cancer. *Genes Cancer. 1* (7): 764–78.

Tschöp, M., Smiley, D.L. and Heiman, M.L., 2000. Ghrelin induces adiposity in rodents. *Nature*, *407*(6806), pp.908-913.

Van Der Lely, A.J., Tschöp, M., Heiman, M.L. and Ghigo, E., 2004. Biological, physiological, pathophysiological, and pharmacological aspects of ghrelin. *Endocrine reviews*, *25*(3), pp.426-457.

Vestergaard, E.T., Djurhuus, C.B., Gjedsted, J., Nielsen, S., Møller, N., Holst, J.J., Jørgensen, J.O.L. and Schmitz, O., 2008. Acute effects of ghrelin administration on glucose and lipid metabolism. *The Journal of Clinical Endocrinology & Metabolism*, *93*(2), pp.438-444.

Von Hoff, D.D., Layard, M.W., Basa, P., Davis Jr, H.L., Von Hoff, A.L., Rozencweig, M. and Muggia, F.M., 1979. Risk factors for doxorubicin-induced congestive heart failure. *Ann Intern Med*, *91*(5), pp.710-717.

Walter, P. and Ron, D., 2011. The unfolded protein response: from stress pathway to homeostatic regulation. *Science*, *334*(6059), pp.1081-1086.

Wang, X., Wang, X.L., Chen, H.L., Wu, D., Chen, J.X., Wang, X.X., Li, R.L., He, J.H., Mo, L., Cen, X. and Wei, Y.Q., 2014. Ghrelin inhibits doxorubicin cardiotoxicity by inhibiting excessive autophagy through AMPK and p38-MAPK. *Biochemical pharmacology*, *88*(3), pp.334-350.

Wren, A.M., Small, C.J., Ward, H.L., Murphy, K.G., Dakin, C.L., Taheri, S., Kennedy, A.R., Roberts, G.H., Morgan, D.G.A., Ghatei, M.A. and Bloom, S.R., 2000. The novel hypothalamic peptide ghrelin stimulates food intake and growth hormone secretion. *Endocrinology*, *141*(11), pp.4325-4328.

Young, B., Woodford, P. and O'Dowd, G., 2013. *Wheater's functional histology: a text and colour atlas*. Elsevier Health Sciences.

Zámbó, V., Simon-Szabó, L., Szelényi, P., Kereszturi, É., Bánhegyi, G. and Csala, M., 2013. Lipotoxicity in the liver. *World journal of hepatology*, *5*(10), p.550.

Zaret, K.S. and Grompe, M., 2008. Generation and regeneration of cells of the liver and pancreas. *Science*, *322*(5907), pp.1490-1494.

Zhang, K. and Kaufman, R.J., 2008. From endoplasmic-reticulum stress to the inflammatory response. *Nature*, *454*(7203), pp.455-462.

Zhang, W., Chen, X.P., Zhang, W.G., Zhang, F., Xiang, S., Dong, H.H. and Zhang, L., 2009. Hepatic non-parenchymal cells and extracellular matrix participate in oval cell-mediated liver regeneration. *World journal of gastroenterology: WJG*, *15*(5), p.552.

Zhou, S., Heller, L.J. and Wallace, K.B., 2001. Interference with calcium-dependent mitochondrial bioenergetics in cardiac myocytes isolated from doxorubicin-treated rats. *Toxicology and applied pharmacology*, *175*(1), pp.60-67.

Appendix A

Normalization graphs for western blot and loading controls

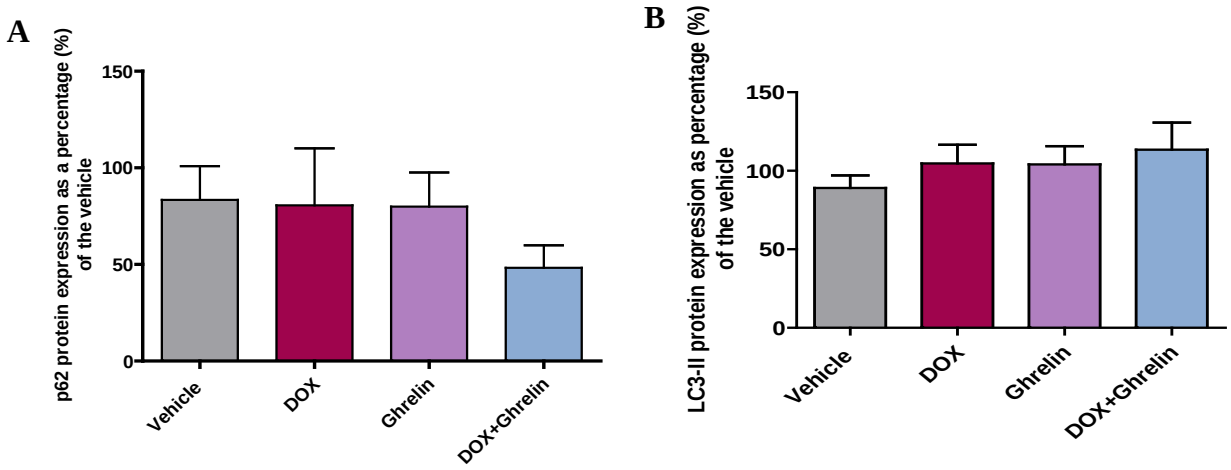

Fig. 4.1: Normalization of relative protein expression of p62 (A) and LC3-II (B). The lane analysis is shown where protein expression of p62 and LC3-II was normalized to total lane protein and the results are expressed as a percentage (%) of the vehicle. Animals were treated (i.p) with saline (vehicle), DOX, ghrelin and a combination of the two. Results are presented as mean ± SEM (n = 5-6). Abbreviations: **DOX** – doxorubicin

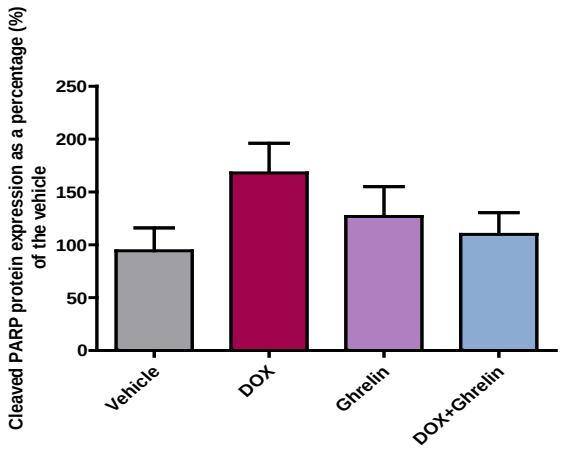

Fig. 4.2: Normalization of relative protein expression of cleaved PARP. The lane analysis is shown where protein expression cleaved PARP was normalized to total lane protein and the results are expressed as a percentage (%) of the vehicle. Animals were treated (i.p) with saline (vehicle), DOX, ghrelin and a combination of the two. Results are presented as mean ± SEM (n = 5-6). Abbreviations: **DOX** – doxorubicin

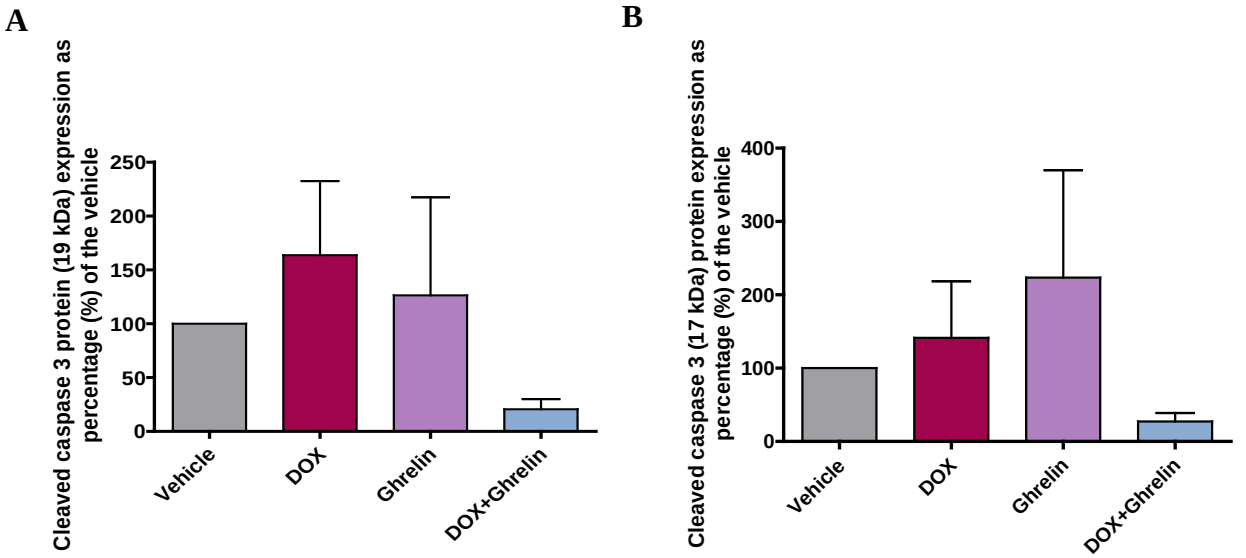

Fig. 4.3: Normalization of relative protein expression of cleaved caspase 3 (A) 19 kDa (B) 17 kDa. The lane analysis are shown where protein expression of cleaved caspase 3 (19 kDa and 17 kDa) was normalized to total lane protein and the results are expressed as a percentage (%) of the vehicle. Animals were treated (i.p) with saline (vehicle), DOX, ghrelin and a combination of the two. Results are presented as mean ± SEM (n = 3-5). Abbreviations: **DOX** – doxorubicin

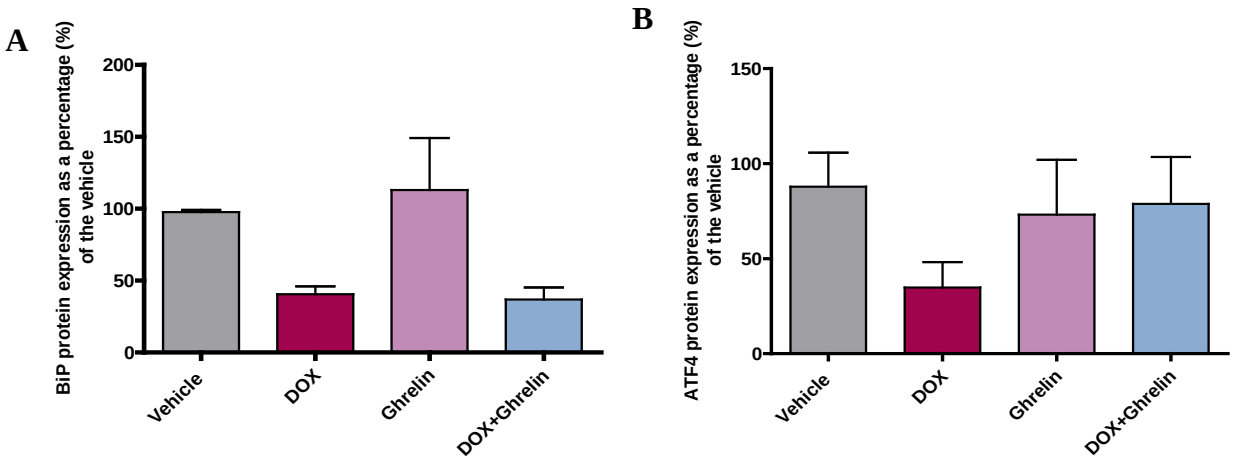

Fig. 4.4: Normalization of relative protein expression of BiP (A) and ATF4 (B). The lane analysis are shown where protein expression of BiP and ATF4 was normalized to total lane protein and the results are expressed as a percentage (%) of the vehicle. Animals were treated (i.p) with saline (vehicle), DOX, ghrelin and a combination of the two. Results are presented as mean ± SEM (n = 5-6). Abbreviations: **DOX** – doxorubicin

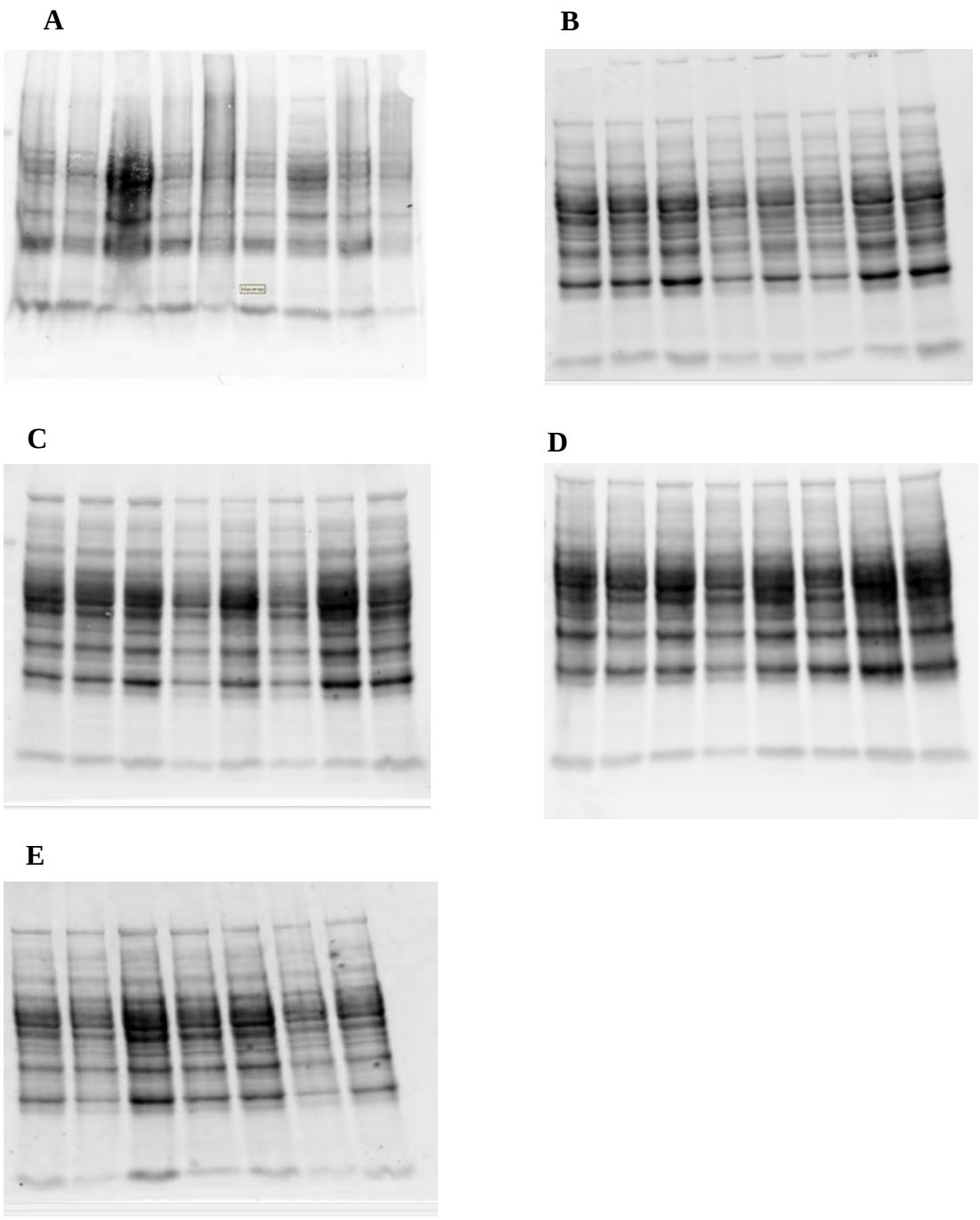

Fig. 4.5: Loading controls for the western blots. Membrane activation which indicates loading control for the western blot bands where (A) Cleaved caspase 3 (B) Cleaved PARP (C) p62 (D) LC3-I and LC3-II and (E) BiP and ATF4

Appendix B

Ethical clearance letter for animal study.

UNIVERSITEIT·STELLENBOSCH·UNIVERSITY
jou kennisvennoot • your knowledge partner

Approved with Stipulations

Date: 29-Apr-2016

PI Name: Goldswain, Toni T

Protocol #: SU-ACUD15-00038

Title: Investigating the role of the RISK and SAFE pathways, through ghrelin stimulation, in an in vivo rat model of chronic Doxorubicin-induced cardiotoxicity.

Dear Toni Goldswain, the Response to Modifications submission was reviewed on 26-Apr-2016 by Research Ethics Committee: Animal Care and Use via committee review procedures and was approved on condition that the following stipulations are adhered to:

1. South African Veterinary Council authorisation for Dr Bester is not addressed in the response to modification. Sodium Pentobarbital is a scheduled substance, the committee recommend a suitable person be responsible for euthanasia using this substance. By suitable, referring to a person registered with SAVC or alternatively authorised by SAVC to do this procedure.

Applicants are reminded that they are expected to comply with accepted standards for the use of animals in research and teaching as reflected in the South African National Standards 10386: 2008. The SANS 10386: 2008 document is available on the Division for Research Developments website www.sun.ac.za/research.

As provided for in the Veterinary and Para-Veterinary Professions Act, 1982. It is the principal investigator's responsibility to ensure that all study participants are registered with or have been authorised by the South African Veterinary Council (SAVC) to perform the procedures on animals, or will be performing the procedures under the direct and continuous supervision of a SAVC-registered veterinary professional or SAVC-registered para-veterinary professional, who are acting within the scope of practice for their profession.

Please remember to use your protocol number, SU-ACUD15-00038 on any documents or correspondence with the REC: ACU concerning your research protocol.

Any event not consistent with routine expected outcomes that results in any unexpected animal welfare issue (death, disease, or prolonged distress) or human health risks (zoonotic disease or exposure, injuries) must be reported to the committee, by creating an Adverse Event submission within the system.

If you have any questions or need further help, please contact the REC: ACU secretariat at WABEUKES@SUN.AC.ZA or 0218089003.

Sincerely,

Winston Beukes

REC: ACU Secretariat

Appendix C

Preparation of DOX and ghrelin for animal treatment

DOX was prepared as follows:

50 mg DOX (LKT Laboratories, D5794, USA) in 12.5 ml sterile saline to give a stock solution of 4 mg/ml = 4 µg/µL. This solution was vortexed thoroughly.

Animal dose = 2.5 mg/kg = 2.5 µg/g

Example: Animal weight = 118.1 g

118.1 g x 2.5 µg/g

295.25 µg DOX

Stock = 4µg/µL

$$\frac{4\ \mu g}{1\ \mu L} = \frac{295.25\ \mu g}{\chi}$$

X = 73.8125 µL DOX stock (4 µg/µL) and add sterile saline to create a total volume of 200 µl (200 µL is the injection volume)

BUT…multiply by 2 to account for bubbles and wastage.

73.8125 x 2 = 147.625 µL DOX in 253.375 µL saline

Vortex thoroughly

Inject 200 µL

Ghrelin was prepared as follows:

5 mg ghrelin (LKT Laboratories, G2869, USA) was suspended in 5 mL sterile saline to give stock solution of 1 mg/mL = 1 µg/µL. This solution was vortexed thoroughly.

Animal dose: 100 µg/kg = 0.1 µg/g

Example: Animal weight: 118.1 g

118.1 x 0.1 µg/g

11.81 µg ghrelin

Stock = 1 µg/µL

$$\frac{1\ \mu g}{1\ \mu L} = \frac{11.81\ \mu g}{x}$$

X = 11.81 µL of ghrelin stock solution and add sterile saline to create a total volume of 200 µl (200 µL is the injection volume)

BUT…multiply by 2 to account for bubbles and wastage

Inject 200 µL

Appendix D

Liver function tests

Protocol 1: Alanine transaminase activity assay

Alanine Transaminase Activity Assay Kit (colorimetric/Flouremnitric) (Abcam, ab105134, SA) was used for the detection of ALT in the serum. The colorimetric assay was executed according the manufacturer's instructions.

Reagent and sample preparation

1. Thaw the serum on ice
2. The ALT assay buffer is ready to use as supplied. Equilibrate to room temperature before use.
3. Oxired probe warmed at 37°C for 1-5 minutes to thaw the DMSO in the solution.
4. Reconstitute the ALT enzyme mix with 220 µl distilled water and keep on ic e while in use.
5. Reconstitute the ALT substrate with 1.1 ml Assay buffer and keep on ice while in use.
6. Pyruvate standard is ready to use as supplied and keep on ice while in use.
7. Reconstitute the ALT positive control with 100 µl of distilled water and keep on ice while in use.

Assay procedure and detection

1. Prepare a standard to run with the samples:
    a. Prepare a 1 nmol/µl Pyruvate Standard by diluting 5 µl Pyruvate standard in 495 µl of ALT assay buffer .
    b. Use the 1 nmol/µl Pyruvate Standard to prepare the standard curve dilution as described in the table below:

Standard #	Volume of standard (µl)	Assay Buffer (µl)	Final Volume standard in well	Concentration of ALT in well (nmol/well)
1	0	60	20	0

2	6	54	20	2
3	12	48	20	4
4	18	42	20	6
5	24	36	20	8
6	30	30	20	10

2. Set up the reactions wells in clear 96 well plate.
    a. Standard wells = 20 µl of a standard dilution. The standards should be tested in triplicate.
    b. Sample wells = 2-20 µl sample and then adjust the volume to 20 µl with the ALT assay buffer. Sample should be tested in duplicate or triplicate
    c. Positive control = 5-10 µl positive control in a well and then adjust the volume to 20 µl with the ALT assay buffer.

3. Prepare the reaction mixture as described in the table below. Prepare 100 µl of reactioin mix per well. Thus, prepare a master mix of the reaction mix for the amount of standards, positive control and samples tested. This will ensure consistency.

Component	**Colorimetric reaction mix (µl)**
ALT assay buffer	86
Oxired probe	2
ALT enzyme mix	2
ALT substrate	10

4. Add 100 µl of the reaction mix into each well of standard, sample and positive control.
5. Measure the absorbance on a microplate reader (BMG Labtech, SPECTROstar nano, Germany) at 570 nm in a kinetic mode after 10 minutes, every 2 - 3 minutes, for atleast 60 minutes at 37˚C protected from light.

Processing of the results

1. Average the duplicate/triplicate reading for each standard and sample.

2. Subtract the mean absorbance value of the blank (standard #1) from all standard and sample readings.
3. Plot the corrected absorbance values for each standard as a function of the final concentration of pyruvate.
4. Draw the best smooth curve through these points to construct the standard curve. Calculate the trendline equation based on your standard curve data (use the equation that provides the most accurate fit).
5. Calculate the ALT activity for your samples with the following equation:

$$\Delta A570\ nm = A2 - A1$$

Where:

A1 is the sample reading at the T1

A2 is the sample reading at the T2

6. Then use the ΔA570 nm to obtain the B nm of pyruvate generated by ALT during the reaction time (ΔT = A2 – A1).
7. The concentration of pyruvate in the test sample is calculated as:

$$ALT\ activity = \left(\frac{B}{\Delta T x V}\right)\ x\ D$$

ALT activity = nmol/min/ml = mU/ml

Where:

B = Amount of pyruvate from standard curve

ΔT = reaction time

V = original sample volume added to the reaction well in ml

D = sample dilution factor

Unit definition: 1 unit ALT = the amount of ALT that generates 1.0 µmol of pyruvate per min at 37 ˚C.

Protocol 2: Albumin Rat ELISA Kit

The Albumin Rat ELISA Kit albumin (Abcam, ab108790, SA) was used to measure Albumin in the plasma. The ELISA was executed according to the manufacturer's instructions.

Reagent preparation

1. Thaw the plasma on ice
2. Equilibrate all the reagents to room temperature (18-25˚C)
3. Dilute the 10X diluent N concentrate 10-fold with distilled water to produce a 1X diluent.
4. Dilute the 20X wash buffer concentrate 20-fold with distilled water abd mix gently and thoroughly.
5. Add 4.5 ml of the 1X diluent N to the lyophilized biotinylated albumin vial to generate a working solution. Allow the vial to sit for 10 minutes with gentle agitation prior to use. Spin down the 100X streptavidin-peroxidase conjugate (SP conjugate) briefly and dilute the desired amount of the conjugate 100-fold with 1X diluent N.
6. Chromogen substrate ready to use as supplied
7. Albumin standard ready to use as supplied
8. Stop solution ready to use as supplied
9. Albumin Microplate 96 wells ready to use as supplied
10. Sealing tape ready to use as supplied

Standard preparation

1. Reconstitute the albumin standard vial to prepare 50 µg/ml of Albumin standard #1:
    a. Consult the albumin standard vial to determine the mass of protein in the vial.
    b. Calculate the appropriate volume of 1X diluent to add to the albumin standard vial to produce a concentration of 50 µg/ml, by using the following equation:

$$\left(\frac{C_S}{C_F}\right) x\ 1{,}000 = V_D$$

Where:

C_S = starting mass of albumin standard (see vial label) (µg)

C_F = The 50 µg/ml albumin standard #1 final required concentration

V_D = Required volume of 1X Diluent N for reconstitution

c. Briefly spin down your albumin standard vial to collect the contents at the bottom of the tube.
d. Reconstitute the albumin standard vial with the appropriate volume of 1X diluent.
e. Mix gently and thoroughly.
f. Allow to sit for 10 minutes before use

2. Label seven tubes #2-8
3. Add 120 µl of 1X diluent N to tube #2-8
4. To prepare standard #2, add 120 µl of the standard #1 to tube #2 and mix gently
5. To prepare standard #3, add 120 µl of standard #2 into tube #3 and mix gently
6. Prepare subsequent serial dilutions using the table below as a guide:

Standard #	Volume to dilute (µl)	Volume Diluent N (µl)	Total volume (µl)	Starting concentration (µg/ml)	Final Concentration (µg/ml)
1	Step 1				50
2	120	120	240	50.00	25
3	120	120	240	25.00	12.50
4	120	120	240	12.50	6.250
5	120	120	240	6.250	3.125
6	120	120	240	3.125	1.563
7	120	120	240	1.563	0.781
8		120	120	0.00	0

Assay procedure

1. Prepare all the reagents as instructed and equilibrate to room temperature prior to use. The assay is performed at room temperature (18 - 25˚C).
2. Remove excess microplate strips from the plate frame and return them immediately to the foil pouch with the desiccant inside.
3. Add 25 µl of Albumin standard or sample per well and immediately add 25 µl of biotinylated albumin protein to each well, on top of the standard or sample. The standard

should be tested in triplicate and the sample in duplicate/triplicate. Gently ta plate to ensure thorough mixing and break any bubbles that may have formed. Cover the wells with the sealing tape and incubate for 1 hour. Start the hour after the last sample addition.

4. Wash five times with 200 µl of 1X wash buffer manually. Invert the plate each time and decant the contents by tapping it 4-5 times on absorbent paper towel to completely remove the liquid.
5. Add 50 µl of 1X SP conjugate to each well. Gently tap plate to thoroughly coat wells. Break any bubbles that may have formed. Cover wells with sealing tape and incubate for 30 minutes. Turn on the microplate reader and setup the program in advance.
6. Wash microplate as described above
7. Add 50 µl of chromogen substrate per well. Gently tap plate to thoroughly coat the wells. Break any bubbles that may have formed. Incubate for 10 minutes or until the optimal blue colour density has formed.
8. Add 50 µl of stop solution to each well. The colour will change from blue to yellow. Gently tap plate to ensure thorough mixing. Break any bubbles that may have formed.
9. Read the absorbance on a microplate reader immediately at a wavelength of 450 nm.

Calculations to determine concentration of Albumin in the plasma

1. Calculate the mean value of the triplicate/duplicate absorbance readings for each standard and sample.
2. Generate a standard curve by plotting the graph using the standard concentrations on the x-axis and the corresponding mean absorbance on the y-axis.
3. The best fit line can be determined by regression analysis issuing log-log or four parameter logistic curve-fit.
4. Determine the unknown sample concentration from the standard curve and multiply the value by the dilution factor.

Appendix E

Histological procedure for staining paraffin embedded tissue

Protocol 1: Preservation and sectioning of tissue stored in 4% formaldehyde

The entire process of making a histological slide can broadly be divided into six main steps, which are: (1) Tissue collection and fixation (2) Tissue processing (3) Embedding (4) Sectioning (5) Staining and (6) Mounting of the tissue. Each one of these steps has an important function and mistakes at any level could interfere with results obtained during microscopic evaluation of the slide.

Tissue collection and fixation.

Tissue should be harvested from the animal before or immediately after death. This is to minimize tissue degradation due to putrefaction and autolysis that occurs as soon as tissue is removed from the body or after death of the animal. For fixation of samples; place in a specimen tube with 4& formaldehyde solution for a minimum of 48 hours. The fixation stops tissue degradation and ensures that tissue structure is not lost.

Tissue processing.

Section tissues into smaller pieces to be placed into embedding cassettes for tissue processing. The tissue processing procedure are divided into 3 steps: dehydration with a series of alcohols, clearing with xylene and infiltration with paraffin wax. Dehydration with a series of different alcohol concentrations ensures that all water in the tissue are removed. Due to alcohol not mixing with water, the clearing step replaces the alcohol with xylene, which can mix and be replaced with paraffin wax during the infiltration steps. Infiltration with paraffin wax allows for further preservation and sectioning into microscopically thin sections once embedded. The tissue was processed with an automated processor (Sakura Finetechnical Co. Ltd, Tissue Tek II 4634, Japan) and Paraplast wax (Sigma-Aldrich, A6330-4LB, SA) was used for infiltration. The processing protocol is indicated in table 1 below.

Table 1: automated processing protocol

Step #	Solution	Time (min)
1	10% formalin	30
2	70% Ethanol	30
3	96% Ethanol	30
4	96% Ethanol	30
5	99.9% Ethanol	30
6	99.9% Ethanol	30
7	99.9% Ethanol	30
8	Xylene	30
9	Xylene	30
10	Paraffin wax	60
11	Paraffin wax	60
12	Paraffin wax	60

Steps 1-9 is completed at room temperature and steps 10-12 at 60 °C.

Embedding.

Place the processed tissue into a metal embedding mould with the appropriate orientation as this will determine the plane in which tissues are sectioned. Fill the mould with melted paraffin wax and immediately place a cassette on top of the mould. This assembly is then placed on an iced surface to allow the wax to set. After the wax has set the tissue blocks were kept at 20-25°C (room temperature). When embedding tissue, care should be taken to prevent formation of air bubbles in the in the wax, in and around the tissue. Such bubbles make sectioning difficult and may cause holes in the tissue section.

Sectioning.

Two hours prior to sectioning, place the tissue blocks in a freezer to cool. Trim and section the tissue block using a Leica RM 2125 RT microtome to obtain uniform 5µm sections. Place the sections into water at a temperature of approximately 40°C. This allows the tissue to stretch out

before being mounted onto a glass slide. Tissue should be picked up from the water bath with a glass slide at an angle, to prevent the formation of bubbles between the tissue and the glass slide, which will interfere with staining. During the process of sectioning, it is important to ensure that the blade of the microtome is does not become blunt, as this can cause artefacts. Tissue sections must be carefully moved from the microtome to the water bath. As sections are very thin they might tare or fold during this process disrupting tissue structure. Monitor the temperature of the water bath because a too high temperature causes tissue to disintegrate before it could be picked up with a glass slide.

Protocol 2: Haematoxylin and Eosin (H&E) Staining.

The standard H&E staining method, does not stain specific structures or differentiate between different cells within tissue, but allows for the visualization of all the cells that make up a tissue. Haematoxylin and eosin are two different dyes; haematoxylin being basic and staining acidic components of a cells, while eosin is acidic and stains basic cellular components [2]. When animal cells are stained with H&E, the nucleus of the cell is stained blue by haematoxylin and the cytoplasm is stained pink by eosin. Sections stained with H&E allow for the evaluation of gross morphological characterization of tissue. In some cases, different cell types may be apparent if some cells stain lighter than others.

Place slides in an incubator to melt the wax off the tissue. Liver tissue were stained with haematoxylin and eosin with an autostainer (Leica Auto Stainer XL). Automation of the staining procedure, allows for replication of the procedure without human error or variation. The haematoxylin solution should be filtered before each run and eosin solutions must be correctly prepared to ensure correct and optimal staining. H&E staining protocol is shown in Table 3. The autostainer includes steps to deparaffinise, rehydrate and clear the tissue, so that the slide may eventually be permanently mounted.

Table 2: H&E staining protocol

Step #	Solution	Time (min)	Repetitions
1	Oven 60°C	2 min	X1
2	Xylene	5 min	X2
3	Ethanol 99%	2 min	X2
4	Ethanol 96%	2 min	X1

5	Ethanol 70%	2 min	X1
6	Tap water	2 min	X1
7	Haematoxylin	8 min	X1
8	Running water	5 min	X1
9	Eosin	4 min	X1
10	Running water	1 min	X1
11	Ethanol 70%	30 sec	X1
12	Ethanol 96%	30 sec	X2
13	Ethanol 99%	30 sec	X1
14	Xylene	1 min	X1

Mounting

Cover the tissue on the slide with DPX mounting media and place a cover slip ontop. Leave to dry for 48 hours.

The mounting solution should not be stirred too much and the cover slip placed on the slide at an angle, this prevents bubbles from forming. Bubbles will interfere with the visualisation of the tissue under the microscope and if they do occur they should be carefully pushed out by pushing down on the coverslip with a pincet. Mounting of the slides completes the histological slide preparation process. Slides can now be viewed under the microscope and images captured for morphometric analysis.

Quantification of haematoxylin and Eosin images.

Hydropic changes were observed in the H&E staining of the hepatic tissue which are the first structural changes that occur in response to liver damage. They are the formation of non-uniform fluid filled sacs in the cytoplasm of the hepatocytes and was semi-quantified by constructing a grading system (Table 3) where the percentage hydropic changes per 10x image of 4 lobes per rat was determined. An average was then calculated and grades assigned per treatment group.

Table 3: Grading system for ballooning

Percentage (%) change	0 > 25	25 > 50	50 > 75	75 > 100
Grade	Minimal	Mild	Moderate	Severe

The percentage (%) hydropic change was determined by dividing one 10x image per lobe into 100 blocks (see below). The presence of hydropic change within hepatocytes in each block was then determined, and a percentage calculated based on the amount of blocks that had hepatocytes

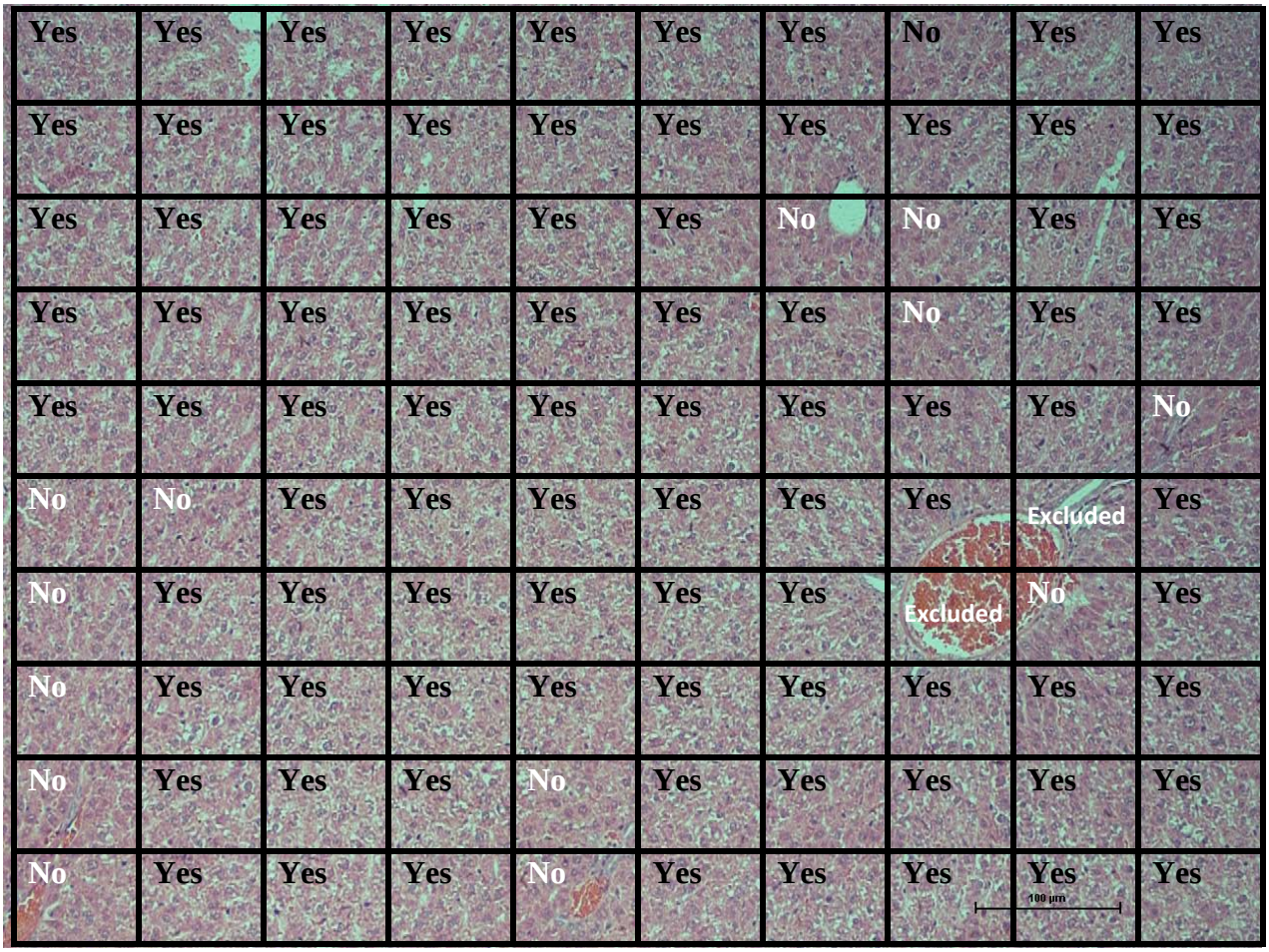

with the hydropic changes. The presence of central veins and portal triads that stretched over an entire block were excluded from the quantification. Those with hydropic received Yes and those with healthy hepatocytes, received NO.

No = 13 blocks Yes = 85 Blocks excluded = 2, thus, total blocks = 98

% hydropic change = 85/98*100 = 86.7%

Protocol 3: Gordon's and Sweets staining for reticulin

Principle:

Reticulin fibres have little natural affinity for silver solutions. Therefore, they need to be treated with potassium permanganate to produce sensitized sites on the fibres where silver deposition can be initiated. The silver is a in a form readily able to precipitate as metallic silver (diamine silver solution). The optimal pH for maximum uptake of silver ions is 9.0. A reducing agent, formalin, causes deposition of silver in the form of metal. Any excess silver in the unprecipitated state is removed by hypo. Gold Chloride treatment renders the preparation permanent and produces a neutral black color of high intensity.

Technical Points:

- Make the silver solution each time. Ammoniacal solutions can be explosive when allowed to dry. Immediately after use neutralise the silver solution with saturated sodium chloride and discard.
- Clean glassware used to prepare the silver solution with glassware cleaning solution. . was thoroughly before use with tap water and use distilled water for the final rinse.
- It is important not to over dissolve the precipitate at any stage as this will result in a decrease in sensitivity.
- Omit step 12 for untoned retics. (i.e, liver specimens)
- Omit step 16 for haematology trephines.

Method:

1. Deparafinise sections with Xylene then take through alcohols to tap water:
    - Xylene, Xylene, 99% alcohol, 99%, 96%, 96%, 70% and lastly, tap water.
    - 5 Minutes in each solution
2. Oxidise in acidified potassium permanganate for 3 minutes
3. Rinse in distilled water
4. Decolourise with 2% oxalic acid for 1 minute.
5. Rinse in distilled water

6. Mordant in 4% iron alum for 10 minutes (upright 45°-degree angle)
7. Rinse in distilled water
8. Impregnate in ammoniacal silvers solution for 11 seconds
9. Rinse quickly in distilled water
10. Immediately reduce with 10% aqueous formalin solution for 2 minutes
11. Wash in running tap water for 2 minutes
12. Tone in 0.2% Gold Chloride for 2 minutes (Omit this step for liver specimens).
13. Rinse in distilled water
14. Fix with 2% aqueous sodium thiophosphate (hypo) for 2 minutes
15. Wash in tap water for 2 minutes
16. Counterstain with neutral red for 2 minutes (Reggie alternatively uses the light green stain – dip slides in solution briefly)
17. Dehydrate (through the alcohol solutions starting at 70% for 5 minutes each and then in xylene for 1 min each) clear and mount.

Reticulin fibers = Black **Nuclei = Red**

Reagent formulae:

1. Acidified Potassium permanganate XE “Potassium permanganate acidified 37”
    a. 0.5% Potassium permanganate ___95 ml (0. 5 dissolved in 100 ml dH2O)
    b. 3% Sulphuric acid_____3 ml (1.5 in 50)
2. Silver solution
    a. To 5 ml of 10% aqueous silver nitrate add strong ammonia drop by drop until the precipitate which firsts forms is just dissolved. Add 5 ml of 3% sodium hydroxide then add strong ammonia drop by drop until the resulting precipitate is almost compltetely dissolved. Make up to 50 ml with dH2O and pour in a clean coplin jar.
3. 2% aqueous Oxalic acid
    a. Oxalic acid (analytical)____ 2g
    b. Distilled water ___100 ml
4. 4% aqueous iron alum
    a. Iron alum (ferric ammonium sulphate) ___ 4g

   b. Distilled water___100 ml
5. 10% formalin
   a. Formaldehyde (Ajax, 37 40g/L) ___ 10 ml
   b. Distilled water____ 100 ml
6. 0.2% gold chloride
   a. Gold Chloride (Sodium tetrachloroaurate, BDH) ___ 2g
   b. Distilled water___100 ml
7. 2% sodium thiosulphate (hypo)
   a. Sodium thiosulphate ___2g
   b. Distilled water___100 ml
8. Neutral red stain – acidified
   a. Neutral red (Cl 500400 ___ 1.0 g
   b. Distilled water___100 ml
   c. Acetic acid ___1.0 ml

Protocol 4: Periodic acid Schiff staining for glycogen

This method is used for the detection of glycogen in tissues such as the liver, cardiac and skeletal muscle in formalin fixed, paraffin-embedded tissue sections, and may be used for frozen sections as well. The glycogen, mucin and fungi will be stained purple and the nuclei will be stained blue.
Fixation: 10% formalin
Section: paraffin sections at 5 µm

Solutions and reagents:

<u>1% periodic acid solution:</u>

1 g periodic acid dissolved in 100 ml distilled water.

<u>Schiff reagent:</u>

Schiff's aldehyde reagent (Merck Millipore, 109034, SA).
Test for Schiff reagent: pour 10 ml of 37% formalin into a watch glass. To this add a few drops of the Schiff reagent to be tested. A good Schiff reagent will rapidly turn a red-purple colour. A

deteriorating Schiff reagent will give a delayed reaction and the colour produced will be a deep blue – purple.

Mayer's haematoxylin solution:

Used as purchased from company (Merck Millipore, SAAR2822001LC, SA).

Procedure:

1. Deparafinize and hydrate to water by placing in the following solutions for 5 min each:
    a. Xylene
    b. Xylene
    c. 99% Alcohol
    d. 99% Alcohol
    e. 96% Alcohol
    f. 96% Alcohol
    g. 70% Alcohol
    h. Tap water – may leave slides in water overnight.
2. Oxidize in 1% Periodic acid solution for 5 min
3. Rinse in distilled water
4. Place in Schiff reagent for 15 min (sections become light pink colour during this step)
5. Wash in lukewarm water for 5 min (Immediately sections turn dark pink colour)
6. Counterstain in Mayer's haematoxylin for 1 min
7. Wash in tap water for 5 min
8. Dehydrate by dipping slides in the alcohol solutions 5 times each and 1 min each in the xylene:
    a. 70% Alcohol
    b. 96% Alcohol
    c. 96% Alcohol
    d. 99% Alcohol
    e. 99% Alcohol
    f. Xylene
    g. Xylene

9. Add coverslip using a synthetic mounting medium (slides should not dry out thus leave slides in xylene while mounting)

Results:

Glycogen, mucin and some basement membranes – red/purple

Fungi - red/purple

Background - Blue

Protocol 4: Masson's trichrome for fibrosis

The Masson's trichrome stain detects type I and III collagen deposition indicative of scarring (fibrosis).

Staining solutions

1. Mayer's haematoxylin solution
2. Acetic Acid Water
    a. Glacial acetic acid -2ml
    b. Distilled water -1000ml
3. Masson Fuchson Ponceau-Orange G
    a. Stock solution – Ponceau (2R) de xylidine -2g
    b. Acid fuchsin -1g
    c. Orange G -2g
    d. Acetic acid water 0.2% -300ml
4. Working solution
    a. No . 3 (MFPOG) -10ml
    b. Acetic acid water 0.2% -90ml
5. Light Green Solution
    a. Light green -0.1g
    b. Acetic acid water 0.2 -100ml
6. Phosphotungstic acid 5%
    a. Phosphotungstic acid -5g
    b. Distilled water -100ml

Method

1. Deparaffinize sections and bring to water.
2. Rinse in distilled water.
3. Stain in haematoxylin for 5min.
4. Run in tape for 3min till dark blue and rinse in distilled water.
5. Stain the sections in filtered working solution of fuchsin ponceau-orangeG for 5-30min (15 minutes for this study)
6. Rinse in acetic acid water.
7. Mordant in 5% phosphotungtic acid solution for 5min.
8. Rinse in acetic acid water for 1min to eliminate the phosphotungstic acid and differentiate the colour tones.
9. Stain in light green solution for 5-20 min. (20)
10. Treat with acetic acid water for 5min.
11. Dehydrate through alcohols.
12. Clear in xylene and mount in DPX mounting medium.

Result

Nuclei	-	black
Cyttoplasm	-	red
Collagen	-	green
Mucin	-	green
Erythrocytes	-	yellow to orange

Protocol 5: Immunohistochemical staining procedure and manual rehydration (ALT)

Follow steps of 1-4 of basic histological procedure:

1) Tissue collection and fixation
2) Tissue processing
3) Embedding
4) Sectioning

Alanine aminotransaminase (ALT) (Santa Cruz biotechnology, Sc-271861, SA) was probed for by IHC using the Bond-Max™ Autostainer (Leica Biosystems, Germany) and the Bond™ Polymer Refine detection kit (Leica Biosystems, DS9800, Germany). Table 3 below indicates the automated staining procedure

Table 3: Automated Immunohistochemical double staining procedure

Step #	Solution	Incubation time (min)	Temperature (°C)
1	Bond wash solution	0	72
2	Bond wash solution	0	72
3	Bond wash solution	0	Room temperature
4	Alcohol	0	Room temperature
5	Alcohol	0	Room temperature
6	Alcohol	0	Room temperature
7	Bond wash solution	0	Room temperature
8	Bond wash solution	0	Room temperature
9	Bond wash solution	0	Room temperature
10	Bond ER solution 1	0	Room temperature
11	Bond ER solution 1	0	Room temperature
12	Bond ER solution 1	20	100
13	Bond ER solution 1	12	Room temperature
14	Bond wash solution	0	35
15	Bond wash solution	0	35
16	Bond wash solution	0	35
17	Bond wash solution	3	Room temperature
18	Peroxide block	5	Room temperature
19	Bond wash solution	0	Room temperature
20	Bond wash solution	0	Room temperature
21	Bond wash solution	0	Room temperature
22	Primary antibody	30	Room temperature

23	Bond wash solution	0	Room temperature
24	Bond wash solution	0	Room temperature
25	Bond wash solution	0	Room temperature
26	Post primary	8	Room temperature
27	Bond wash solution	2	Room temperature
28	Bond wash solution	2	Room temperature
29	Bond wash solution	2	Room temperature
30	Polymer	8	Room temperature
31	Bond wash solution	2	Room temperature
32	Bond wash solution	2	Room temperature
33	Deionized water	0	Room temperature
34	Mixed DAB refine	0	Room temperature
35	Mixed DAB refine	10	Room temperature
36	Deionized water	0	Room temperature
37	Deionized water	0	Room temperature
38	Deionized water	0	Room temperature
39	Haemotoxylin	5	Room temperature
40	Deionized water	0	Room temperature
41	Bond wash solution	0	Room temperature
42	Deionized water	0	Room temperature
43	Primary antibody	15	Room temperature
44	Bond wash solution	0	Room temperature
45	Bond wash solution	0	Room temperature
46	Bond wash solution	0	Room temperature
47	Polymer AP	20	Room temperature
48	Bond wash solution	2	Room temperature
49	Bond wash solution	2	Room temperature
50	Bond wash solution	2	Room temperature
51	Polymer AP	30	Room temperature
52	Bond wash solution	2	Room temperature

53	Bond wash solution	2	Room temperature
54	Bond wash solution	5	Room temperature
55	Bond wash solution	2	Room temperature
56	Bond wash solution	0	Room temperature
57	Deionized water	0	Room temperature
58	Mixed red refine	10	Room temperature
59	Mixed red refine	5	Room temperature
60	Deionized water	0	Room temperature
61	Deionized water	0	Room temperature
62	Deionized water	0	Room temperature
63	Haematoxylin	5	Room temperature
64	Deionized water	0	Room temperature
65	Bond wash solution	0	Room temperature
66	Deionized water	0	Room temperature

The primary antibody used were: Mouse anti-rat alanine transaminase primary antibody at a 1:1000 dilution. Purchased from Santa Cruz biotechnology cat. # sc - 271861

Table 4: Manual rehydration

Step #	Solution	Time	Repetitions
1	Ethanol 70%	5 dips	1
2	Ethanol 96%	5 dips	1
3	Ethanol 99%	5 dips	1
4	Xylene	1 min	2

Cover the tissue on the slide with PDX mounting media and place a cover slip ontop. Leave to dry for 48 hours. The mounting solution should not be stirred too much and the cover slip placed on the slide at an angle, this prevents bubbles from forming. Bubbles will interfere with the visualisation of the tissue under the microscope and if they do occur they should be carefully pushed out by pushing down on the coverslip with a pincet. Mounting of the slides completes the histological slide preparation process. Slides can now be viewed under the microscope and images captured for morphometric analysis.

Appendix F

Oil red O staining of frozen tissue

1. Frozen liver tissue was placed in liquid nitrogen and sectioned into 7 µm thick sections with a cryostat (Leica CM 3050 S Research Cryostat, Leica Biosystems) which was kept at a temperature of -12 ˚C.
2. The sections was then placed onto positively charged Histobond microscope slides (Lasec, GLAS2S13M0810401).
3. The sections were left to defrost
4. Followed by placing in the oil red O staining solution (Sigma-Aldrich, O1391, SA) for 20 minutes.
5. The slides was briefly washed in washed in cold tap water to remove excess staining solution.
6. The sections were then counterstained with 50% crystal violet (Sigma-Aldrich, V5265) for 1 minute.
7. Wash slides in cold tap water for 3 min
8. Leave the sections to air dry
9. Place aqueous mounting media (Sigma-Aldrich, G 0918) onto the sections with a coverslip.

Appendix G

Protocols for oxidative stress analysis

Protocol 1: Tissue preparation for TBARS, conjugated dienes and glutathione assays.

Buffer preparation

1. Phosphate buffer 75 mM, pH 7.4
    a. Weigh 1.035 g sodium di-hydrogen orthophosphate-1-hydrate in 100 ml distilled water and mix until dissolved.
    b. Weigh 1.335 g di-sodium hydrogen orthophosphate dehydrate in 100 ml distilled water and mix until dissolved.
    c. Mix 18 ml of the first solution, sodium di-hydrogen orthophosphate-1-hydrate, with 82 ml of the second solution, di-sodium hydrogen orthophosphate dehydrate.
    d. Adjust the pH of the buffer to 7.4
    e. Store at 4˚C
2. Phosphate buffer 75 mM, pH 7.4 with M_2VP
    a. Prepare the M_2VP by dissolving 8 mg of M_2VP in 0.1 M HCl.
    b. For every 990 µl of phosphate buffer add 10 µl of M_2VP. Prepare a stock solution and work from there

Tissue preparation

1. Thaw frozen liver tissue on ice.
2. Weigh ±100 mg of tissue off and place in a pre-chilled 2ml Eppendorf tube. Weigh two separate pieces off per rat.
3. For the one piece: add phosphate buffer (75 mM, pH 7.4), a ratio of 1/10 (w/v) to the tissue. Example: 100 mg of liver tissue add 1000 µl phosphate buffer add for 96 mg of tissue add 960 µl of the phosphate buffer. This will be used for TBARS, Conjugated Dienes and Glutathione (to measure GSH) assay
4. For the other piece: Add the stock solution of phosphate buffer with M_2VP also at a ratio of 1/10 (w/v) as described above in 3. This will be used for the glutathione assay (to measure GSSG)

5. Homogenize the tissue in the buffer on ice, with a dense homogenizer (Kinematica, POLYTRON® PT 2100 Homogenizer Switzerland) at 22 000 rpm for ±20 seconds until a lysate forms.
6. Sonicate at 10 A for 10 seconds (Qsonica, Misonix Sonicator S-400, USA).
7. Allow the froth to settle for 30 minutes.
8. Centrifuge (Labnet, Spectrafuge 16M, USA) at 12 000 rpm at 4 ˚C for 10 minutes
9. Remove the supernatant and place in a pre-chilled Eppendorf tube. Discard the pellet.
10. Store at – 80 ˚C.

Protocol 2: Conjugated Dienes Assay

1. Use the lysate prepared by only adding the Phosphate buffer (75 mM, pH 7.2), for this assay.
2. Prepare a solution of 2:1 methanol to chloroform by adding, 33 ml methanol to 67 ml chloroform.
3. Place 100 µl of sample into a 2 ml Eppendorf tube
4. Add 500 µl of the 2:1 chloroform to methanol solution to each sample
5. Invert the Eppendorf tube to mix
6. Centrifuge at 14 000 rpm for 1 minute
    a. Two layers form, the top layer is a protein layer and the bottom liquid layer is the conjugated dienes dissolved in the solution.
    b. Pipette 200 µl of the bottom into a new labelled Eppendorf tube. Take care not to remove the protein layer as well.
7. Leave the new Eppendorf tube with 200 µl of the sample, at 4˚C overnight over a flow of nitrogen (in the fridge) for the solution to evaporate and the conjugated dienes to stay behind in the tube. Do not close the lids of the Eppendorf tubes.
8. The following day, the solution will have evaporated.
9. Add 1000 µl of cyclohexane to each Eppendorf tube
10. Vortex for ±20 seconds

11. Transfer 300 µl of the sample and the cyclohexane as the blank to the wells of clear 96 well UVplate (Thermoscientific Inc, Microplate Uv Flat Bttm CS40, Netherlands). Test blank and samples in triplicate.

Measure the absorbance (Thermo Electron Corporation, Multiskan spectrum, Finland) at 230 nm immediately

Protocol 3: TBARS assay

Materials and reagents required:

1. Clear 96 well plate
2. A heating water bath set at 90 ˚C
3. Vortex
4. Centrifuge
5. Pipettes
6. O.11M Thiobarturic acid (TBA)
7. 0.2M Orthophosphoric acid (OPA)
8. 4mM 3,5-Di-tert-4-butylhydroxytoluene (BHT)

Assay procedure

1. Use the lysate prepared by only adding the Phosphate buffer (75 mM, pH 7.2), for this assay.
2. Add 50 µl of sample into a 2 ml Eppendorf tube.
3. Add 6.25 µl 4Mm BHT to each sample
4. Add 50 µl of ortho-phosphoric acid to each sample
5. Vortex to mix
6. Add 6.25 µl 0.11M TBA reagent to each sample
7. Vortex to mix
8. Punch a hole in the lid of each Eppendorf tube
9. Heat at 90 ˚C in the water bath for 45 minutes. Be strict with time and temperature for every repeat. All the samples should be placed into and removed out of the water bath simultaneously. The heat catalyse the reaction.
10. To stop the reaction, place samples in an ice bath for 2 minutes (or until needed).

11. Add 1000 µl of Butanol (100%) to each sample and invert the Eppendorf tube to mix. Use your finger to cover the hole in the lid.
12. Centrifuge at 14 000 rpm for 1 minute at room temperature.
13. Transfer 300 µl of the top layer to the wells of clear 96 well plate. Use the butanol as the blank. Test samples in triplicate.
14. Measure the absorbance (Thermo Electron Corporation, Multiskan spectrum, Finland) immediately at 532 nm.

Protocol 4: Glutathione assay

This assay consists of two parts: measurement of reduced glutathione (GSH) and measurement of oxidized glutathione (GSSG). The assay procedure remains the same but the samples are prepared differently.

To measure GSH use the lysate prepared by only adding the phosphate buffer (75 mM,pH 7.4) and for the measurement of GSSG, use the lysate prepared by adding the phosphate buffer with M_2VP solution.

Materials and reagents required:

1. Phosphate buffer (75 mM, pH 7.4)
2. I vial reduced nicotinamide adenine dinucleotide phosphate (NADPH) (Sigma-Aldrich, N6785) (1 mM). Add 12 ml in phosphate buffer (75 mM, pH 7.4) to 1 vial NADPH.
3. 5,5'-dithiobis-(2-nitrobenzoic acid (DTNB) (Sigma-Aldrich, D21820) 30 mM in phosphate buffer (75 mM, pH 7.4)
4. Standard solution (GSH - 3µm) (GSSG – 1.5 µM) in phosphate buffer (75 mM, pH 7.4)
5. Glutathione reductase (Sigma Aldrich, G3664, SA) [16 µl in 984 µl phosphate buffer (75 mM, pH 7.4)]

Assay procedure:

1. Prepare a standard curve and a dilution series of your samples to determine at what dilution the samples should be at to fall within the standard curve.
2. Prepare the standard curve as follows:

	Blank	**1**	**2**	**3**	**4**	**5**
GSH (µl)	0	167	333	500	667	833

Phosphate buffer (75 mM, pH 7.4)	1000	833	667	500	333	167

3. A standard should be tested prepared for each plate and test. Add 50 µl of standards and samples to the wells of a clear 96 well plate.
4. Add 50 µl of the DTNB to each well using a multichannel.
5. Add 50 µl of the glutathione reductase using a multichannel.
6. Add 50 µl NADPH to each well as quickly as possible (30 seconds max)
7. Measure absorbance at 412 nm every 30 seconds for 3 minutes.
8. Use linear slope of the standards to calculate concentration of samples

Appendix H

Protocol for western blotting

Protocol 1: Reagent preparation for western blot

Modified Radio immunoprecipitation assay buffer (RIPA) buffer

1. Dissolve 790 mg Tris base and 900 mg Sodium Chloride (NaCl) in 75 ml distilled water. Adjust the pH of the solution to 7.4 using Hydrochloric acid (HCl).
2. Add 10 ml of 10% triton x100 to the solution
3. Add 2. 5 ml of 10% Na-deoxycholate and stir until the solution is clear
4. Add 1 ml of 100 mM EDTA to the solution followed by adjusting the volume of the solution to 100 ml with distilled water
5. Aliquot the buffer in 10 ml amounts and store at 4 ˚C until day of use.
6. On the day of use add the following:
    a. PMSF: 10 µl/ml RIPA buffer (half-life 30 minutes)
    b. 200 mM NaF: 5 µl/ml RIPA buffer
    c. Na_2VO_3: 5 µl/ml RIPA buffer
    d. Phosphatase and protease inhibitor cocktail: 42 µl/1ml RIPA buffer

10X TBS

1. Dissolve 24.2 g Tris and 80 NaCl in 600 ml distilled water.
2. Adjust pH to 7.6 with HCl
3. Make up to 1000 ml with distilled water

1X TBS-T

1. Mix 100 ml of the 10X TBS with 900 ml distilled water.
2. Add 1 ml Tween
3. Mix well do not adjust pH

Laemmli's loading buffer

First prepare stock solution A.

1. 38 ml distilled water
2. Add 10 ml of 0.5 M Tris (pH 6.8)
3. Add 8 ml glycerol
4. 16 ml 10% Sodium dodecyl sulphate (SDS)
5. 4 ml of 0.05% Bromophenol blue

On the day of use prepare a working solution of Laemmli's loading buffer by adding mercapto-ethanol: for every 850 µl Solution A, add 150 µl mercapto-ethanol.

Running buffer

Dilute 10X running buffer to 1X running buffer:

1. 100 ml 10X running buffer with 900 ml distilled water.
2. Mix well

5% Blocking buffer

1. 5 ml Parmalat fat free milk dissolved in 95 ml 1X TBS-T
2. Mix well
3. Use 50 ml of this solution per membrane

Protocol 2: Sample preparation

1. Frozen liver tissue was used for Western blot analysis. Thaw liver tissue on ice.
2. Add 300 µl of the modified RIPA buffer to each 2 ml Eppendorf tube with tissue.
3. On ice, homogenize the tissue with a dense homogenizer (Kinematica, POLYTRON® PT 2100 Homogenizer Switzerland) at 22 000 rpm for ±20 seconds.
4. Place samples back on ice and allow froth to settle for 60 minutes.
5. Centrifuge at 14 000 rpm at 4˚C for 60 minutes
    a. 3 layers form: a top fat layer, a middle protein layer and at the bottom, the pellet.
6. Remove the middle protein layer with a 23-gauge needle attached to a 1 ml syringe. Insert the 23-gauge needle attached to a 1 ml syringe into the side, at the middle, of the Eppendorf tube to remove the protein lysate.
7. Place the protein lysate into a pre-chilled 2 ml Eppendorf tube.
8. To ensure that the lysate is free of fat and cellular debris contaminants, centrifuge the lysate again at 14 000 rpm at 4 ˚C for 40 minutes.

9. Remove the protein lysate and discard the pellet.

Protein concentration determination

The Direct Detect ™ Spectrometer (Merck Millipore, DDHW00010-WW, Germany) was used to determine the protein concentration within each lysate. This system measures the absorbance of amide bonds in protein chains using infrared quantitation thereby determines intrinsic components of every protein without relying on amino acid composition, dye binding properties and redox potential.

1. Apply 2 µl of sample into positions 2-4 of the direct detect card. Position 1 is for the blank. Use the modified RIPA buffer as the blank.
2. Insert the card vertically into the slot in the top of the sampling accessory with the card notch facing towards the center of the instrument
3. The instrument will dry the sample and then take protein concentration measurements in mg/ml.

Sample preparation for loading

1. Determine the volume of lysate required to load 30 µg of protein into the wells by using this equation: $\frac{(30x1000)}{\text{protein concentration (µg/ml)}}$
2. Add the appropriate volume of lysate to 20 µl laemmli's buffer.
3. Punch a hole in Eppendorf tube and boil at 95˚C for 5 minutes before loading into the wells of the gel for electrophoresis.

Protocol 3: Sodium dodecyl sulphate polyacrylamide gel electrophoresis (SDS-PAGE).

1. Use the 1 mm glass plates and assemble to pour gels.
2. Prepare the 12% TGX stain-free™ FastCast™ acrylamide gels according to the manufacturer's instructions (Bio-Rad, 1610183, SA).
3. Use a Pasteur pipette to first pour the resolving gel into the assembled glass plates until about 2 cm under the brim of the front plate, then immediately pour the stacking gel and fill to the brim of the front plate.
4. Immediately insert the 10 well comb being careful not to form bubbles.
5. Allow gels to set for 40 minutes.

6. Once the gels have set in the glass plates, remove the combs and lace in the U-shaped adapter with the short plate facing inwards. This will form a center in the adapter called a buffer dam. NB: two gels is required to form the buffer dam, if only running one gel, use an insert called a buffer dam in the place of the second gel.
7. Place the assembly in a gel tank and fill the buffer dam with 1X running buffer.
8. Start loading samples and a protein marker into the wells using the gel loading tips.
9. Place the lid of the tank on top of the tank with the appropriate leads (black to black and red to red) and connect to the power pack.
10. Run at 90 V until the blue frontline and the smallest standard of the protein marker reaches the bottom of the gel.
11. Remove the gel from the gel plates and active the gels in the ChemiDoc™ XRS+ system (Bio-Rad, USA).
12. Transfer onto a PVDF membrane. (Bio-Rad, Trans-Blot® Turbo™ ready-to-assemble mini low fluorescent PVDF transfer kit, 1707274, USA)
    a. Soak transfer stack in the transfer buffer supplied by transfer kit and prepared as manufacturer indicates.
    b. Place the PVDF membrane in 100% methanol for ±30 seconds and then in the transfer buffer.
    c. Assemble the transfer stack and membrane in the TransBlot® Turbo™ Transfer System (Bio-Rad, USA) with the transfer stack placed down first, roll out any bubbles or wrinkles that may have formed on the transfer stack and then place the membrane on top. NB: Do not roll the membrane.
    d. After the gel have been activated, place the gel on top of the membrane. Roll out any bubbles that may have formed.
    e. Soak the second transfer stack in the transfer buffer and place on top of the gel. Give a final role.
    f. Place the lid of the cassette on top, and place the cassette into the TransBlot® Turbo™ Transfer System (Bio-Rad, USA).
    g. Transfer for 30 min at 25 V.
13. After transfer, take an image of the membrane in the ChemiDoc™ XRS+ system

14. Place membrane in methanol for 30 seconds and then air dry the membrane. This is to fix the proteins into the membrane. Wet the membrane in methanol again in order for it to interact with hydrophilic solutions
15. Place the membrane in 5% blocking buffer for 60 minutes. Place on belly dancer at a very low speed.
16. Wash membrane 3x 5mins in 1x TBS-T
17. Place membrane in primary antibody (see table 2.1 below for list of antibodies) on a rotator overnight at 4 ˚C.
18. Wash membrane 3x 5mins in 1x TBS-T
19. Place membrane in secondary antibody for 60 minutes at room temperature on a rotator.
20. Wash membrane 3x 5mins in 1x TBS-T
21. Image in ChemiDoc™ XRS+ system. Place membrane in ChemiDoc™ XRS+ system and cover the membrane in ECL (Bio-Rad, 1705061, USA). The bands are viculaized with the Image Lab™ software and discrepancies in loading were corrected for by using total protein normalization.

Table 2.1. List of primary and secondary antibodies used for Western blotting

Primary Antibodies			
Name	**Size (kDa)**	**Company (catalogue number)**	**Dilution**
Cleaved Caspase-3	17, 19	Cell Signalling Technology (9662)	1:1 000
Cleaved PARP	89	Cell Signalling Technology (5625)	1:1 000
BiP	68	Cell Signalling Technology (3177)	1:1 000
ATF4	48	Cell Signalling Technology (11815)	1:1 000
LC3	16, 18	Cell Signalling Technology (3868)	1:1 000
p62	62	Cell Signalling Technology (5114)	1:1 000
ALT	48	Santa Cruz Biotechnology (Sc-271861)	1:1 000
	Secondary Antibodies		
Anti-Rabbit IgG HRP-linked	0	Cell Signalling Technology (7074)	1:10 000

Anti-mouse IgG HRP-linked	0	Cell Signalling Technology (58802)	1:10 000

Abbreviations: **PARP**: Poly (ADP-ribose) polymerase, **BiP**: immunoglobulin heavy chain-binding protein, **ATF4**: Activating Transcription Factor 4, **LC3**: microtubule associated protein 1 light chain 3, **ALT**: alanine transaminase.

Appendix I

Reagents used

Reagent	Cat#	Company
,5-Di-tert-4-butylhydroxytoluene (BHT)	442377	Sigma-Aldrich
5,5'-dithiobis-(2-nitrobenzoic acid) (DTNB)	D21820	Sigma-Aldrich
Acetic acid water	600113	Radchem
aqueous mounting media	G 0918	Sigma-Aldrich,
Butanol	B7906	Sigma-Aldrich
crystal violet	V5265	Sigma-Aldrich
Doxorubicin	D5794	LKT Laboratories
DPX mountant	D0738NN00500	Associated Chemical Enterprises
Formaldehyde	1.00496.5000	Merck Millipore,
Ghrelin	G2869	LKT Laboratories
Glutathione reductase	G3664	(Sigma Aldrich
Iron alum	103776	Merck Millipore,
Light green solution	L1886	Sigma-Aldrich
Mayer's haematoxylin	SAAR2822001LC	Merck Millipore
NADPH Sigma-Aldrich, N6785)	Sigma-Aldrich	N6785
Oil red O staining solution	O1391	Sigma-Aldrich
Ortho-phosphoric acid (OPA)	1.00573.2500	Merck Millipore
Oxalic acid	6153-56-6,	Radchem

Paraplast® wax	A6330-4LB	Sigma-Aldrich,
Potassium permanganate	109930	Merck Millipore,
Sodium triphosphate	T5041	Sigma-Aldrich
Xylene	1086619190	Merck Millipore

Appendix J:

Permissions/copyright from journals for the use of figures

Figure 1.2: Representation of the hepatic lobule and hepatic acinus and the arrangement of the hepatocytes and sinusoids.

ELSEVIER LICENSE
TERMS AND CONDITIONS

Dec 13, 2017

This Agreement between Ms. Carmelita Abrahams ("You") and Elsevier ("Elsevier") consists of your license details and the terms and conditions provided by Elsevier and Copyright Clearance Center.

License Number	4242440139249
License date	Dec 05, 2017
Licensed Content Publisher	Elsevier
Licensed Content Publication	Anaesthesia & Intensive Care Medicine
Licensed Content Title	Liver: functional anatomy and blood supply
Licensed Content Author	Iain Campbell
Licensed Content Date	Feb 1, 2006
Licensed Content Volume	7
Licensed Content Issue	2
Licensed Content Pages	3
Start Page	49
End Page	51
Type of Use	reuse in a thesis/dissertation
Intended publisher of new work	other
Portion	figures/tables/illustrations
Number of figures/tables/illustrations	1
Format	both print and electronic
Are you the author of this Elsevier article?	No
Will you be translating?	No
Original figure numbers	Figure 3: Lobule
Title of your thesis/dissertation	Chronic doxorubicin-induced toxicity: Effect on hepatic tissue
Expected completion date	Feb 2018
Estimated size (number of pages)	75
Requestor Location	Ms. Carmelita Abrahams 6 Speyer Drive Silversands Kuils River Cape town, Western cape 7580 South Africa Attn: Ms. Carmelita Abrahams
Publisher Tax ID	ZA 4110266048
Total	0.00 USD
Terms and Conditions	

INTRODUCTION

terms and conditions. These terms and conditions, together with CCC's Billing and Payment terms and conditions (which are incorporated herein), comprise the entire agreement between you and publisher (and CCC) concerning this licensing transaction. In the event of any conflict between your obligations established by these terms and conditions and those established by CCC's Billing and Payment terms and conditions, these terms and conditions shall control.

14. Revocation: Elsevier or Copyright Clearance Center may deny the permissions described in this License at their sole discretion, for any reason or no reason, with a full refund payable to you. Notice of such denial will be made using the contact information provided by you. Failure to receive such notice will not alter or invalidate the denial. In no event will Elsevier or Copyright Clearance Center be responsible or liable for any costs, expenses or damage incurred by you as a result of a denial of your permission request, other than a refund of the amount(s) paid by you to Elsevier and/or Copyright Clearance Center for denied permissions.

LIMITED LICENSE

The following terms and conditions apply only to specific license types:

15. **Translation**: This permission is granted for non-exclusive world **English** rights only unless your license was granted for translation rights. If you licensed translation rights you may only translate this content into the languages you requested. A professional translator must perform all translations and reproduce the content word for word preserving the integrity of the article.

16. **Posting licensed content on any Website**: The following terms and conditions apply as follows: Licensing material from an Elsevier journal: All content posted to the web site must maintain the copyright information line on the bottom of each image; A hyper-text must be included to the Homepage of the journal from which you are licensing at http://www.sciencedirect.com/science/journal/xxxxx or the Elsevier homepage for books at http://www.elsevier.com; Central Storage: This license does not include permission for a scanned version of the material to be stored in a central repository such as that provided by Heron/XanEdu.

Licensing material from an Elsevier book: A hyper-text link must be included to the Elsevier homepage at http://www.elsevier.com . All content posted to the web site must maintain the copyright information line on the bottom of each image.

Posting licensed content on Electronic reserve: In addition to the above the following clauses are applicable: The web site must be password-protected and made available only to bona fide students registered on a relevant course. This permission is granted for 1 year only. You may obtain a new license for future website posting.

17. **For journal authors:** the following clauses are applicable in addition to the above:

Preprints:

A preprint is an author's own write-up of research results and analysis, it has not been peer-reviewed, nor has it had any other value added to it by a publisher (such as formatting, copyright, technical enhancement etc.).

Authors can share their preprints anywhere at any time. Preprints should not be added to or enhanced in any way in order to appear more like, or to substitute for, the final versions of articles however authors can update their preprints on arXiv or RePEc with their Accepted Author Manuscript (see below).

If accepted for publication, we encourage authors to link from the preprint to their formal publication via its DOI. Millions of researchers have access to the formal publications on ScienceDirect, and so links will help users to find, access, cite and use the best available version. Please note that Cell Press, The Lancet and some society-owned have different preprint policies. Information on these policies is available on the journal homepage.

Accepted Author Manuscripts: An accepted author manuscript is the manuscript of an article that has been accepted for publication and which typically includes author-incorporated changes suggested during submission, peer review and editor-author communications.

Authors can share their accepted author manuscript:

- immediately

1. The publisher for this copyrighted material is Elsevier. By clicking "accept" in connection with completing this licensing transaction, you agree that the following terms and conditions apply to this transaction (along with the Billing and Payment terms and conditions established by Copyright Clearance Center, Inc. ("CCC"), at the time that you opened your Rightslink account and that are available at any time at http://myaccount.copyright.com).

GENERAL TERMS

2. Elsevier hereby grants you permission to reproduce the aforementioned material subject to the terms and conditions indicated.

3. Acknowledgement: If any part of the material to be used (for example, figures) has appeared in our publication with credit or acknowledgement to another source, permission must also be sought from that source. If such permission is not obtained then that material may not be included in your publication/copies. Suitable acknowledgement to the source must be made, either as a footnote or in a reference list at the end of your publication, as follows:

"Reprinted from Publication title, Vol /edition number, Author(s), Title of article / title of chapter, Pages No., Copyright (Year), with permission from Elsevier [OR APPLICABLE SOCIETY COPYRIGHT OWNER]." Also Lancet special credit - "Reprinted from The Lancet, Vol. number, Author(s), Title of article, Pages No., Copyright (Year), with permission from Elsevier."

4. Reproduction of this material is confined to the purpose and/or media for which permission is hereby given.

5. Altering/Modifying Material: Not Permitted. However figures and illustrations may be altered/adapted minimally to serve your work. Any other abbreviations, additions, deletions and/or any other alterations shall be made only with prior written authorization of Elsevier Ltd. (Please contact Elsevier at permissions@elsevier.com). No modifications can be made to any Lancet figures/tables and they must be reproduced in full.

6. If the permission fee for the requested use of our material is waived in this instance, please be advised that your future requests for Elsevier materials may attract a fee.

7. Reservation of Rights: Publisher reserves all rights not specifically granted in the combination of (i) the license details provided by you and accepted in the course of this licensing transaction, (ii) these terms and conditions and (iii) CCC's Billing and Payment terms and conditions.

8. License Contingent Upon Payment: While you may exercise the rights licensed immediately upon issuance of the license at the end of the licensing process for the transaction, provided that you have disclosed complete and accurate details of your proposed use, no license is finally effective unless and until full payment is received from you (either by publisher or by CCC) as provided in CCC's Billing and Payment terms and conditions. If full payment is not received on a timely basis, then any license preliminarily granted shall be deemed automatically revoked and shall be void as if never granted. Further, in the event that you breach any of these terms and conditions or any of CCC's Billing and Payment terms and conditions, the license is automatically revoked and shall be void as if never granted. Use of materials as described in a revoked license, as well as any use of the materials beyond the scope of an unrevoked license, may constitute copyright infringement and publisher reserves the right to take any and all action to protect its copyright in the materials.

9. Warranties: Publisher makes no representations or warranties with respect to the licensed material.

10. Indemnity: You hereby indemnify and agree to hold harmless publisher and CCC, and their respective officers, directors, employees and agents, from and against any and all claims arising out of your use of the licensed material other than as specifically authorized pursuant to this license.

11. No Transfer of License: This license is personal to you and may not be sublicensed, assigned, or transferred by you to any other person without publisher's written permission.

12. No Amendment Except in Writing: This license may not be amended except in a writing signed by both parties (or, in the case of publisher, by CCC on publisher's behalf).

13. Objection to Contrary Terms: Publisher hereby objects to any terms contained in any purchase order, acknowledgment, check endorsement or other writing prepared by you, which terms are inconsistent with these terms and conditions or CCC's Billing and Payment

- via their non-commercial person homepage or blog
- by updating a preprint in arXiv or RePEc with the accepted manuscript
- via their research institute or institutional repository for internal institutional uses or as part of an invitation-only research collaboration work-group
- directly by providing copies to their students or to research collaborators for their personal use
- for private scholarly sharing as part of an invitation-only work group on commercial sites with which Elsevier has an agreement

- After the embargo period
  - via non-commercial hosting platforms such as their institutional repository
  - via commercial sites with which Elsevier has an agreement

In all cases accepted manuscripts should:

- link to the formal publication via its DOI
- bear a CC-BY-NC-ND license - this is easy to do
- if aggregated with other manuscripts, for example in a repository or other site, be shared in alignment with our hosting policy not be added to or enhanced in any way to appear more like, or to substitute for, the published journal article.

Published journal article (JPA): A published journal article (PJA) is the definitive final record of published research that appears or will appear in the journal and embodies all value-adding publishing activities including peer review co-ordination, copy-editing, formatting, (if relevant) pagination and online enrichment.
Policies for sharing publishing journal articles differ for subscription and gold open access articles:
Subscription Articles: If you are an author, please share a link to your article rather than the full-text. Millions of researchers have access to the formal publications on ScienceDirect, and so links will help your users to find, access, cite, and use the best available version.
Theses and dissertations which contain embedded PJAs as part of the formal submission can be posted publicly by the awarding institution with DOI links back to the formal publications on ScienceDirect.
If you are affiliated with a library that subscribes to ScienceDirect you have additional private sharing rights for others' research accessed under that agreement. This includes use for classroom teaching and internal training at the institution (including use in course packs and courseware programs), and inclusion of the article for grant funding purposes.
Gold Open Access Articles: May be shared according to the author-selected end-user license and should contain a CrossMark logo, the end user license, and a DOI link to the formal publication on ScienceDirect.
Please refer to Elsevier's posting policy for further information.
18. **For book authors** the following clauses are applicable in addition to the above:
Authors are permitted to place a brief summary of their work online only. You are not allowed to download and post the published electronic version of your chapter, nor may you scan the printed edition to create an electronic version. **Posting to a repository:** Authors are permitted to post a summary of their chapter only in their institution's repository.
19. **Thesis/Dissertation**: If your license is for use in a thesis/dissertation your thesis may be submitted to your institution in either print or electronic form. Should your thesis be published commercially, please reapply for permission. These requirements include permission for the Library and Archives of Canada to supply single copies, on demand, of the complete thesis and include permission for Proquest/UMI to supply single copies, on demand, of the complete thesis. Should your thesis be published commercially, please reapply for permission. Theses and dissertations which contain embedded PJAs as part of the formal submission can be posted publicly by the awarding institution with DOI links back to the formal publications on ScienceDirect.

Elsevier Open Access Terms and Conditions
You can publish open access with Elsevier in hundreds of open access journals or in nearly 2000 established subscription journals that support open access publishing. Permitted third

Figure 1.3: Hepatic glycogen synthesis and breakdown.

Figure 1.4: Transamination and deamination reactions to metabolize amino acids

ELSEVIER LICENSE
TERMS AND CONDITIONS

Dec 13, 2017

This Agreement between Ms. Carmelita Abrahams ("You") and Elsevier ("Elsevier") consists of your license details and the terms and conditions provided by Elsevier and Copyright Clearance Center.

License Number	4242431413254
License date	Dec 05, 2017
Licensed Content Publisher	Elsevier
Licensed Content Publication	Anaesthesia & Intensive Care Medicine
Licensed Content Title	Metabolic functions of the liver
Licensed Content Author	Vikramjit Mitra,Jane Metcalf
Licensed Content Date	Feb 1, 2012
Licensed Content Volume	13
Licensed Content Issue	2
Licensed Content Pages	2
Start Page	54
End Page	55
Type of Use	reuse in a thesis/dissertation
Intended publisher of new work	other
Portion	figures/tables/illustrations
Number of figures/tables/illustrations	2
Format	both print and electronic
Are you the author of this Elsevier article?	No
Will you be translating?	No
Original figure numbers	Illustration of amino acid transamination and amino acid deamination
Title of your thesis/dissertation	Chronic doxorubicin-induced toxicity: Effect on hepatic tissue
Expected completion date	Feb 2018
Estimated size (number of pages)	75
Requestor Location	Ms. Carmelita Abrahams 6 Speyer Drive Silversands Kuils River Cape town, Western cape 7580 South Africa Attn: Ms. Carmelita Abrahams
Publisher Tax ID	ZA 4110266048
Total	0.00 USD
Terms and Conditions	

Figure 1.6: The Harber-Weiss and Fenton reaction.

ELSEVIER LICENSE
TERMS AND CONDITIONS

Dec 13, 2017

This Agreement between Ms. Carmelita Abrahams ("You") and Elsevier ("Elsevier") consists of your license details and the terms and conditions provided by Elsevier and Copyright Clearance Center.

License Number	4242440733850
License date	Dec 05, 2017
Licensed Content Publisher	Elsevier
Licensed Content Publication	Pharmacological Reports
Licensed Content Title	Anthracycline-induced cardiotoxicity: Overview of studies examining the roles of oxidative stress and free cellular iron
Licensed Content Author	Tomáš Šimůnek,Martin Štěrba,Olga Popelová,Michaela Adamcová,Radomír Hrdina,Vladimír Geršl
Licensed Content Date	January–February 2009
Licensed Content Volume	61
Licensed Content Issue	1
Licensed Content Pages	18
Start Page	154
End Page	171
Type of Use	reuse in a thesis/dissertation
Intended publisher of new work	other
Portion	figures/tables/illustrations
Number of figures/tables/illustrations	1
Format	both print and electronic
Are you the author of this Elsevier article?	No
Will you be translating?	No
Original figure numbers	Illustration of the Haber-Weiss reaction and the Fe (iron) catalyzed Haber-Weiss reaction
Title of your thesis/dissertation	Chronic doxorubicin-induced toxicity: Effect on hepatic tissue
Expected completion date	Feb 2018
Estimated size (number of pages)	75
Requestor Location	Ms. Carmelita Abrahams 6 Speyer Drive Silversands Kuils River Cape town, Western cape 7580 South Africa Attn: Ms. Carmelita Abrahams
Publisher Tax ID	ZA 4110266048
Total	0.00 USD
Terms and Conditions	

Figure 1.3: Hepatic glycogen synthesis and breakdown.

Figure 1.4: Transamination and deamination reactions to metabolize amino acids

ELSEVIER LICENSE
TERMS AND CONDITIONS

Dec 13, 2017

This Agreement between Ms. Carmelita Abrahams ("You") and Elsevier ("Elsevier") consists of your license details and the terms and conditions provided by Elsevier and Copyright Clearance Center.

License Number	4242431413254
License date	Dec 05, 2017
Licensed Content Publisher	Elsevier
Licensed Content Publication	Anaesthesia & Intensive Care Medicine
Licensed Content Title	Metabolic functions of the liver
Licensed Content Author	Vikramjit Mitra,Jane Metcalf
Licensed Content Date	Feb 1, 2012
Licensed Content Volume	13
Licensed Content Issue	2
Licensed Content Pages	2
Start Page	54
End Page	55
Type of Use	reuse in a thesis/dissertation
Intended publisher of new work	other
Portion	figures/tables/illustrations
Number of figures/tables/illustrations	2
Format	both print and electronic
Are you the author of this Elsevier article?	No
Will you be translating?	No
Original figure numbers	Illustration of amino acid transamination and amino acid deamination
Title of your thesis/dissertation	Chronic doxorubicin-induced toxicity: Effect on hepatic tissue
Expected completion date	Feb 2018
Estimated size (number of pages)	75
Requestor Location	Ms. Carmelita Abrahams 6 Speyer Drive Silversands Kuils River Cape town, Western cape 7580 South Africa Attn: Ms. Carmelita Abrahams
Publisher Tax ID	ZA 4110266048
Total	0.00 USD
Terms and Conditions	

Figure 1.6: The Harber-Weiss and Fenton reaction.